SOLAR CORONAL STABILITY PROBLEMS

Ian S. Hardie

A Thesis Submitted for the Degree of PhD
at the
University of St Andrews

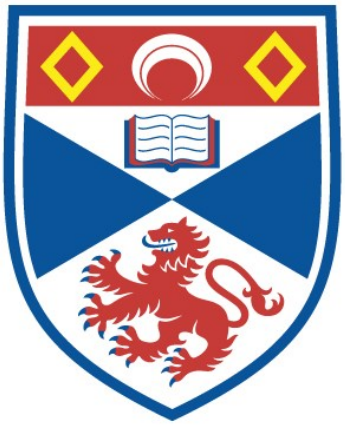

1993

Solar Coronal Stability Problems

Ian S. Hardie

Thesis submitted for the degree of Doctor of Philosophy of the University of St. Andrews

16 March 1993

Abstract

Magnetohydrodynamic stability theory provides a powerful tool for understanding and testing hypothesized mathematical and physical models of observed phenomena on the surface of the Sun. In this thesis, the problem of applying the 'correct' boundary conditions at the photospheric/coronal interface used in modelling coronal arcades is tackled. Then some aspects of the stability of coronal loops and arcades are investigated using a Fourier truncated series approximation for the equation of motion.

The problem involving the boundary conditions has been the subject of a controversy for the past decade with two principal conditions suggested, the 'rigid-wall' conditions where all perturbations vanish at the interface, and 'flow-through' conditions where flows parallel to the equilibrium magnetic field take place.

By modelling the photosphere and corona as two different density regions and then varying the ratio of the densities of the two regions, growth rates and eigenfunctions of both ideal and resistive modes are investigated in order to follow the evolution of the modes as the density ratio is increased. In order to simplify the analysis, the 2-D equations are reduced to 1-D equations by taking a WKB approximation for the spatial variations across the field to give a localized ballooning approach with ordinary differential equations along the fieldlines.

Stability of coronal loops to kink modes transformed to localized modes by increasing the poloidal wavenumber, m, is investigated. Two fields generated numeri-

cally from the Grad-Shafranov equation and three analytic fields are investigated in detail and the effect of pressure on the marginal loop length is found, both for near force-free conditions such as is found in the solar corona, and away from force-free conditions. It was found that for near force-free conditions, kink modes are the most unstable with localized modes the most stable. As pressure and pressure gradients become important, there is a reversal in the most unstable modes with localized modes the most unstable.

Declarations

I, Ian Stuart Hardie, hereby certify that this thesis has been composed by myself, that it is a record of my own work, and that it has not been accepted in partial or complete fulfilment of any other degree or professional qualification.

Signed: Date 16·3·93

I was admitted to the Faculty of Science of the University of St. Andrews under Ordinance General No. 12 on 1 October 1988 and as a candidate for the degree of Ph.D. on 1 October 1989.

Signed Date 16·3·93

I hereby certify that the candidate has fulfilled the conditions of the Resolution and Regulations appropriate to the Degree of Ph.D.

Signature of Supervisor.. Date 16/3/93

In submitting this thesis to the University of St. Andrews I understand that I am giving permission for it to be made available for use in accordance with the regulations of the University Library for the time being in force, subject to any copyright vested in the work not being affected thereby. I also understand that the title and abstract will be published, and that a copy of the work may be made and supplied to any *bona fide* library or research worker.

Acknowledgements

I would like to thank everyone who has helped me in the creation of this thesis.

Dr Alan Hood, my supervisor, who has guided me for the past few years, without his suggestions this thesis would not have been possible.

Also, everyone in the Solar Theory group and in the Department of Mathematical and Computational Sciences including Colin D.C. Steele, Christopher Ridgway, Neil R. Strachan and Gordon Inverarity, the co-occupants of room 223.

Financial support was provided by S.E.R.C., the Science and Engineering Research Council.

Finally, and most important of all, I would like to thank my parents, Stuart L.S. and Davina L.H. for their guidance, moral and financial support over the years since 1965, and my sisters, Grace, Hazel, Fiona and Shona for being there.

Dedication

This thesis is dedicated to my parents.

Contents

1 Introduction

1.1 Magnetohydrodynamics

The Sun, like most of the universe, is a plasma. A plasma is often described in literature as an ionized gas but such a simple definition belies the many underlying complexities. Thus, electromagnetic effects are important in the description of the plasma on a macroscopic scale. The simplest model comprises combining Maxwell's equations with the equations of fluid dynamics to give what is termed Magnetohydrodynamics. The MHD equations form a self-contained system of eight equations in eight primary variables ($\mathbf{B}$, $\mathbf{v}$, p, ρ) and are valid provided that flow velocities are small compared to the speed of light ($v \ll c$).

Maxwell's equations are

$$\nabla \times \mathbf{B} = \mu\epsilon\frac{\partial \mathbf{E}}{\partial t} + \mu\mathbf{j}, \tag{1.1}$$

$$\nabla \times \mathbf{E} = -\frac{\partial \mathbf{B}}{\partial t}, \tag{1.2}$$

$$\nabla \cdot \mathbf{B} = 0, \tag{1.3}$$

$$\nabla \cdot \mathbf{E} = \frac{\rho_c}{\epsilon}, \tag{1.4}$$

where

$\mathbf{B}$ is magnetic induction, loosely described as magnetic field,

$\mathbf{E}$ is the electric field,

$\mathbf{j}$ is plasma current density,

ρ_c is electric charge density,

μ is coefficient of magnetic permeability,

ϵ is coefficient of electric permittivity.

Assuming typical lengthscales of L and time T, the ratio of the second term to the first term in equation (1.1) in order of magnitude, is given by

$$EL/Tc^2B, \tag{1.5}$$

and equation (1.2) by

$$E/L \approx B/T. \tag{1.6}$$

Using (1.6), (1.5) reduces to

$$v^2/c^2, \tag{1.7}$$

where v $(= L/T)$ is a typical plasma flow velocity.

Thus, for $v^2 \ll c^2$, the second term in equation (1.1) can be ignored, leaving

$$\mathbf{j} = \frac{1}{\mu}\nabla \times \mathbf{B}. \tag{1.8}$$

Writing Ohm's Law as

$$\mathbf{j} = \sigma\left(\mathbf{E} + \mathbf{v} \times \mathbf{B}\right), \tag{1.9}$$

where σ is the electric conductivity, states that the plasma current density is proportional to the total electric field. Then, using equation (1.8), equations (1.2) and (1.9) are rewritten as

$$\frac{\partial \mathbf{B}}{\partial t} = \nabla \times (\mathbf{v} \times \mathbf{B}) - \nabla \times \left(\frac{1}{\mu\sigma}\nabla \times \mathbf{B}\right), \tag{1.10}$$

Defining the magnetic diffusivity as

$$\eta = \frac{1}{\mu\sigma}, \tag{1.11}$$

and taking η to be constant, then equation (1.10) may be rewritten as

$$\frac{\partial \mathbf{B}}{\partial t} = \nabla \times (\mathbf{v} \times \mathbf{B}) + \eta \nabla^2 \mathbf{B}, \tag{1.12}$$

The presence of the velocity term in the induction equation (1.12) indicates that the evolution of the magnetic field is coupled to the evolution of the plasma treated as a fluid.

1.2 MHD equations

The MHD equations used in this thesis are

$$\rho \frac{D\mathbf{v}}{Dt} = -\nabla p + \mathbf{j} \times \mathbf{B}, \tag{1.13}$$

$$\frac{\partial \mathbf{B}}{\partial t} = \nabla \times (\mathbf{v} \times \mathbf{B}) + \eta \nabla^2 \mathbf{B}, \tag{1.14}$$

$$\frac{D\rho}{Dt} + \rho \nabla \cdot \mathbf{v} = 0, \tag{1.15}$$

$$\frac{\rho^\gamma}{\gamma - 1} \frac{D}{Dt}\left(\frac{p}{\rho^\gamma}\right) = \frac{\mathbf{j}^2}{\sigma}. \tag{1.16}$$

$\frac{D}{Dt} \equiv \frac{\partial}{\partial t} + \mathbf{v} \cdot \nabla$ is the time derivative following the fluid.

Equation (1.13) is the equation of motion and relates the inertial force to that of the plasma pressure gradient and the dominant part of the Lorentz force. The effect of gravity has been neglected in this equation as it severely complicates the analysis when using cylindrical coordinates.

Equation (1.14) is the induction equation. The ratio of the second term, the adjection term, to the third term, the diffusive term is known as the magnetic Reynolds number,

$$R_m = \frac{Lv}{\eta}, \tag{1.17}$$

where L, v and η represent typical lengthscales, velocities and diffusivities in the plasma. In the solar corona, taking $\eta = 10^9 T^{-3/2} m^2 s^{-1}$ (see Priest, 1982), $T = 2 \times 10^6 K$, $v = 10^6 m s^{-1}$, $L = 3 \times 10^6 m$ gives a value for R_m of 10^{13}.

Equation (1.15) is the mass conservation equation, and indicates that mass is not being created or destroyed in the region under consideration.

Equation (1.16) is the energy equation. Thermal conduction and radiative effects have been neglected from this equation. In the adiabatic limit, given by $\eta = 0$, $p \propto \rho^\gamma$, where γ, the ratio of specific heats, is usually taken to be 5/3, except when considering isothermal variations, when it is taken to be unity.

1.3 Basic MHD Plasma Waves

Before investigating complex MHD problems, it is useful in a physical sense to determine the basic waves which propagate in a MHD plasma.

In order to keep the analysis simple, start with a unidirectional magnetic field infinite in extent with uniform background plasma pressure and density.

$$\mathbf{B} = B_0 \mathbf{e}_z, \tag{1.18}$$

$$p = p_0, \tag{1.19}$$

$$\rho = \rho_0, \tag{1.20}$$

To investigate the wave motions of this configuration linearize all quantities

$$X(\mathbf{r},t) = X_0 + X_1(\mathbf{r},t), \tag{1.21}$$

where $X_1(\mathbf{r},t)$ is a small order perturbation to the equilibrium quantities. Write the perturbation

$$X_1(\mathbf{r},t) = X_1 e^{i(\mathbf{k}\cdot\mathbf{r}-\omega t)}, \tag{1.22}$$

with

$$\mathbf{k} = k_\perp \mathbf{e}_y + k_\parallel \mathbf{e}_z, \tag{1.23}$$

where the y-z plane has been chosen to coincide with the wavevector $\mathbf{k}$.

Substituting expression (1.22) into the linearized ideal MHD equations from equations (1.13), (1.14), (1.15) and (1.16) with $\eta = 0$

$$-i\omega\rho_0\mathbf{v} = -i\mathbf{k}p_1 + \mathbf{j}_1 \times \mathbf{B}_0, \tag{1.24}$$

$$-i\omega\mathbf{B}_1 = i\mathbf{k} \times (\mathbf{v} \times \mathbf{B}_0), \tag{1.25}$$

$$-i\omega\rho_1 + i\rho_0\mathbf{k}\cdot\mathbf{v} = 0, \tag{1.26}$$

$$-\rho_0 p_1 + \gamma p_0 \rho_1 = 0, \tag{1.27}$$

with

$$\mathbf{j}_1 = \frac{i}{\mu}\mathbf{k} \times \mathbf{B}_1, \tag{1.28}$$

$$\mathbf{k}\cdot\mathbf{B}_1 = 0, \tag{1.29}$$

Substituting equations (1.25) to (1.29) into the equation of motion (1.24) and defining the Alfvén speed v_A, and the acoustic speed c_s,

$$v_A^2 = \frac{B_0^2}{\mu \rho_0}, \tag{1.30}$$

$$c_s^2 = \frac{\gamma p_0}{\rho_0}, \tag{1.31}$$

gives

$$\left(\omega^2 - k_\parallel^2 v_A^2\right) \mathbf{v} = \left[\left(c_s^2 + v_A^2\right) k_\perp v_y + c_s^2 k_\parallel v_z\right] \mathbf{k} - k_\parallel v_A^2 \left(k_\perp v_y + k_\parallel v_z\right) \mathbf{e}_z, \tag{1.32}$$

The x-component of equation (1.32) gives the Alfvén wave frequency

$$\omega^2 = k_\parallel^2 v_A^2, \tag{1.33}$$

The y and z components of equation (1.32) lead to the dispersion relation

$$\omega^4 - \omega^2 k^2 \left(c_s^2 + v_A^2\right) + k^2 k_\parallel^2 c_s^2 v_A^2 = 0, \tag{1.34}$$

with solution given by the fast and slow magnetoacoustic wave frequencies

$$\omega^2 = \frac{1}{2} k^2 \left(c_s^2 + v_A^2\right) \left[1 \pm \sqrt{1 - 4\alpha^2}\right], \tag{1.35}$$

with

$$\alpha^2 = \frac{k_\parallel^2}{k^2} \frac{c_s^2 v_A^2}{\left(c_s^2 + v_A^2\right)^2}, \tag{1.36}$$

For localized modes with $k_\parallel << k_\perp$, $k_\perp \to \infty$, expanding (1.35)

$$\omega_s^2 = k_\parallel^2 \frac{c_s^2 v_A^2}{c_s^2 + v_A^2} + \cdots, \tag{1.37}$$

$$\omega_f^2 = k_\perp^2 \left(c_s^2 + v_A^2\right) - k_\parallel^2 \frac{c_s^2 v_A^2}{c_s^2 + v_A^2} + \cdots, \tag{1.38}$$

In a non-uniform medium the Alfvén and magnetoacoustic modes couple, making mode identification more complicated.

1.4 Stability

Stability theory is very important in relation to observed phenomena on the Sun. Any model suggested to explain solar phenomena such as coronal loop and arcade structures and prominence models must be tested for stability. If the model is found to be unstable on a timescale that is shorter than the observed lifetime, then it is not relevant and has to be rejected or modified by introducing either extra or different conditions. This may result in a closer correspondence to the observed phenomena.

There are two main methods for testing stability. The normal mode approach is used in this thesis and will be described later. The energy method can be used for ideal MHD and is based on the fact that the sum of the total potential and kinetic energies is constant. A decrease in the potential energy will lead to an increase in the kinetic energy of the system representing an instability. By linearizing the perturbed ideal MHD equations an expression for the change in the potential energy (δW) is obtained. If any perturbation $\boldsymbol{\xi}$ gives a negative value for the change in potential energy, δW, then the system is unstable. A positive value of δW means the system is stable to that particular perturbation (but possibly could still be unstable to other perturbations). The method was first used by Bernstein et al., 1958. Take the force operator

$$\rho_0 \frac{\partial^2 \boldsymbol{\xi}_0}{\partial t^2} = \mathbf{F}(\boldsymbol{\xi}) = -\nabla p_1 + \mathbf{j}_1 \times \mathbf{B}_0 + \mathbf{j}_0 \times \mathbf{B}_1, \tag{1.39}$$

the change in potential energy is the work done by the force to displace the plasma

$$\delta W = -\frac{1}{2}\int \boldsymbol{\xi}\cdot\mathbf{F}(\boldsymbol{\xi})\,dV, \tag{1.40}$$

where the integration is over the volume of the plasma.

The advantage of the energy method is when seeking stability but not growth rates or oscillation frequencies, it is necessary to look for a perturbation which decreases the potential energy. More complicated equilibria can be investigated this way. Its drawback is it cannot be used when non-ideal effects are included such as resistivity or viscosity and the normal mode approach has to be used.

An equilibrium is assumed or derived from the magnetostatic equation ($\frac{\partial}{\partial t} \equiv 0$)

$$\frac{1}{\mu}(\nabla\times\mathbf{B})\times\mathbf{B} = \nabla p. \tag{1.41}$$

Many such equilibrium fields have been derived, and some of these fields have been named after the authors who first used them, such as the Gold-Hoyle field (Gold and Hoyle, 1960) and Anzer field (Anzer, 1968). The next step is to perturb the equilibrium field by introducing small variations as follows

$$\begin{aligned}
\mathbf{B} &= \mathbf{B}_0 + \mathbf{B}_1 \\
p &= p_0 + p_1 \\
\rho &= \rho_0 + \rho_1 \\
\mathbf{v} &= \mathbf{0} + \mathbf{v}
\end{aligned} \tag{1.42}$$

where $\mathbf{B}_0$, p_0, ρ_0 are equilibrium quantities, and $\mathbf{B}_1$, p_1, ρ_1, $\mathbf{v}$ are perturbed variables such that the ratios of equilibrium to perturbed quantities are large. The equations are linearized and time-dependence is assumed by looking for normal modes of the form $f(\mathbf{r},t) = f(\mathbf{r})\, e^{\sigma t}$. σ is termed the growth rate and if the real part of σ is positive then the equilibrium is linearly unstable since the perturbed variables will grow in time. Likewise, for σ negative or purely imaginary, the equilibrium is stable. In many problems several or sometimes an infinite set of normal modes exist, and if one or more of these modes give a positive value for σ, then the equilibrium is declared unstable. The normal mode method will be used throughout this thesis.

1.5 Stability modes

To illustrate the various instability modes, consider a cylindrically symmetric magnetic flux tube with an azimuthal magnetic field

$$\mathbf{B} = B_\theta(r)\, \mathbf{e}_\theta, \tag{1.43}$$

and pressure p from the equilibrium equation

$$\frac{dp}{dr} + \frac{B_\theta}{\mu r}\frac{d}{dr}(rB_\theta) = 0. \tag{1.44}$$

Then Fourier analyse the linearized equations of motion in the poloidal and axial directions

$$\boldsymbol{\xi} = \boldsymbol{\xi}(r)\, e^{i(m\theta + kz)}. \tag{1.45}$$

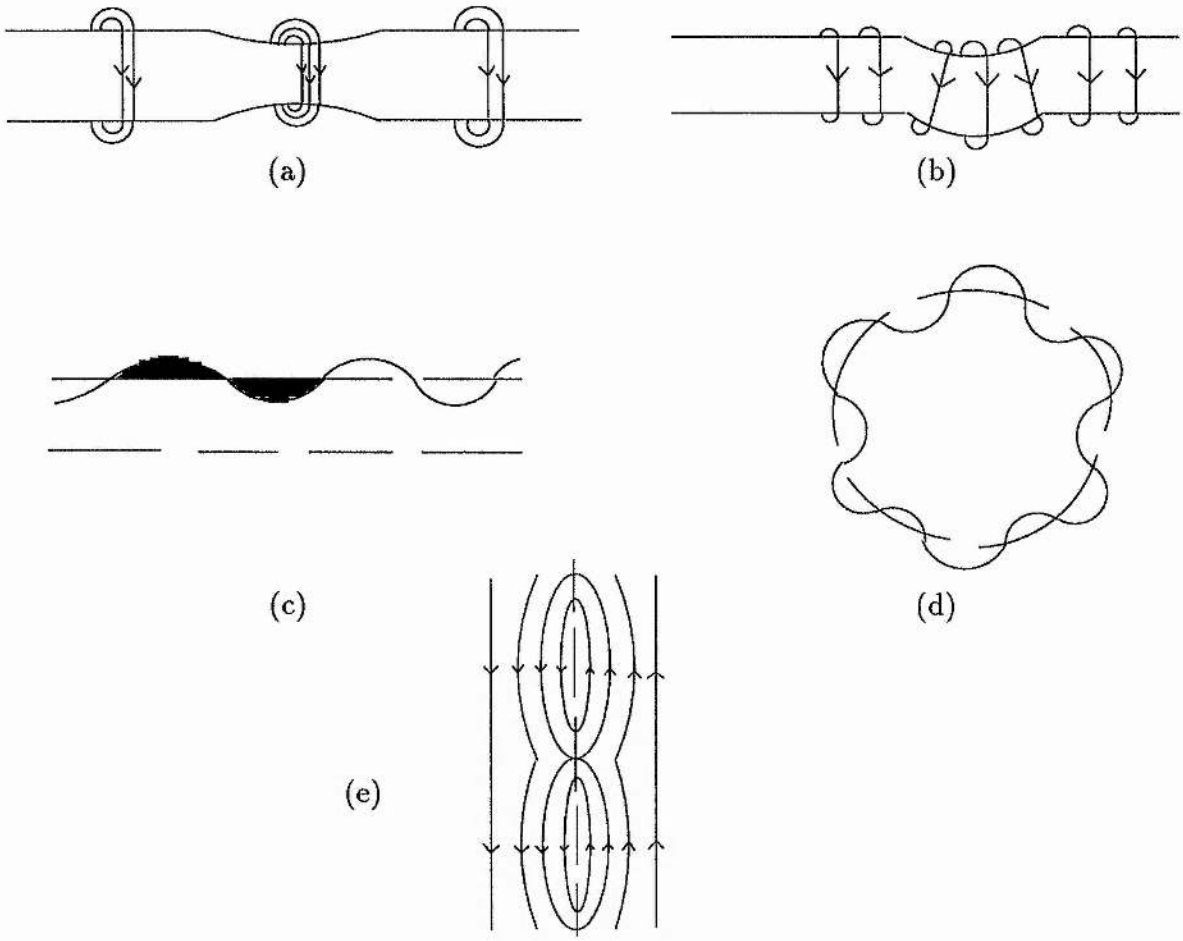

Figure **1.1**: Diagrams of (a) Sausage mode (b) Kink mode (c) Interchange mode (d) Flute mode, and (e) Resistive tearing mode.

Sausage modes are obtained by setting $m = 0$. Physically a sausage mode instability is caused by a perturbed constriction of the flux tube leading to an increased azimuthal magnetic field and increased magnetic tension force causing the flux tube to further constrict (see figure 1.1). This mode can be stabilized by

the introduction of an axial component to the magnetic field as this gives rise to stabilizing magnetic tension forces at the constricted part of the flux tube.

Kink modes are obtained by setting $m = 1$. Physically a displacement of the flux tube perpendicular to the axis causes the magnetic field on the inside of the displaced tube to be concentrated and rarefied on the outer part of the displaced tube leading to the kink growing in size. The introduction of an axial component of the magnetic field gives a stabilizing component of magnetic tension.

Interchange or flute modes occur when two flux surfaces at different radii interchange. Interchange modes are driven by pressure gradients.

Ballooning modes are given by perturbations with long wavelengths along the magnetic field and short wavelengths across the magnetic field. The oscillations give rise to oppositely directed magnetic tension forces which combine with pressure gradients to give regions of favourable and unfavourable curvature resulting in localized instabilities. Ballooning modes were used by Hood (1986) to investigate the effect of line-tying on flux tube stability. Line-tying converts a one dimensional problem into two dimensions. Making use of the ratio of the wavelength of the perturbations along the magnetic field to the wavelength of the perturbation across the equilibrium magnetic field, the equations are converted from two dimensional partial differential equations to one dimensional ordinary differential equations along the magnetic fieldlines which are easier to solve.

Resistive tearing instabilities occurs at the boundary between two sheared mag-

netic fields. The fieldlines reconnect to form magnetic islands by tearing along the interface separating the two opposite magnetic fields. If this change in topology leads to a lower potential energy state a tearing instability occurs.

1.6 Coronal loops and arcades

Observations indicate that much of the plasma in the corona of the Sun is in the form of loops. The loops are believed to trace out lines of force of the magnetic field emerging from beneath the photosphere. A study of loops can give a physical insight into the structure of the solar magnetic field. Coronal loops have been divided into two categories, 'cool' loops with temperatures ranging from $20000 - 1 \times 10^6$ K and 'hot' loops with temperatures greater than 1×10^6 K. Active region cool loop systems can last for up to 5-6 hours. Widths vary from 300-2000 km and heights from 40000-50000 km. Active region hot loop systems last up to several days with widths from 3000-12000 km and heights from 50 000-250 000 km (see Bray et. al., 1991). The Alfvén travel time of a loop is several minutes. Given the long observed lifetimes, coronal loops must be stable. Stability is applicable in explaining the long lifetimes of many phenomena such as prominences and flares. Prominences are coronal structures which have a typical temperature 100 times less and density 100 times greater than surrounding coronal values. They are stable for up to 300 days (see Priest, 1988).

Flares are observed to be sudden brightenings on the surface of the Sun. The

energy released by a flare (up to 10^{25} W, see Svestka, 1976) must come from the magnetic field since no other source of such large quantities of energy is available to drive the flare. Flares occur in the corona of the Sun and from observations, the magnetic field is thought to be in the form of either coronal loops or coronal arcades.

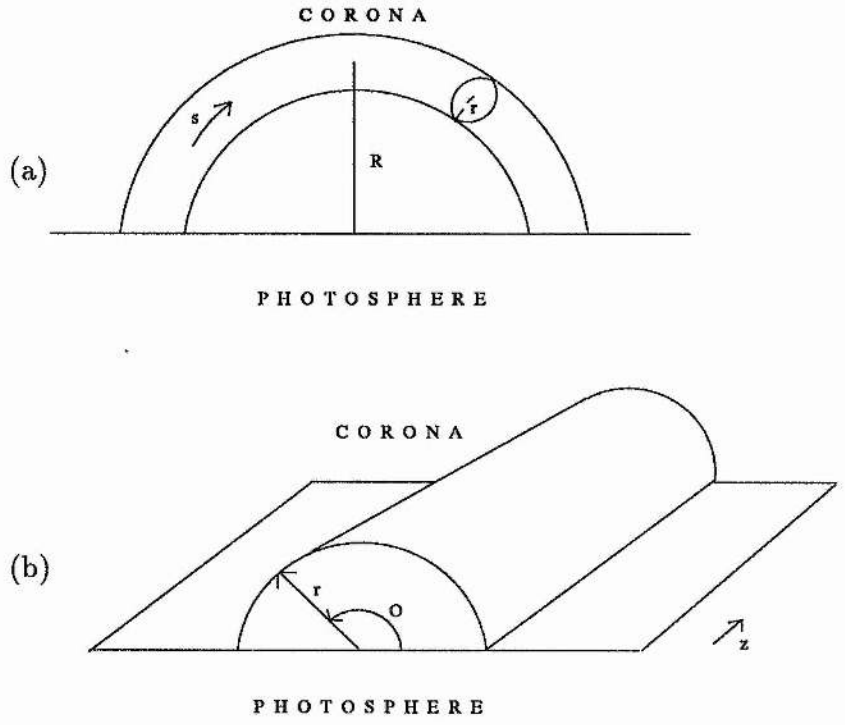

Figure **1.2**: Diagrams of (a) Coronal loop (b) Coronal arcade.

The generally accepted scenario is that convective motions in the photosphere cause the footpoints of the coronal magnetic field to move. Since the photospheric density is 10^8 times that of the corona and since the magnetic field is essentially frozen into plasma, these motions cause stress (and hence energy) to build up over

several days in the form of electric currents in the non-potential field structure. At some point a loss of equilibrium or an instability occurs and there is a large release of energy over 20-30 minutes. This is known as a flare.

Flares have been divided into two main classes (see Priest, 1982):-

(1) Small loop flares (or compact flares) with an energy release of 10^{21} -10^{22} W. Most flares are of this type. An individual loop appears to brighten without a substantial change of shape.

(2) Large two-ribbon flares with an energy release of up to 3×10^{25} W which generally occur in arcade structures. In this case there is a substantial restructuring and simplification of the field.

It is therefore important to investigate stability in relation to both loop and arcade structures.

1.7 A Brief Review of Stability Theory

Solar flares involve a rapid release of magnetic energy that is thought to be stored in the preflare coronal magnetic field. Thus it is important to demonstrate that the coronal field is stable to MHD disturbances in order to store the necessary energy in situ but that an instability can be triggered if some critical threshold is exceeded. Anzer (1968) was the first to investigate the ideal MHD stability of coronal fields. He suggested that convective motions in the penumbrae of sunspots twists the field and so stores magnetic energy in the magnetic fields until it is released by instabilities.

However, he found that all force-free cylindrically symmetric fields were unstable to $m = 1$ kink modes. This suggested that the flare energy could not be stored in the corona.

Raadu (1972) realized that the magnetic field is strongly stabilized by the extremely dense photosphere. To simulate the photosphere he proposed that the magnetic footpoints are anchored by *line-tying* due to the high inertia of the photospheric plasma. Thus, he argued that coronal disturbances must vanish at the photosphere, so that

$$\xi_\perp = 0, \tag{1.46}$$

there. Since he only considered force-free fields and used the energy method, it is only the perpendicular displacement, (perpendicular to the equilibrium magnetic field), that enters the analysis. The inclusion of a finite gas pressure introduces the parallel component of the displacement and the boundary conditions regarding this component have been the subject of some debate.

Hood and Priest (1979) included a radial pressure gradient but restricted their choice of displacements so that

$$\xi_\parallel \equiv 0. \tag{1.47}$$

Nonetheless, they showed that kink instabilities were present when the loop was sufficiently twisted. In addition, they proved that force-free loops were stable if the twist, $\Phi = LB_\theta/rB_z$, was less than 2π.

Einaudi and Van Hoven (1981, 1983) included a parallel component of the veloc-

ity (or equivalently the displacement) and suggested that this need not vanish but should merely satisfy conditions that preserved the total energy of the corona. For a loop they selected the flow-through conditions

$$\xi_\perp = 0, \text{ at z=0,L}$$

$$\xi_{||}(0) = \xi_{||}(L), \frac{\partial \xi_z}{\partial z}(0) = \frac{\partial \xi_z}{\partial z}(L) \tag{1.48}$$

These conditions simplify the manipulation of the energy integral and allow for incompressible displacements while still conserving the total energy. However, Rosner *et al* (1986) and Cargill *et al* (1986) have argued, on basis of timescales and physical arguments, that equation (1.48) is unlikely to be realized in practice since it assumes that the photosphere can respond quickly to coronal perturbations and that it requires one end of the loop to 'know' what is happening at the other end simultaneously. Nonetheless, because the flow-through conditions allow the elimination of a positive term in the energy integral, stability obtained using equation (1.48) guarantees stability for the 'rigid-wall' conditions.

Hood (1986) investigated line-tying conditions by modelling the corona and photosphere as two different uniform density plasmas and using localized ballooning modes to let the plasma select its own conditions. Investigating the most unstable flux surface he found that the rigid-wall conditions were the most appropriate conditions when the photospheric to coronal density ratio is large. This confirms the intuitive approach described above that the photosphere cannot move fast enough

in response to coronal motion. However, his analysis breaks down when the growth rate approaches marginal stability and $|\rho_p \sigma^2|$ is no longer large.

When instabilities evolve on a slower timescale, the situation may change. For example, Hood, Van der Linden and Goossens (1989) investigated thermal (or radiative) instabilities and they found that substantial flow across the photospheric boundary was possible when the growth rate was sufficiently small. Cargill and Hood (1989) in their investigation of thermal instabilities in a sheared magnetic field have argued that a variety of thermal and magnetic boundary conditions should be used until the realistic conditions are proved.

One important effect that must be included in solar flare and coronal heating models is the influence of resistivity, since this is essential for the magnetic topology to change and release of magnetic energy during a flare as it relaxes to a lower energy state. Resistive ballooning modes with rigid wall line-tying have been investigated by Velli and Hood (1986, 1987). They obtain a resistive mode, with a growth depending on a fractional power of resistivity, $(\eta)^{\frac{1}{3}}$, when the equilibrium is close to ideal marginal stability. Velli and Hood (1989) included line-tying in a simple current sheet. They considered slab geometry and a magnetic field with an inversion in the line-of-sight component so that a singular surface exists. Line-tying helps to stabilize the tearing mode by effectively discretizing the wavenumber in the line-tied direction, although 'modes' must be coupled together in order to satisfy the imposed boundary conditions. This then stabilizes the tearing mode beyond a simple

discretization.

Hassam (1989) has cast doubt on the applicability of line-tying in stabilizing the tearing mode. He argues that the tearing mode evolves so slowly that there is plenty of time for the photospheric flows to develop. However, the instability he considers appears to be driven down in the photosphere whereas it is important to see the effect of disturbances initiated in the corona.

The problem then is to understand the correct form of the boundary conditions at the coronal/photospheric interface. To answer this, we investigate in chapter 2 the behaviour of both the ideal and resistive ballooning modes as the photospheric to coronal density ratio and the resistivity are varied, although this is only valid for localized modes. Chapters 3, 4 and 5 investigate stability bounds for global modes for coronal loops and arcades. In chapter 3, the general method of solution is described while in chapter 4 it is applied to several equilibria in an in-depth study. The effect of pressure and pressure gradients on the various modes from the $m = 1$ kink mode up to localized modes is investigated. Chapter 5 describes the general method of solution for arcades.

2 Resistive Ballooning Line-Tied Boundary Conditions

2.1 Introduction

In this chapter the form of the boundary conditions at the coronal/photospheric interface is investigated. The growth rates and eigenfunctions of both ideal and resistive modes are investigated as the photospheric to coronal density ratio and resistivity are varied.

Firstly a simple model of a transverse wave on a two density string is considered in order to gain an idea of a sharp boundary between corona and photosphere in section 2.2. Then a model equilibrium and the stability equations that are used in section 2.3 are developed. Section 2.4 describes the construction of a normal mode from the ballooning approach and how plots of growth rate against radius should be interpreted. In the next section, the general dispersion relation is given and several limits are investigated analytically that provide bounds for the subsequent more general situations. Finally, section 2.6 presents the solutions of the dispersion relation for general density ratio and resistivity values.

The stabilizing influence of the magnetic field is minimized by considering perturbations with short wavelength across the magnetic field but long wavelengths

parallel to the magnetic field (see Connor et al., 1979) since this reduces the energy required to overcome magnetic tension.

Taking a WKB approximation for the spatial variations across the field converts the MHD equations from a set of partial differential equations to a set of ordinary differential equations with derivatives along the magnetic field.

In order to simplify the analysis, we consider an azimuthal magnetic field so that the derivatives are with respect to the azimuthal component.

2.2 Simple model of boundary

In this section, a simple model of line-tying of a transverse wave on an elastic string of two different densities is considered.

Represent the displacement of the string on either side of the change in density by y_1 and y_2 where

$$y_1 = y_{\text{incident}} + y_{\text{reflected}}, \tag{2.1}$$

$$y_2 = y_{\text{transmitted}}, \tag{2.2}$$

where

$$y_{\text{incident}} = A_i e^{2\pi i(nt - k_1 x)}, \tag{2.3}$$

$$y_{\text{reflected}} = A_r e^{2\pi i(nt + k_1 x)}, \tag{2.4}$$

$$y_{\text{transmitted}} = A_t e^{2\pi i(nt - k_2 x)}, \tag{2.5}$$

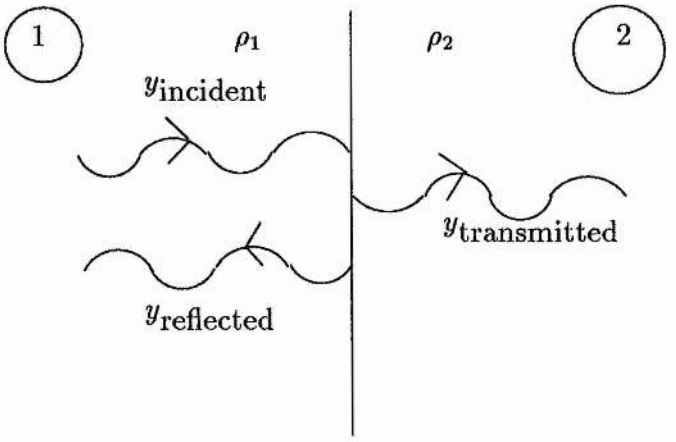

Figure **2.1**: Diagram showing an incident wave transmitting and reflecting across a boundary.

Since the string is continuous, $y_1 = y_2$ for all t. Also the slopes $\partial y_1/\partial x = \partial y_2/\partial x$ for all t. The two boundary conditions imply

$$A_i + A_r = A_t, \tag{2.6}$$

$$k_1 \left(-A_i + A_r\right) = -k_2 A_t, \tag{2.7}$$

which have solution

$$A_r = \frac{k_1 - k_2}{k_1 + k_2} A_i, \tag{2.8}$$

$$A_t = \frac{2k_1}{k_1 + k_2} A_i, \tag{2.9}$$

Representing region 1 by the corona and region 2 by the photosphere and taking a constant magnetic field and a density ratio of 10^8, then an Alfvén wave has velocity (see Hood, 1992)

$$V_{A_1} = \frac{B}{\sqrt{\mu\rho_1}} = \frac{n}{k_1}, \tag{2.10}$$

$$V_{A_2} = \frac{B}{\sqrt{\mu\rho_2}} = \frac{n}{k_2}, \tag{2.11}$$

giving

$$A_r = \frac{-1+\sqrt{\frac{\rho_c}{\rho_p}}}{1+\sqrt{\frac{\rho_c}{\rho_p}}} A_i = -0.9998 A_i, \tag{2.12}$$

$$A_t = \frac{2\sqrt{\frac{\rho_c}{\rho_p}}}{1+\sqrt{\frac{\rho_c}{\rho_p}}} A_i = 1.9998 \times 10^{-4} A_i, \tag{2.13}$$

Thus a disturbance initiated in the corona is essentially totally reflected at the boundary with the photosphere. From expressions (2.3) and (2.4), the perpendicular velocity components of the wave will vanish at the interface.

2.3 Equations

The magnetohydrodynamic equations considered are

$$\rho\frac{D\mathbf{v}}{Dt} = -\nabla p + \mathbf{j}\times\mathbf{B}, \tag{2.14}$$

$$\frac{\partial\rho}{\partial t} + \nabla\cdot(\rho\mathbf{v}) = 0, \tag{2.15}$$

$$\frac{\partial\mathbf{B}}{\partial t} = \nabla\times(\mathbf{v}\times\mathbf{B}) + \eta\nabla^2\mathbf{B}, \tag{2.16}$$

$$\nabla\cdot\mathbf{B} = 0, \tag{2.17}$$

$$\frac{Dp}{Dt} = \frac{\gamma p D\rho}{\rho Dt} - (\gamma-1)\,\mu\eta j^2. \tag{2.18}$$

where the momentum equation (2.14) consists of forces due to a pressure gradient and a Lorentz force, the induction equation (2.16) involves a uniform resistivity, and (2.18) is the energy equation with ohmic heating included.

We will consider an arcade consisting of a cylindrically symmetric azimuthal magnetic field, B_θ, and gas pressure, p, that are functions of r, but with a density, ρ, that is a function of r and θ. The photosphere and corona are taken as two distinct regions of densities ρ_p and ρ_c, separated by a sharp transition region at $\theta = \pm\pi/2$. The idea is to see how the amplitude of the eigenfunction at $\theta = \pm\pi/2$ and the growth rate respond to changes in the density ratio ρ_p/ρ_c for various values of the dimensionless resistivity parameter η. The plasma beta, in such a model, is larger than typical solar coronal values but the emphasis here is to see how both stable and unstable modes are modified by the density ratio. To produce a ballooning instability requires a β of order unity, since the instability is driven by an adverse pressure gradient.

The equilibrium equation is given by

$$\frac{d}{dr}\left[\mu p + \frac{{B_\theta}^2}{2}\right] = -\frac{{B_\theta}^2}{r}. \tag{2.19}$$

Linearizing about this basic state and taking all perturbed quantities of the form $f(r,\theta,z)e^{\sigma t}$, equations (2.14) to (2.18) reduce to

$$\rho_0\sigma\mathbf{v}_1 = -\nabla p_1 + \frac{1}{\mu}(\nabla\times\mathbf{B}_1)\times\mathbf{B}_0 + \frac{1}{\mu}(\nabla\times\mathbf{B}_0)\times\mathbf{B}_1, \tag{2.20a}$$

$$\sigma\rho_1 + \nabla\cdot(\rho_0\mathbf{v}_1) = 0, \tag{2.20b}$$

$$\sigma \mathbf{B}_1 = \nabla \times (\mathbf{v}_1 \times \mathbf{B}_0) + \eta \nabla^2 \mathbf{B}_1, \tag{2.20c}$$

$$\nabla \cdot \mathbf{B}_1 = 0, \tag{2.20d}$$

$$\sigma p_1 + \mathbf{v}_1 \cdot \nabla p_0 = -\gamma p_0 \nabla \cdot \mathbf{v}_1 + 2(\gamma - 1)\, \eta \mathbf{j}_0 \cdot (\nabla \times \mathbf{B}_1). \tag{2.20e}$$

To simplify these equations further, we make the ballooning approximation and take a WKB approximation for the spatial variations across the field, namely $f(\theta)\, e^{in(S(r)+z)}$ where $n \gg 1$ is the ratio of equilibrium to perturbation length scales. The ohmic heating term in equation (2.20e), of order ηn 'drops out' by comparison with the resistive term in equation (2.20c), of order ηn^2 which is of order unity (see Appendix A). From the leading order equation we find that $(\mu p_1 + B_\theta B_{1\theta}) = O(1/n)$ (see Hood *et.al.* 1989). Equations (2.20a) to (2.20e) reduce to

$$\frac{1}{r}\frac{dv_{1\theta}}{d\theta} + \left[\left(\frac{\gamma\mu p + {B_\theta}^2}{\gamma\mu p {B_\theta}^2}\right)\mu p' + \frac{2}{r}\right] v_{1r} + \left[\frac{\left(\gamma\mu p + {B_\theta}^2\right)\sigma}{\gamma\mu p {B_\theta}^2} + \frac{\eta n^2 k^2}{{B_\theta}^2}\right]\mu p_1 = 0, \tag{2.21a}$$

$$\frac{1}{r}\frac{dp_1}{d\theta} + \rho\sigma v_{1\theta} + \frac{p'}{B_\theta} B_{1r} = 0. \tag{2.21b}$$

$$k^2 \frac{B_\theta}{r}\frac{dB_{1r}}{d\theta} + \frac{2\mu}{r} p_1 - \mu\rho\sigma k^2 v_{1r} = 0, \tag{2.21c}$$

$$\frac{B_\theta}{r}\frac{dv_{1r}}{d\theta} - \left(\sigma + \eta n^2 k^2\right) B_{1r} = 0. \tag{2.21d}$$

where $k^2 = 1 + (S')^2$ is the square of the wavevector. Eliminating p_1 from equation (2.21c) using (2.21a) and differentiating (2.21d) with respect to θ to eliminate $dB_{1r}/d\theta$ gives

$$\left[\left(\gamma\mu p + {B_\theta}^2\right)\sigma + \eta n^2 k^2 \gamma\mu p\right] \frac{{B_\theta}^2 k^2}{2\mu}\frac{d^2 v_{1r}}{d\theta^2} - \left(\sigma + \eta n^2 k^2\right) {B_\theta}^2 \gamma p \frac{dv_{1\theta}}{d\theta}$$

$$-\left(\sigma+\eta n^2k^2\right)\left[\left(\gamma\mu p+{B_\theta}^2\right)\frac{\rho\sigma^2r^2k^2}{2}+r{B_\theta}^2p'\right.$$

$$\left.+2{B_\theta}^2\gamma p+r\gamma\mu pp'+\frac{\eta n^2k^2\gamma\mu p\rho\sigma r^2k^2}{2}\right]v_{1r}=0, \qquad (2.21e)$$

Similarly, eliminating p_1 from equation (2.21b) using the derivative of (2.21a) with respect to θ, and (2.21d) to eliminate B_{1r} gives

$$\left(\sigma+\eta n^2k^2\right)\frac{{B_\theta}^2\gamma p}{r}\frac{d^2v_{1\theta}}{d\theta^2}-\left(\sigma+\eta n^2k^2\right)\left[\left(\gamma\mu p+{B_\theta}^2\right)\sigma+\eta n^2k^2\gamma\mu p\right]r\rho\sigma v_{1\theta}$$

$$+\left[\frac{2{B_\theta}^2\gamma p\left(\sigma+\eta n^2k^2\right)}{r}+\eta n^2k^2p'{B_\theta}^2\right]\frac{dv_{1r}}{d\theta}=0, \qquad (2.21f)$$

Thus, the stability equations reduce to two coupled second order O.D.E.'s.

To illustrate the ideas, we will use the example equilibrium

$$\mathbf{B}=B_0\left[0,\frac{r}{1+r^2},0\right]$$

$$p=\frac{1}{2}\frac{{B_0}^2}{\mu}\frac{1}{\left(1+r^2\right)^2}$$

with

$$\rho=\frac{{B_0}^2}{\mu}\frac{\rho^*}{\left(1+r^2\right)^2}$$

since the results for ideal MHD are already known (Hood, 1986). The asterisk will be omitted, and isothermal disturbances, with γ as unity, are taken for simplicity. Equations (2.21e) and (2.21f) reduce to

$$\left[\left(1+2r^2\right)\sigma+\eta n^2k^2\right]k^2\frac{d^2v_{1r}}{d\theta^2}-2\left(\sigma+\eta n^2k^2\right)\frac{dv_{1\theta}}{d\theta}$$

$$-\left(\sigma+\eta n^2k^2\right)\left[\frac{-4r^2}{1+r^2}+\left(1+2r^2\right)\rho\sigma^2k^2+\eta n^2k^2\rho\sigma\right]v_{1r}=0, \qquad (2.22a)$$

$$\left(1+r^2\right)\left(\sigma+\eta n^2k^2\right)\frac{d^2v_{1\theta}}{d\theta^2}+2\left[\left(1+r^2\right)\sigma+\eta n^2k^2\left(1-r^2\right)\right]\frac{dv_{1r}}{d\theta}$$

$$-\left(1+r^2\right)\left[\left(1+2r^2\right)\sigma+\eta n^2k^2\right]\left(\sigma+\eta n^2k^2\right)\rho\sigma v_{1\theta}=0. \qquad (2.22b)$$

In the ideal limit, $\eta n^2k^2=0$, with $k^2=1$, equations (2.22a) and (2.22b) reduce to those of Hood (1986).

Since in each region, all coefficients are independent of θ, we take $v_{1r}, v_{1\theta}$ of the form $e^{im\theta}$, so that a fourth order equation in m is obtained

$$m^4+\frac{1}{k^2}\left[\frac{-4}{1+r^2}+2\left(1+r^2\right)\rho\sigma^2k^2+2\eta n^2k^2\rho\sigma\right]m^2$$
$$+\frac{\rho\sigma}{k^2}\left(\sigma+\eta n^2k^2\right)\left[\frac{-4r^2}{1+r^2}+\left(1+2r^2\right)\rho\sigma^2k^2+\eta n^2k^2\rho\sigma\right]=0, \qquad (2.23a)$$

or in terms of k^2 as

$$\eta n^2\rho^2\sigma^2\left[\left(1+2r^2\right)\sigma+\eta n^2\right]k^4$$
$$+\left[m^4+2\left(1+r^2\right)m^2\rho\sigma^2+\left(1+2r^2\right)\rho^2\sigma^4\right]k^2$$
$$+\eta n^2\rho\sigma\left[2m^2+\rho\sigma^2-\frac{4r^2}{1+r^2}\right]k^2$$
$$-\frac{4}{1+r^2}\left[m^2+r^2\rho\sigma^2\right]=0, \qquad (2.23b)$$

Thus, there are four roots for m in each region, $\pm m_1$, $\pm m_2$ in the corona and $\pm m_3$, $\pm m_4$ in the photosphere.

2.4 Construction of the WKB solution

To illustrate how we use the WKB approach, consider a uniform density in the ideal MHD limit. Without the coronal/photospheric interface, the equilibrium reduces to a Z pinch and m must take integer values. The standard approach is to

set $S'(r) \equiv 0$ and obtain σ^2 as a function of radius. This is shown in figure 2.2 for $m = 0$ and $m = 1$. The problem is how to interpret this figure in terms of actual normal modes. To do this we consider first the $m = 0$ mode. Equation (2.23b) then defines the radial wavenumber $(S')^2$ as a function of r and σ^2 as

$$(S')^2 = \frac{4r^2}{(1+r^2)(1+2r^2)\sigma^2} - 1. \tag{2.24}$$

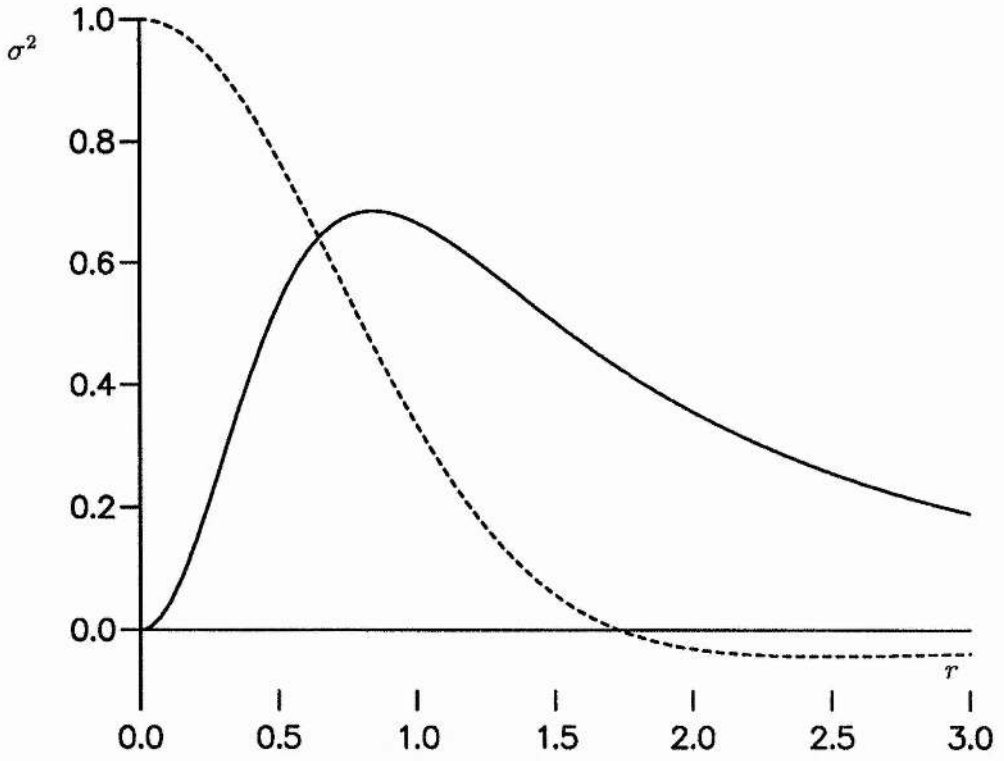

Figure **2.2**: Square of the growth rate, σ^2, as a function of the radial coordinate, r, in the uniform density ideal approximation, with poloidal wavenumbers, $m = 0$ (solid curve) and $m = 1$ (dashed curve).

This is shown in figure 2.3 for two different values of σ. The solutions are

evanescent where $(S')^2$ is negative and oscillatory where $(S')^2$ is positive.

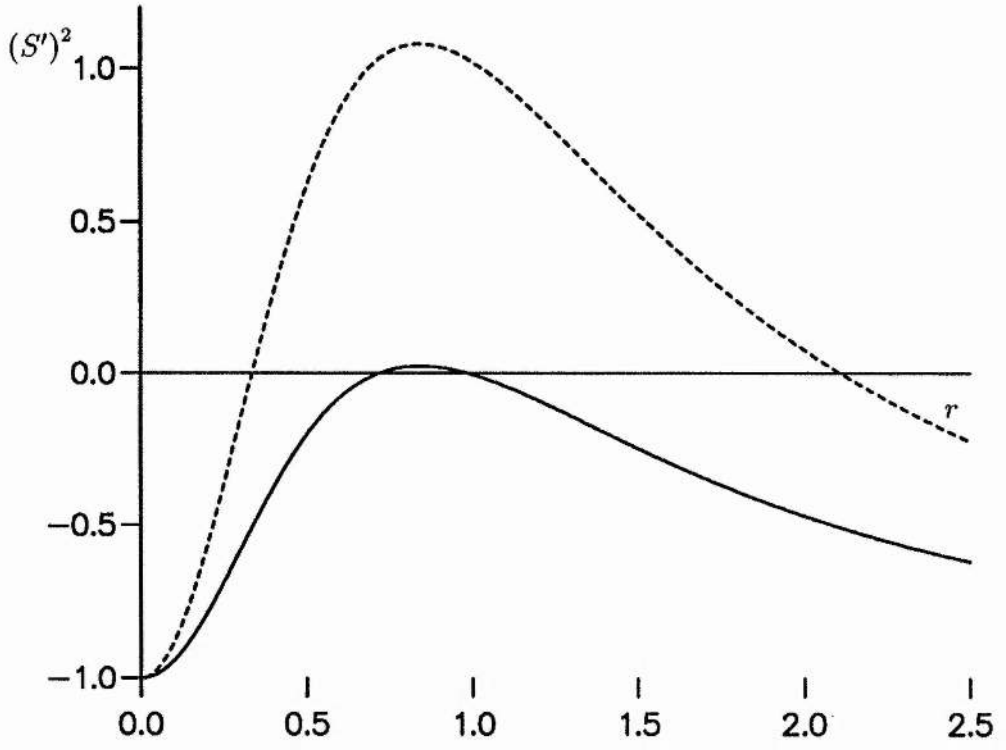

Figure **2.3**: The radial wavenumber $(S')^2$ as a function of radius, r, with the square of the growth rate given by $\sigma^2 = 0.67$ (solid curve) and $\sigma^2 = 0.33$ (dashed curve).

In the neighbourhood of $(S')^2 = 0$ there is a turning point and the solutions on either side of this point can be connected using Airy functions. Having obtained $(S')^2$, the growth rate is determined by requiring that the oscillatory part of the solution has the "correct" number of oscillations to match onto the evanescent solutions. This generates a Bohr-Sommerfeld condition of the form

$$\int_a^b S'(r)\, dr = \frac{(M+\alpha)\,\pi}{n}, \tag{2.25}$$

where M is the number of radial nodes, α is a number of order unity and a, b are the zeros of $S'(r)$. σ^2 is then adjusted until equation (2.25) is satisfied. An alternative way of using equation (2.25) is to specify σ^2, evaluate the integral on the left hand side of (2.25) and then determine the value of n. As long as $n \gg 1$ we have a valid solution. The actual value of α is determined by treating the turning points and boundary conditions in detail but if a is not too close to zero α is approximately 1/2.

The link between the WKB approach and the standard normal mode approach can be seen by studying the Hain-Lüst equation (Goedbloed, 1983). For the uniform, in the θ direction, density case, the linearized ideal MHD equations can be reduced to one 2^{nd} order differential equation for the radial velocity, the Hain-Lüst equation, for variations of the form $f(r)\exp(im\theta + inz + \sigma t)$, that in the limit of large n reduces to $(m = 0)$

$$\frac{\sigma^2}{n^2}\frac{d}{dr}\left\{\frac{1}{r\left(1+r^2\right)^2}\left(1-\frac{2\sigma^2}{n^2\left(1+2r^2\right)}\right)\frac{dX}{dr}\right\}$$
$$+\left\{-\frac{\sigma^2}{r\left(1+r^2\right)^2}+\frac{4r}{\left(1+r^2\right)^3\left(1+2r^2\right)}+O\left(\frac{1}{n^2}\right)\right\}X=0, \qquad (2.26a)$$

where $X = rv_r$.

Hence, to leading order the Hain-Lüst equation becomes

$$\frac{d^2X}{dr^2}-\frac{\left(1+5r^2\right)}{r\left(1+r^2\right)}\frac{dX}{dr}+n^2\left(-1+\frac{4r^2}{\sigma^2\left(1+r^2\right)\left(1+2r^2\right)}\right)X=0. \qquad (2.26b)$$

Applying the WKB technique to equation (2.26b) for the radial variation means that the first derivative term is neglected and equation (2.24) is recovered. Thus,

by replacing $(S')^2$ by $-1/n^2\ d^2/dr^2$ from equation (2.24) we can in fact recover the leading order differential equation, except for the first derivative term. The first derivative however, is only of importance near $r = 0$ when n is large (ie for $nr < 1$). Notice that correction terms in equation (2.26a) remain asymptotically small even in the neighbourhood of the zeros of $S'(r)$. If $S'(a) = 0$, setting

$$x = (r - a)\, n^{2/3}, \tag{2.27a}$$

in equation (2.26a) generates Airy's equation in the form

$$\frac{d^2X}{dx^2} + CxX = O\left(n^{-2/3}\right), \tag{2.27b}$$

where $C = 2\left(1 - 2a^4\right)/a\left(1 + a^2\right)\left(1 + 2a^2\right)$. Neglecting the corrections of $O\left(n^{-2/3}\right)$, this is equivalent to the Airy's equation generated direct from equation (2.24). Therefore the equation derived from (2.24) agrees with the leading order behaviour of the Hain-Lüst equation, (2.26a).

The behaviour of the $m = 1$ mode is slightly different. From figure 2.2 it is seen that σ is a monotonically decreasing function of radius. This means that $S'(r) = 0$ at only one radius, r=c, say. Hence we have a one turning point problem. For $r < c$ the eigenfunction is oscillatory and for $r > c$ evanescent. Matching the two solutions, through Airy's equation, the WKB expression for the eigenvalue becomes

$$n \int_0^c S'(r) dr = (M + 3/4)\pi, \tag{2.28a}$$

where

$$(S')^2 = -1 + \frac{4\left(1 + \sigma^2 r^2\right)}{\left(1 + r^2\right)\left(1 + 2\left(1 + r^2\right)\sigma^2 + \left(1 + 2r^2\right)\sigma^4\right)}. \tag{2.28b}$$

In deriving (2.28a) it has been assumed that the eigenfunction is zero at $r = 0$. Notice that, again, the differential equation derived from (2.28b) agrees with the leading behaviour of the Hain-Lüst equation, for large n, except near $r = 0$ ($nr < 1$). Table 2.1 illustrates the above relationships for the growth rate.

	n	M	Hain-Lüst	Ballooning	Integral
	10	0	0.7731	0.7837	0.7832
	10	4	0.5565	0.5614	0.5612
m=0	30	0	0.8114	0.8126	0.8126
	30	4	0.7078	0.7087	0.7087
	10	0	0.9152	0.8584	0.8571
m=1	10	4	0.3139	0.2760	0.2756
	30	0	0.9687	0.9509	0.9507
	30	4	0.7300	0.7164	0.7163

Table **2.1**: Values of the growth rate obtained numerically using Hain-Lüst, Ballooning and integral equations for the ideal uniform density $m = 0$ and $m = 1$ modes. M is the number of internal radial nodes.

The number of internal nodes is taken as either 0 or 4 and results for the sausage (rows 1–4) and kink (rows 5–8) modes are presented for $n = 10$ and 30. The column labelled Hain-Lüst represents the growth rates calculated from the numerical solution to the Hain-Lüst equation. The "ballooning" column gives σ as calculated

from the differential equations generated from equations (2.24) and (2.28b). The "integral" column gives σ when using equations (2.25) and (2.28a).

Now we are in a position to interpret figure 2.2. Basically, the curve shows all the possible values for the growth rate. The radius (for a given value of σ) gives the location at which the eigenfunction changes its character from exponential to oscillatory (or vice versa). However, for every value of σ given by figure 2.2 there is a possible normal mode that depends on the value of n (as long as n is large) and the number of nodes.

The inclusion of resistivity does not radically alter the above approach. Neglecting the root corresponding to pure diffusion in the derivation of (2.23a), it is clearly seen that the ballooning approach generates a 4^{th} order differential equation

$$\frac{d^4v}{d\theta^4} - \frac{1}{k^2}\left[\frac{-4}{(1+r^2)} + 2\left(1+r^2\right)\rho\sigma^2k^2 + 2\eta n^2k^2\rho\sigma\right]\frac{d^2v}{d\theta^2}$$
$$+\left[\frac{-4r^2}{(1+r^2)} + \left(1+2r^2\right)\rho\sigma^2k^2 + \eta n^2k^2\rho\sigma\right]\left(\sigma + \eta n^2k^2\right)\frac{\rho\sigma}{k^2}v = 0, \qquad (2.29)$$

Again this equation agrees with the leading order behaviour, for large n, of the actual linearized equations away from the origin (ie. the equations are valid for $nr \gg 1$). Factorising into a pair of 2^{nd} order equations reveals that one factor is simply the ideal equation modified by resistivity whereas the other equation admits the possibility of a new resistive mode. For each of these two equations, normal mode solutions can be constructed in the manner described above.

In the rest of this chapter, we are not concerned with the detailed solutions for the eigenfunctions for a given growth rate. Instead, we investigate the allowable

values for the growth rate, σ, by setting $(S')^2 \equiv 0$ and plotting σ as a function of r. Given a value for σ, the above analysis shows that there is a normal mode solution that depends on the value of n and the number of radial nodes. The radius at which σ attains this value corresponds to the radius at which the nature of the solution changes from oscillatory to evanescent (or vice versa).

When the density is non-uniform, in the θ direction, the same approach can, in principle, be carried out but the actual derivation of the normal mode is substantially more complicated. Instead we select a typical radius and see the effect on this value for the growth rate as the photospheric density is varied. Generally speaking the variation of σ is similar at all radii. However, following this approach we are unable to follow the same normal mode as we have no guarantee that n and the number of radial modes will remain the same.

In section 2.5 we begin by constructing the general dispersion relation before discussing the two extreme limits of uniform density and infinite photospheric density. Then the way in which one solution evolves into the other is investigated by varying the photospheric density in section 2.6.

2.5 Dispersion relation

Consider initially even modes, about $\theta = 0$, for v_{1r} and odd modes for $v_{1\theta}$, which we shall write as v_r and v_θ.

$$v_{rc} = a \cos m_1\theta + b \cos m_2\theta, \tag{2.30a}$$

$$v_{rp} = c\cos m_3(\pi-\theta) + d\cos m_4(\pi-\theta), \tag{2.30b}$$

$$v_{\theta c} = A\sin m_1\theta + B\sin m_2\theta, \tag{2.30c}$$

$$v_{\theta p} = C\sin m_3(\pi-\theta) + D\sin m_4(\pi-\theta), \tag{2.30d}$$

where subscript p refers to the photospheric, and c refers to the coronal regions.

Equation (2.22) is used to write A, B, C and D in terms of a, b, c and d and matching (2.30a) to (2.30d) across the coronal/photospheric boundary, $\theta = \pm\pi/2$, using continuity of normal velocity, total pressure, normal magnetic field and tangential electric field by equating $(v_r)_c = (v_r)_p$, $d(v_r)_c/d\theta = d(v_r)_p/d\theta$, $d(v_\theta)_c/d\theta = d(v_\theta)_p/d\theta$ and $(v_\theta)_c = (v_\theta)_p$ gives the dispersion relation

$$\begin{vmatrix} 1 & 1 & 1 & 1 \\ \frac{E_c-m_1^2F}{m_1}\tan m_1\frac{\pi}{2} & \frac{E_c-m_2^2F}{m_2}\tan m_2\frac{\pi}{2} & \frac{E_p-m_3^2F}{m_3}\tan m_3\frac{\pi}{2} & \frac{E_p-m_4^2F}{m_4}\tan m_4\frac{\pi}{2} \\ E_c-m_1^2F & E_c-m_2^2F & E_p-m_3^2F & E_p-m_4^2F \\ m_1\tan m_1\frac{\pi}{2} & m_2\tan m_2\frac{\pi}{2} & m_3\tan m_3\frac{\pi}{2} & m_4\tan m_4\frac{\pi}{2} \end{vmatrix} = 0, \tag{2.31a}$$

where

$$E_c = -\frac{1}{2}\left[\frac{-4r^2}{1+r^2} + \left(1+2r^2\right)\rho_c\sigma^2 + \eta n^2\rho_c\sigma\right], \tag{2.31b}$$

$$E_p = -\frac{1}{2}\left[\frac{-4r^2}{1+r^2} + \left(1+2r^2\right)\rho_p\sigma^2 + \eta n^2\rho_p\sigma\right], \tag{2.31c}$$

$$F = \frac{1}{2}\frac{(1+2r^2)\,\sigma + \eta n^2}{\sigma + \eta n^2}. \tag{2.31d}$$

and m_1, m_2, m_3 and m_4 are solutions to (2.23a).

This dispersion relation is now solved analytically for two special density limits.

2.5.1 Uniform Density

In this extreme we take $\rho_p = \rho_c = 1$, and we have to solve equation (2.23) with the condition that m is an integer to satisfy the periodicity of the disturbances. Several simple cases, for particular values of the radius, are described. This is equivalent to a ballooning mode analysis of a Z-pinch.

Analysing equation (2.23a), with $(S')^2 = 0$, $k^2 = 1$, it is clear that the only unstable modes occur for $m = 0$ and $m = 1$. The behaviour of σ as ηn^2 varies is typified by the particular radius $r = 1$. In this case, equation (2.23a) factorizes to

$$\left[m^2 + \sigma\left(\sigma + \eta n^2\right)\right]\left[m^2 - 2 + \sigma\left(3\sigma + \eta n^2\right)\right] = 0, \tag{2.32}$$

giving the solutions

$$\sigma = -\frac{\eta n^2}{2} \pm \frac{1}{2}\left[\left(\eta n^2\right)^2 - 4m^2\right]^{\frac{1}{2}}, \tag{2.33a}$$

$$\sigma = -\frac{\eta n^2}{6} \pm \frac{1}{6}\left[\left(\eta n^2\right)^2 - 12\left(m^2 - 2\right)\right]^{\frac{1}{2}}, \tag{2.33b}$$

Equation (2.33a) corresponds to the slow mode whereas (2.33b) describes the Alfvén mode. Notice, from (2.33b) that there are ideal unstable solutions for $m = 0$ and 1. For all values of m, the roots eventually become real if ηn^2 is sufficiently large. For example, σ as a function of ηn^2 for $m = 1$ is shown in figure 2.4. The unstable Alfvén mode has a reduced growth rate as ηn^2 increases but remains unstable

whereas the stable root has an increased damping rate. The two damped oscillatory slow modes become two damped real modes for $\eta n^2 > 2$. This point coincides with the damped Alfvén mode only for $r = 1$. For $r \neq 1$ there is no coincidence of 3 roots. The behaviour for other values of m is readily obtained from (2.33).

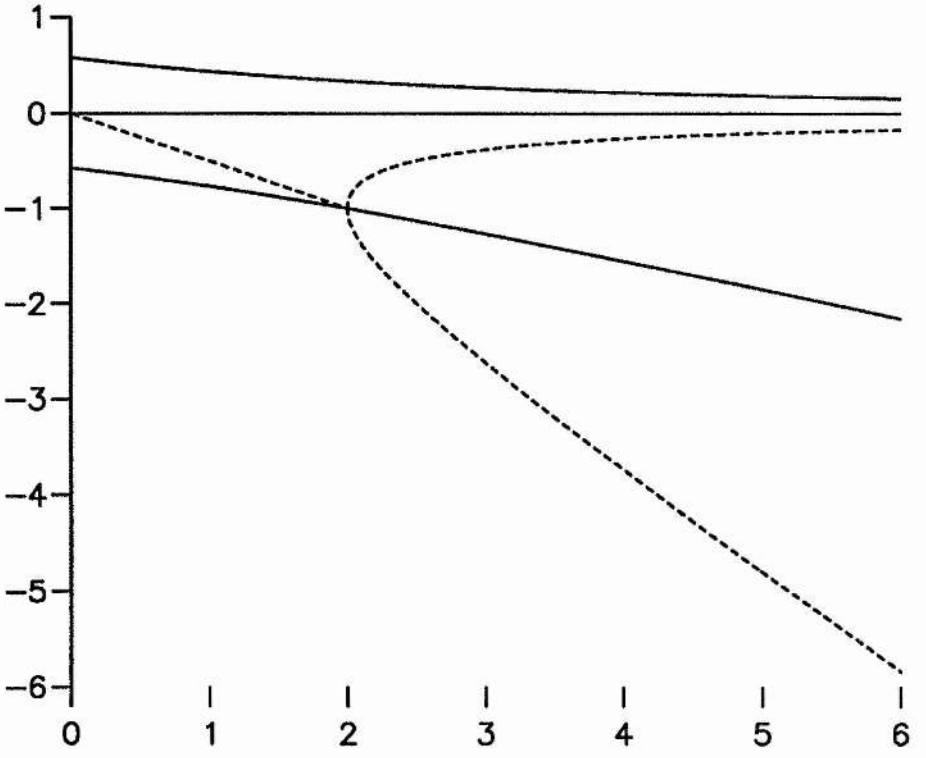

Figure **2.4**: Growth rate, σ, as a function of ηn^2, corresponding to uniform density with radial coordinate, $r = 1.0$, and poloidal wavenumber, $m = 1$. The dashed curves correspond to equation (2.33a), whereas the solid curves correspond to equation (2.33b).

2.5.2 Infinite density limit

Taking $\rho_c = 1, \rho_p = \rho$ and $|\rho\sigma^2|, |\rho\sigma| \gg 1$, the dispersion relation (2.31) reduces to

$$\frac{E_c - {m_1}^2 F}{m_1} \tan m_1 \frac{\pi}{2} = \frac{E_c - {m_2}^2 F}{m_2} \tan m_2 \frac{\pi}{2}. \tag{2.34}$$

where E_c and F are given by expressions (2.31), (see Velli and Hood, 1986), since if we represent the term in the i^{th} row and j^{th} column of the dispersion relation (2.31) by κ_{ij}, then the leading order contributions are

$$\kappa_{13} = O(1) \qquad \kappa_{14} = O(1)$$
$$\kappa_{23} = O\left((\rho\sigma)^{\frac{1}{2}}\right) \qquad \kappa_{24} = O(1)$$
$$\kappa_{33} = O(\rho\sigma) \qquad \kappa_{34} = O\left((\rho\sigma)^{\frac{1}{2}}\right)$$
$$\kappa_{43} = O\left((\rho\sigma)^{\frac{1}{2}}\right) \qquad \kappa_{44} = O\left((\rho\sigma)^{\frac{1}{2}}\right)$$

Hence the contribution from $\kappa_{33} \times \kappa_{44}$ dominates all other product contributions from columns 3 and 4.

2.5.2.1 small r

Before investigating the numerical solutions to the dispersion relation, it is informative to analyse the behaviour of σ in the neighbourhood of the origin, $r = 0$. Through this approach the singular nature of the resistive problem and the actual number (and form) of the roots are clearly seen.

With $r = 0$, equation (2.23a) factorizes as

$$\left[m^2 - 2m + \sigma\left(\sigma + \eta n^2\right)\right]\left[m^2 + 2m + \sigma\left(\sigma + \eta n^2\right)\right] = 0, \tag{2.35}$$

and taking $\pm m_1, \pm m_2$ as solutions of equation (2.35), for small r, there is an infinity of solutions of the form

$$\sigma = -\frac{\eta n^2}{2} \pm \frac{1}{2}\left(\left(\eta n^2\right)^2 - 4m_1 m_2\right)^{\frac{1}{2}}, \tag{2.36a}$$

$$m_2 = m_1 + 2, \tag{2.36b}$$

to first order, where m_1 and m_2 are integer values in order to satisfy the dispersion relation (2.34).

Using equations (2.36a) and (2.36b) and substituting integer values for m_1, we obtain the small r perturbation expansions, in the following forms

$$\sigma = \pm\left(r - \frac{13}{8}r^2 + \ldots\right), \quad \eta n^2 = 0, m_1 = 0, \tag{2.37a}$$

$$\sigma = \pm i\sqrt{3}\left(1 - \frac{1}{2}r^2 + \ldots\right), \quad \eta n^2 = 0, m_1 = 1, \tag{2.37b}$$

$$\sigma = \frac{1}{\eta n^2}r^2 + \ldots, \quad \eta n^2 \neq 0, \quad \eta n^2 \gg r, m_1 = 0, \tag{2.37c}$$

$$\sigma = -\eta n^2 + \left[\frac{\left(-2 + 5(\eta n^2)^2\right) \pm \sqrt{4 - 52(\eta n^2)^2 + 9(\eta n^2)^4}}{2\eta n^2}\right] r^2 + \ldots, \quad \eta n^2 \neq 0, \quad \eta n^2 \gg r, m_1 = 0, \tag{2.37d}$$

The different forms for $m_1 = 0$, namely (2.37a) and (2.37c), illustrates the singular nature of the stability problem. Thus, the inclusion of resistivity may produce a pronounced effect when comparing with the ideal results.

Looking at any particular solution of equations (2.36a) and (2.36b) with $m_1 \neq 0$, then

$$\sigma_{real} = -\frac{\eta n^2}{2}$$

$$\sigma_{imag} = \left(4m_1m_2 - \left(\eta n^2\right)^2\right)^{\frac{1}{2}}$$

$$\sigma = \sigma_{real} \pm i\sigma_{imag}$$

and as ηn^2 increases, $|\sigma_{imag}|$ reduces until $(\eta n^2)^2 - 4m_1m_2 = 0$ when $\sigma_{imag} = 0$. Then, for $(\eta n^2)^2 - 4m_1m_2 > 0$, σ becomes purely real and negative. As $\eta n^2 \to \infty$, σ asymptotes to the values 0 and $-\eta n^2$.

The implications of the above results are now discussed. In the ideal limit there are two types of modes namely the Alfvén and slow modes. Because of the boundary conditions introduced by the dense photosphere, these modes are now coupled together. By analysing the behaviour of the dispersion relation in the neighbourhood of $r = 0$ we can see that there are two ideal modes. The oscillatory solution is stable and generates the pair of σ values given by (2.37b). The marginally stable mode (at $r = 0$) generates a stable and unstable solution given by (2.37a). The inclusion of resistivity produces a surprise. The unstable mode given by (2.37a) is now modified to (2.37c) with the change in character of the expansion illustrating the singular nature of the ideal limit. (2.37d) is the resistive analogue to the negative root of (2.37a). For small ηn^2, we have two solutions emanating from $\sigma = -\eta n^2$ given by equation (2.37d). These solutions cease to exist at $r = 0$ for ηn^2 satisfying $4 - 52(\eta n^2)^2 + 9(\eta n^2)^4 < 0$ since complex conjugate roots of this kind do not satisfy the stability equations. The appearance and disappearance of roots (due to varying ηn^2) is important in understanding the behaviour for general radius.

2.5.2.2 General r

Dispersion relation (2.34) together with the fourth order equation (2.23), have been solved numerically for different values of r and ηn^2 and the results are now discussed. Consider first the infinite density limit.

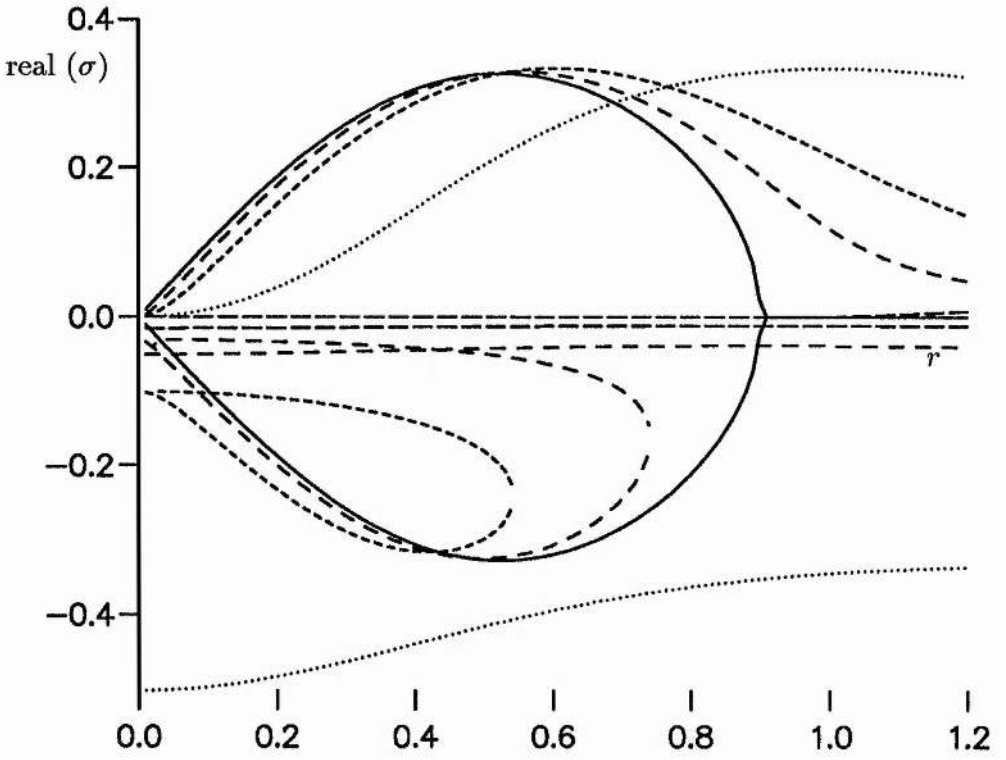

Figure **2.5**a: Real component of the growth rate, σ, as a function of the radial coordinate, r, in the infinite density ratio approximation in the ideal limit (solid curve), and also $\eta n^2 = 0.05$, 0.1, 0.5 and 1.0 (dashed curves of decreasing length).

Figure 2.5 shows the variation of the real and imaginary parts of σ with the radius for various values of ηn^2. Curves for larger values of ηn^2 are shown by

shorter dashes. In figure 2.5a, the solid curve shows the ideal Alfvén modes are purely real for $r < 0.9$. For $r > 0.9$, the ideal Alfvén modes are stable. Figure 2.5b clearly illustrates the region at which stable Alfvén modes appear. In addition, the slow mode is stable for all values of r. Notice that in the region $r > 0.9$ the unstable mode is a purely real mode that owes its existence to resistivity. The allowable normal mode growth rates are similar to the ideal values but the radial extent (of the oscillatory part) of the eigenfunction is more extended. Two solutions of complex type exist for non-zero ηn^2 which merge and disappear at a value of ηn^2 less than 0.05. One of these two roots is tabulated below.

ηn^2	σ
0.00	(0.00×10^{0}, 0.2202)
0.01	(6.13×10^{-5}, 0.2188)
0.02	(8.61×10^{-5}, 0.2141)
0.03	(2.84×10^{-5}, 0.2050)
0.04	(-2.01×10^{-4}, 0.1872)

Table **2.2**: Values of the growth rate obtained for small ηn^2 at $r = 1.0$. This solution merges with its complex conjugate pair and disappears for greater values of ηn^2.

One overstable and one damped oscillatory solutions for $\eta n^2 = 0.03$ can be shown to exist. As ηn^2 is increased, the solution with the smaller imaginary value of σ increases, whereas the solution with the larger imaginary value of σ decreases.

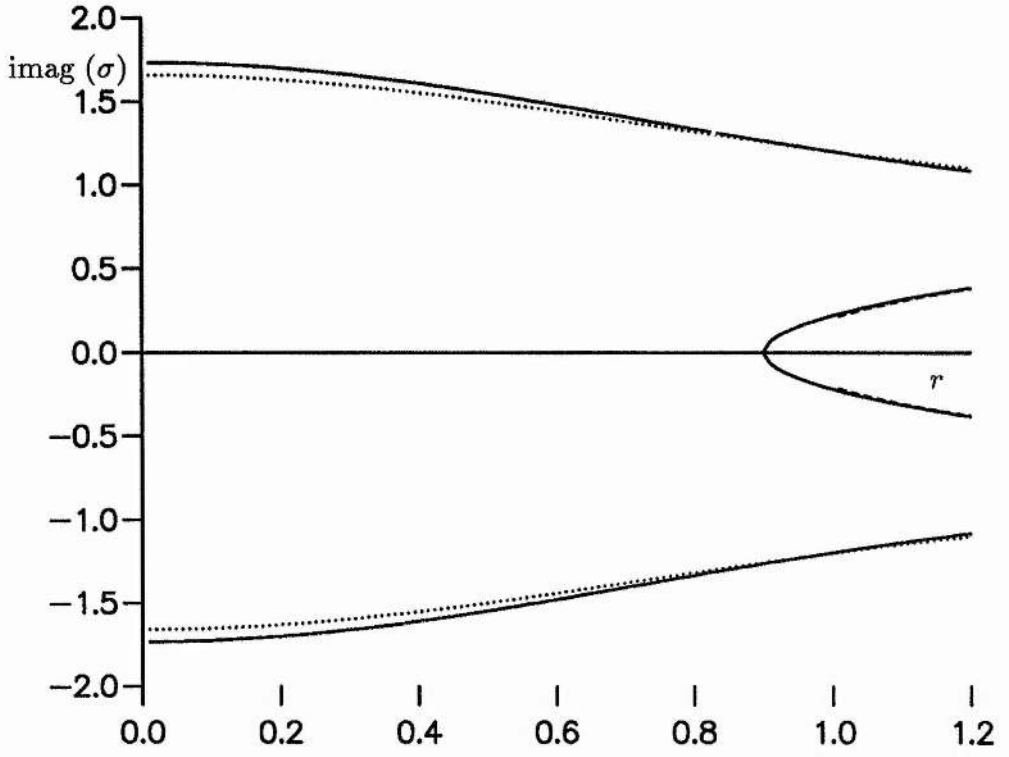

Figure **2.5**b: Oscillatory component of the growth rate, σ, as a function of the radial coordinate, r, in the infinite density ratio approximation in the ideal limit (solid curve), and for $\eta n^2 = 0.5$ and 1.0 (dashed curves of decreasing length).

Thus we have two roots coming together and disappearing. The difference between these disappearing roots and the previous mentioned roots is that in this case, the oscillatory component is non-zero at the point of disappearance. As ηn^2 decreases from 0.03, the larger imaginary value of σ limits to the ideal oscillatory solution shown in figure 2.5b, whereas the smaller imaginary value of σ approaches zero in the limit as ηn^2 tends to zero. For the ideal case, this limit is not a solution of

dispersion relation (2.34) since F in (2.31c) is indeterminate.

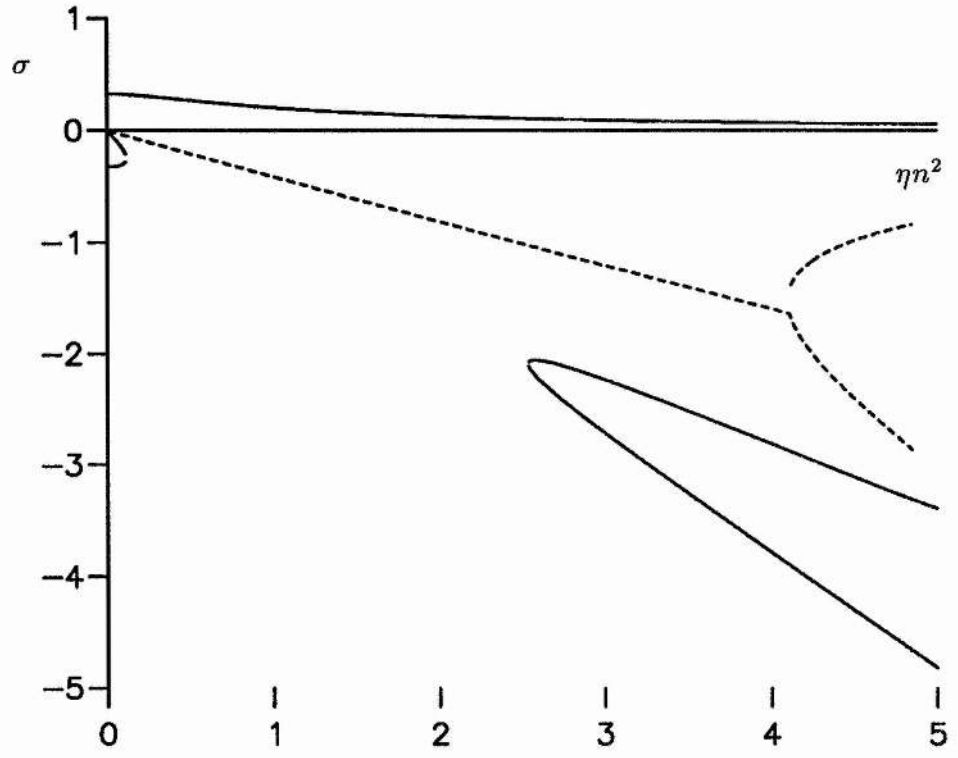

Figure **2.6**: Growth rate, σ, as a function of ηn^2, in the infinite density ratio approximation with radial coordinate, $r = 0.5$. Solid curves correspond to the Alfvén mode , dashed curves to the slow mode.

Two damped modes emerge from $r = 0$, $\sigma = -\eta n^2$ and coalesce at a radius (less than 0.9) that decreases with ηn^2. For a fixed value of the radius, increasing ηn^2 will cause these two roots to approach each other, coalesce and disappear. This is borne out by figure 2.6, which shows the behaviour of the real part of the growth rate as ηn^2 is increased for the flux surface at $r = 0.5$. Notice that there are two

roots that coalesce and then reappear at a larger value of ηn^2. This is identical to the points of coalescence at $r = 0$ which occur (at $\eta n^2 = 0.08, 5.7$) when the square root term in (2.37d) changes from real to imaginary and back to real again, as ηn^2 is increased.

To apply the rigid wall line-tying conditions, the photospheric density must be sufficiently large that $|\rho\sigma^2| \gg 1$. Then starting at the ideal limit, $\eta n^2 = 0$, there are four fundamental roots to the dispersion relation, namely the real unstable and stable Alfvén modes, and the purely imaginary slow modes. As ηn^2 increases the slow mode becomes damped with a damping rate of $\eta n^2/2$, and the frequency is reduced until at $\eta n^2 \approx 4.1$ the frequency is zero and above this there are two real stable modes. The growth rate of the unstable Alfvén mode is reduced but remains unstable. This is in contrast with the results found in Velli and Hood (1986). However, Velli and Hood investigated regions of ideal marginal stability given by $r \approx 0.9$ in figure 2.5, and in that region it is clear that resistivity increases the growth rate.

A new resistive mode emerges from the origin that merges with the stable Alfvén mode at $\eta n^2 = 0.11$. The two modes then reappear at $\eta n^2 = 2.54$ as two purely real stable modes. Interestingly enough, there are no complex conjugate roots between these values of ηn^2. This has been verified by plotting, the real and imaginary parts of dispersion relation (2.34) as a function of the real part of σ for various values of the imaginary part of σ. For $\eta n^2 = 0.11$, the imaginary part of (2.34) is only zero

for $\sigma_i = 0$ and the real part of (2.34) is zero, (with $\sigma_i = 0$) at two distinct values of σ_r, giving the two roots. However, when $\eta n^2 = 0.12$, although the imaginary part of (2.34) is zero for $\sigma_i = 0$, the real part of (2.34) (with $\sigma_i = 0$) does not possess any zeros indicating there are no solutions to the dispersion relation.

When $r = 1$, the plasma is ideally stable and at $\eta n^2 = 0$, there are the 4 frequencies, the larger values of $|\sigma_i|$ correspond to the slow modes and the smaller values to the Alfvén modes. As ηn^2 increases the slow modes are again damped with a rate proportional to $\eta n^2/2$. The purely real resistive ballooning mode, is clearly seen emanating from the origin and soon reaches a maximum value before slowly decreasing. Beyond $\eta n^2 = 2.5$, two real roots emerge.

2.6 General ρ

The previous section has presented the behaviour of the growth rate as the resistivity parameter, ηn^2, is varied for two particular photospheric density limits. Obviously the realistic density ratio lies in between. In this section we vary the density ratio and investigate how the solutions for uniform density evolve into the infinite density limit. In addition, it is important to remember that the infinite density limit is valid as long as $|\rho\sigma^2| \gg 1$. This means that a mode that is initially unstable in the uniform density limit cannot pass through marginal stability as the photospheric density increases (since at marginal stability the linearized equations are independent of ρ.).

To proceed, equations (2.22a) and (2.22b) have been solved numerically using a fourth order Runga-Kutta-Merson method with density profile given by

$$\rho = \frac{1}{2}\left[(1+\rho_p) + (1-\rho_p)\tanh\lambda\left(\frac{\pi}{2} - |\theta|\right)\right] \tag{2.38}$$

where λ has been taken to be 1000 to give a steep density transition from $\rho = 1$ to $\rho = \rho_p$ as θ is increased across the boundary $\theta = \pi/2$. A typical value of the radius is selected to illustrate the influence on the growth rates of increasing ρ_p.

2.6.1 Ideal Case

Firstly, consider an ideal plasma. The values of r are selected as they are typical of the uniform and infinite density limits. At $r = 0.5$ and 1, the uniform density limit has both the kink and sausage modes unstable whereas there is only one unstable mode for $r = 0.5$ in the infinite density limit and there are no unstable roots at $r = 1$. For $r = 2$ only the sausage mode is unstable in the uniform density limit and there are no unstable roots in the infinite density limit. Thus these three values of r cover the different cases and we now consider how these ideal modes evolve as the photospheric density varies. The behaviour of σ for $r = 0.5$, as ρ_p varies is shown in figure 2.7a for the kink-type and sausage-type modes. The former tends to a finite value that is given by the infinite density value, whereas the latter tends to zero. The growth rate of the kink-type mode is given by $\sigma \approx \sigma_\infty + c_1\rho^{-1/3}$ for large ρ, whereas the sausage-type mode is given by $\sigma \approx c_2\rho^{-1/2}$. Notice that for the sausage mode $|\rho\sigma^2|$ is not large and so, not surprisingly, this mode is not picked up by the

infinite density limit.

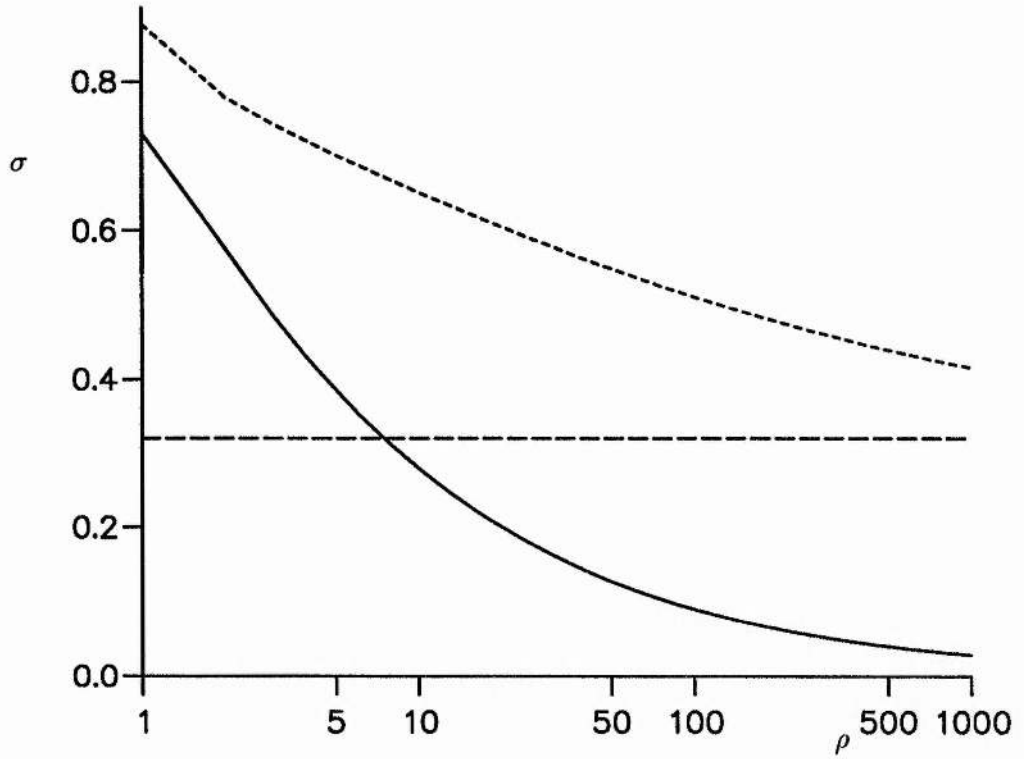

Figure **2.7**a: Growth rate, σ, as a function of the density ratio, ρ, with radial coordinate, $r = 0.5$, in the ideal limit. The infinite density ratio limit is shown as a dashed horizontal line. The kink-type mode is shown by a dashed curve, the sausage-type by a solid curve.

The kink-type growth rate is larger in value than the sausage-type growth rate. The type of mode is identified at $\rho_p = 1$ and followed as ρ_p increases. The amplitude of the velocity eigenfunctions of the kink-type mode at the $\theta = \pm\pi/2$ boundary tends to 0 as ρ is increased. The amplitude of the velocity eigenfunctions of the sausage-type mode tend to a non-zero finite limit although the growth rate tends

to 0 as ρ increases indicating that there is a flow across the boundary. Using a normalisation of $v_r = 1$ at $\theta = 0$, the relationship between velocity and density is shown in figure 2.7b. The eigenfunction for the kink-type mode, has a maximum at $\theta = 0$ and minimum at $\theta = \pm\pi/2$, whereas, for the sausage-type mode, it has a minimum at $\theta = 0$ and maximum at $\theta = \pm\pi/2$. Since, in the corona, the radial velocity has the form

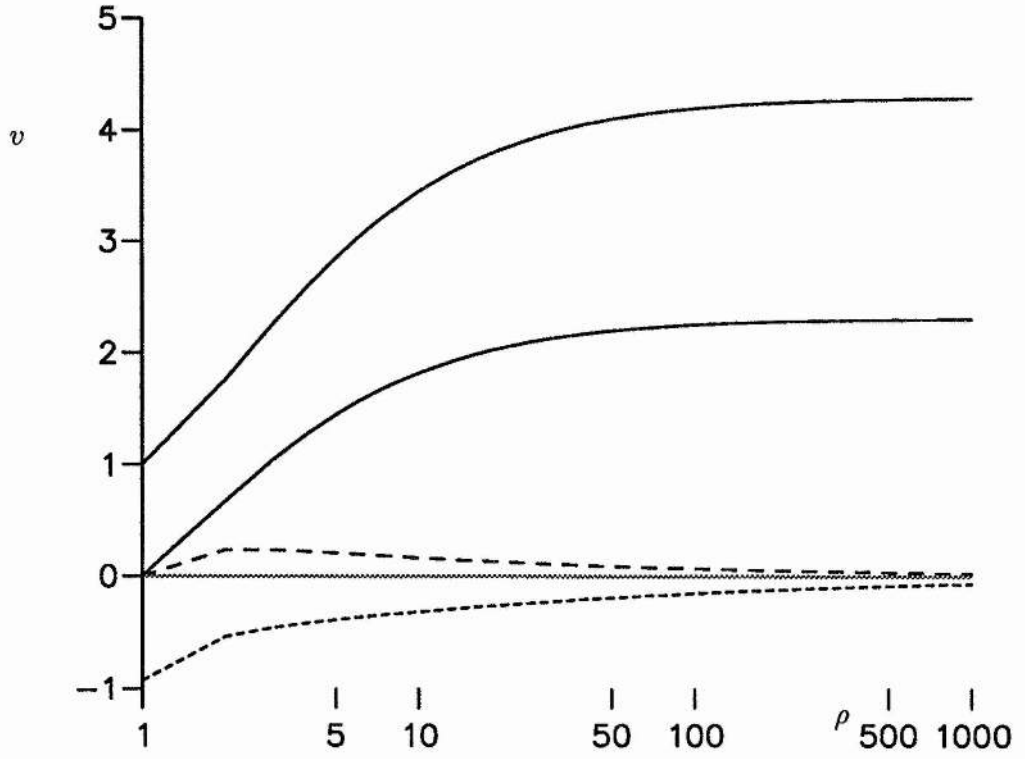

Figure **2.7**b: Radial (upper) and poloidal (lower) velocities at the photospheric/coronal boundary, $\theta = \pi/2$, for unstable modes corresponding to figure 2.7a.

$$v_r = a\cos m_1\theta + b\cos m_2\theta \tag{2.39}$$

this can be explained by a and b having the same sign for the kink-type mode, and opposite signs for the sausage mode. For $r = 1.0$, the sausage-type growth rate is larger in value than the kink-type growth rate, with both types of mode tending to 0 as ρ is increased. The amplitude of the kink-type velocity eigenfunctions tends to a finite non-zero limit and again the growth rate tends to 0 as ρ is increased. In contrast to $r = 0.5$, the sausage-type mode has a maximum at $\theta = 0$ and a minimum at $\theta = \pm\pi/2$, and the kink-type mode has a minimum at $\theta = 0$ and a maximum at $\theta = \pm\pi/2$. The growth rate of the sausage-type mode is given by $\sigma \approx c_2\rho^{-1/3}$ for large ρ, whereas the kink-type mode is given by $\sigma \approx c_1\rho^{-1/2}$. Hence, the sausage mode satisfies rigid wall line-tying conditions but the kink mode, since $|\rho\sigma^2|$ is not large, does not.

For $r = 2.0$, there is no unstable kink-type mode since $\sigma^2 < 0$ for $r > \sqrt{3}$. The sausage-type growth rate is similar to the case $r = 1.0$ with σ tending to 0 as ρ tends to ∞. The growth rate is given by $\sigma \propto \rho^{-1/2}$.

In contrast to Hood (1986), we have found that for unstable solutions tending to marginal stability as ρ tends to infinity, flows can occur across the photosphere/corona boundary. These flows do not satisfy either of the 'rigid-wall' or 'flow-through' conditions since v_r, perpendicular to the magnetic field, is non-zero. For solutions which remain unstable as ρ tends to infinity, we have found agreement

with Hood (1986) that for large photospheric/coronal density ratios, the line-tying conditions are best simulated by taking all velocity amplitudes to be zero at the photospheric boundary.

2.6.2 non-zero ηn^2

We now investigate how the growth rates are influenced by the inclusion of resistivity. Again 3 values of r are used as above.

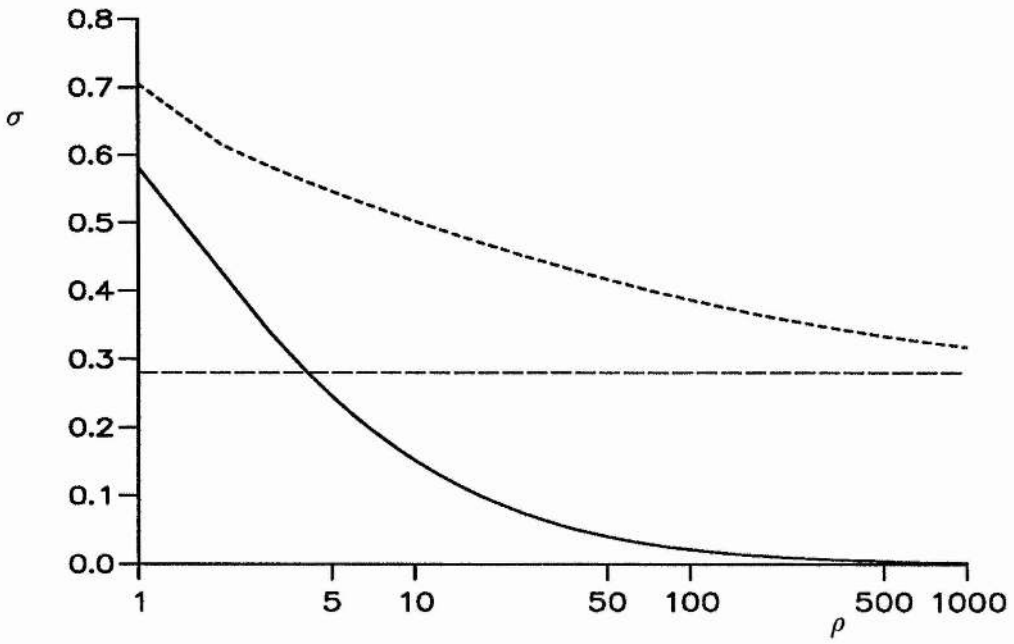

Figure **2.8**a: Growth rate, σ, as a function of the density ratio, ρ, with radial coordinate, $r = 0.5$, and $\eta n^2 = 0.5$. The infinite density ratio limit is shown as a dashed horizontal line. The kink-type mode is shown by a dashed curve, the sausage-type by a solid curve.

For $r = 0.5$, see figure 2.8, the behaviour of the growth rates is similar to the ideal

case with the amplitude of the kink-type velocity eigenfunctions tending to zero as ρ is increased. Figure 2.8a shows the behaviour of the kink-type (dashed curve) and sausage-type (solid curve) growth rates as the photospheric density varies. Again, the former tends to a non-zero value given by the infinite density limit, whereas the latter tends to zero. However, the velocity eigenfunctions do not go to zero, since a contribution to the ballooning equations will come from the second order derivative of the perturbed magnetic field with respect to the poloidal angle, θ. This will introduce diffusive terms, which vary as $\eta\rho\sigma$, into the two coupled second order ordinary differential equations for v_r and v_θ given by equations (2.22a) and (2.22b). The growth rate, σ, tends to a non-zero positive value as the density ratio, ρ tends to infinity, and $\eta\rho\sigma$ will cease to be small compared to $\eta n^2 k^2$ and so a small non-zero velocity will remain with an amplitude dependent on the diffusion timescale (see Velli, Einaudi and Hood, 1990).

The amplitude of the sausage-type eigenfunctions at $\theta = \pm\pi/2$ seem to tend to ∞ as ρ is increased for the resistive $r = 0.5$ case. However, since we are normalising the amplitude of the radial velocity eigenfunction to unity at $\theta = 0$, we have calculated $v_r/(a+b)$ from expression (2.41), and $a+b$ tends to zero as ρ is increased. Again, the sausage-type eigenfunction, v_r, has a minimum at $\theta = 0$ and maximum at $\theta = \pm\pi/2$ and the kink-type eigenfunction, v_r, has a maximum at $\theta = 0$ and a minimum at $\theta = \pm\pi/2$. The sausage-type growth rate, $\sigma \approx \sigma_\infty + c\rho^{-1}$, is independent of the value of ηn^2. The kink-type growth rate varies approximately as $\rho^{-0.41}$ for $\eta n^2 = 0.5$,

and $\rho^{-0.42}$ for $\eta n^2 = 1.0$, somewhere between the $-1/3$ and $-1/2$ values obtained for the ideal case.

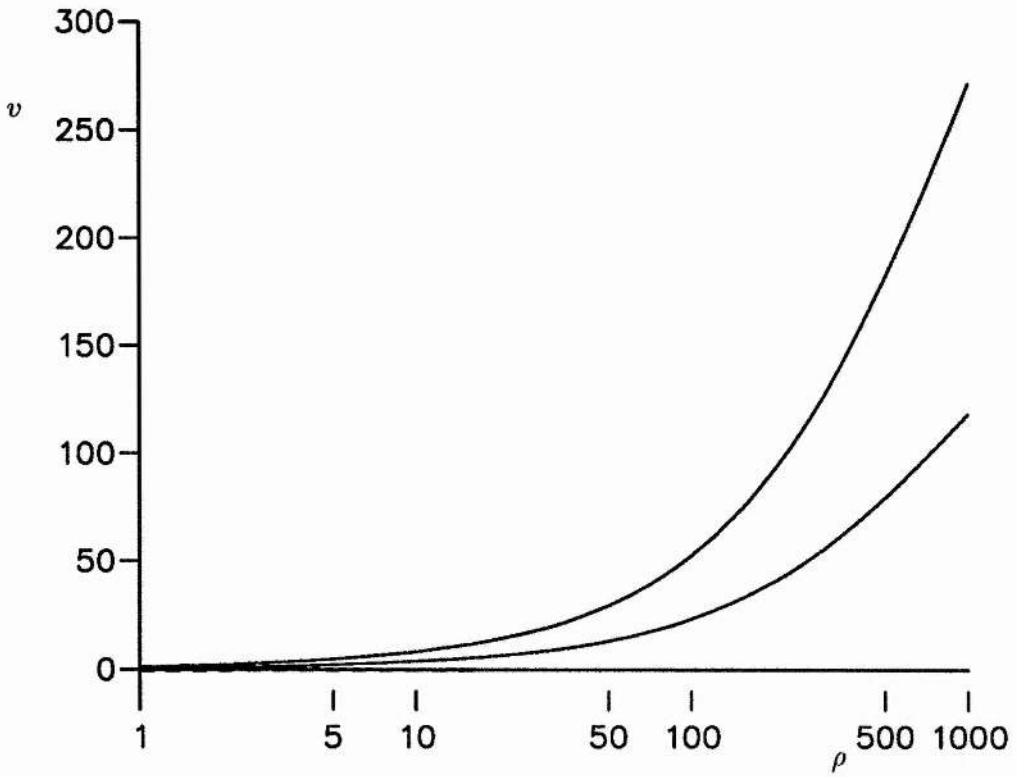

Figure **2.8**b: Radial (upper) and poloidal (lower) velocities at the photospheric/coronal boundary, $\theta = \pi/2$, for unstable modes corresponding to figure 2.8a.

For $r = 1.0$ and $r = 2.0$, there exists a resistive instability in the infinite density case, whereas no ideal instability is present. Both the sausage-type and kink-type, for $r = 1.0$, have maxima of v_r at $\theta = 0$, minima of v_r at $\theta = \pm\pi/2$ indicating a and b of the same sign in expression (2.41). The amplitude of the sausage-type velocity

eigenfunctions tends to zero as ρ is increased. As explained above, the velocity eigenfunctions do no go to zero but will tend to a small, non-zero, value dependent on the diffusion timescale with extra terms in the coupled ordinary differential equations due to the second order derivative of the perturbed magnetic field.

The amplitude of the kink-type radial velocity eigenfunction tends to a non-zero value, with the growth rate tending to 0 as ρ is increased. The kink-type growth rate, $\sigma \approx c\rho^{-1}$, for $r = 1.0$, whereas the kink-type mode is non-existent for $r = 2.0$. The sausage-type growth rate varies approximately as $\rho^{-0.43}$ for $r = 1.0$, $\eta n^2 = 0.5$, and $\rho^{-0.45}$ for the cases $r = 1.0$, $\eta n^2 = 1.0$ and for $r = 2.0$, $\eta n^2 = 0.5$ and 1.0, somewhere between the power values $-1/3$ and $-1/2$ obtained for the ideal case.

2.7 Discussion

In this chapter, we have looked at the behaviour of both ideal and resistive ballooning modes as the photospheric to coronal density ratio, resistivity and radius are varied in order to investigate the correct form of the boundary conditions at the photosphere/corona interface.

A detailed derivation of how the ballooning (or WKB) approach can be used to construct a normal mode is presented and the interpretation of the growth rate curves as a function of radius is clarified. Basically, we are selecting the radius at which the character of the eigenfunction changes from oscillatory to exponential. All the values of σ predicted by the $\sigma - r$ curves are in fact realizable by suitably

adjusting the wavenumber n and the number of radial nodes. Choosing a particular value of r allows us to predict the influence of resistivity and the photospheric density on the behaviour of attainable normal modes. We have looked at a larger range of parameters than has previously been attempted, with the resistivity parameter, ηn^2, extending beyond the maximum value of 10^{-2} used in Velli and Hood (1986) up to a value of 6.0, in order to follow the development of some of the modes as the resistivity is varied. Unless anomalous resistivity is used, such high values of ηn^2 are unlikely to be achieved in the solar corona. Previous attention has been focused on a particular value of the radius. This chapter has shown that the effect of resistivity on unstable modes can be different depending on the value of the radius chosen. In the case of an infinite density ratio, resistivity decreases the growth rate for small r, whereas beyond ideal marginal stability, $r = 0.9$, resistivity causes an increase in the growth rate, the region investigated by Velli and Hood (1986). Our analysis has looked at small perturbations about a cylindrical magnetostatic equilibrium where the coronal and photospheric pressures and magnetic fields depend on the radius, and are independent of the poloidal angle, θ, and toroidal z direction. The large wave-number, n, in the radial and z directions for the perturbed quantities, gives slow variations along the field lines but rapid variations across them.

The two types of boundary conditions that are commonly considered are the 'rigid-wall' conditions where all perturbations of the eigenfunction vanish, and the 'flow-through' conditions where perturbations of the eigenfunction are allowed along

the field lines. Hood (1986) investigated the ideal case with $r = 0.5$, and found that for the most unstable mode, the kink-type mode, the 'rigid-wall' conditions were the most appropriate as the density ratio becomes large. He also found the governing equation in the infinite-density ratio case when the corona becomes detached from the photosphere, indicating agreement with the 'rigid-wall' conditions. However, the density ratio is not infinite, but of the order of 10^8, and it is not obvious that a large finite ratio should give similar results to an infinite ratio. This chapter has shown that there exists a second series of instabilities which tend to marginal stability as the infinite density ratio is approached. In this case, flows parallel and perpendicular to the magnetic field were found if $|\rho\sigma^2|$ remains finite. This is in agreement with Cargill *et al.* (1986), who suggested that either all three components of the perturbed eigenfunction vanish or none at all.

Summarising then,

(i) if there is an unstable (or stable) mode in the uniform density (untied) limit and a corresponding unstable (or stable) mode in the infinite density limit, then the growth rate simply evolves from one to the other as the photospheric density increases and the photosphere can be represented by the rigid wall conditions.

(ii) if there is an instability in the uniform density limit but no instability in the infinite density limit then there may indeed be flows across the coronal/photospheric interface. However, the growth rates will be small since $|\rho_p\sigma^2|$ remains finite (or zero) for large ρ_p.

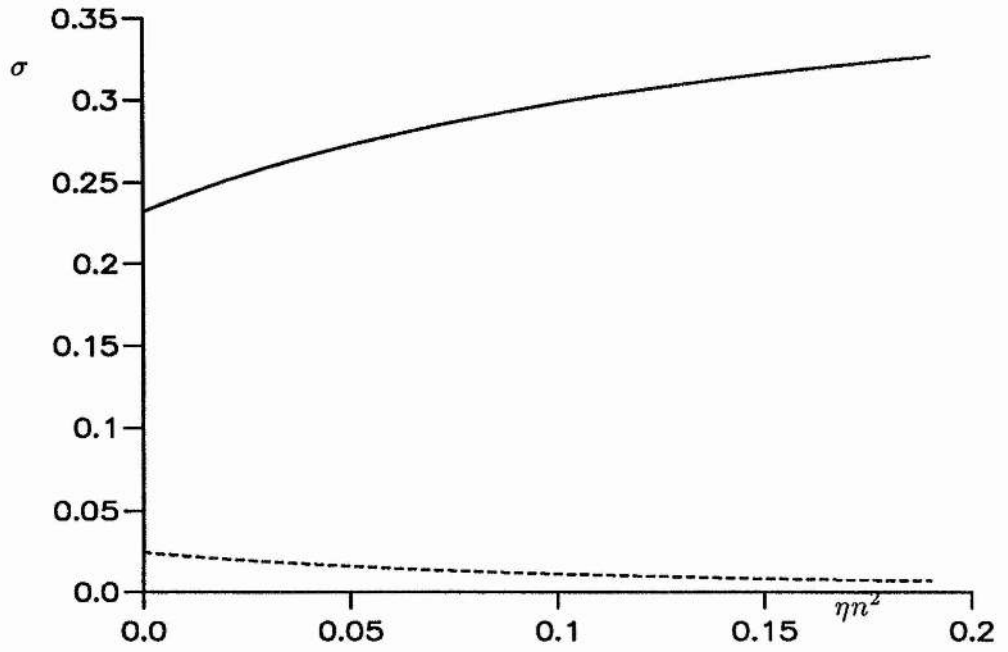

Figure **2.9**: Growth rate, σ, as a function of the resistivity parameter, ηn^2, for $r = 1$ and $\rho_p = 1000$ corresponding to a sausage-type mode (solid curve) and a kink-type mode (dashed curve).

(iii) for a fixed value of ρ_p, increasing resistivity, through ηn^2, results in differing effects depending on the value of radius chosen. This is illustrated in the infinite density limit, where the growth rate is decreased for small r, whereas beyond marginal stability, $r > 0.9$, resistivity causes an increase in the growth rate. Figure 2.9 shows the growth rate, σ, against the resistivity parameter, ηn^2, for $r = 1$ and $\rho_p = 1000$. The most unstable mode (solid curve), which has evolved from the uniform density sausage mode (solid curve) shown in figure 2.2, becomes more unstable with increasing ηn^2, as is the case for the infinite density limit shown in figure 2.5a. The other mode (dashed curve) has σ decreasing as ηn^2 increases. This instability has evolved

from the uniform density kink mode (dashed curve) shown in figure 2.2. For large values of ρ_p, diffusive terms, varying as $\eta\rho_p$, eliminated in the ballooning equations by comparison with ηn^2, will no longer be small and extra diffusive terms are introduced into the equations. Small non-zero velocities will result at the boundary indicating flows contrary to both the rigid-wall and flow-through conditions.

The calculations presented have ignored the transition region, viscosity, thermal and gravitational effects which would severely complicate the analysis. Also, it has been suggested that non-linear effects may enhance the instabilities obtained by linear analysis or even lead to an explosive instability.

3 Equilibrium and Equations of Motion for Coronal Loops

3.1 Introduction

In chapter 2, the form of the boundary conditions at the photosphere/ corona interface was investigated using localized modes. In this chapter, global modes will be used to investigate stability of a flux tube. The stability of coronal loops to kink modes transformed into localized modes by increasing the poloidal wavenumber, m, is investigated. A code was developed that is applied to numerically generated 1–D equilibria based on the 2–D Grad-Shafranov equation.

Zweibel and Boozer (1985) looked at the effect of small twist. They showed that the main part of the loop has a constant cross-sectional area with all radial variations confined to a boundary layer near the photospheric ends. Lothian and Hood (1989) also investigated small twist and developed a theory for the central part of the loop in terms of a simple one-dimensional model. Browning and Hood (1989) extended the work of Lothian and Hood (1989) to include the effect of large twist. Lothian and Hood (1992) included pressure effects as well as the footpoint displacement and find that nonequilibrium can occur if the pressure is sufficiently large. Robertson, Hood and Lothian (1990) used the one-dimensional model with entropy as a specified function of the flux function, A. Loop stability has been

investigated by Mikic, Schnack and Van Hoven (1990), Van der Linden, Goossens and Kerner (1990) and Goedbloed (1990). Foote and Craig (1990) and De Bruyne and Hood (1992) have investigated a variety of modes in addition to the kink mode.

Mikic, Schnack and Van Hoven (1990) investigated the equilibrium and stability of a twisted magnetic flux tube using a time-dependent MHD model. Starting from an initial uniform background axial magnetic field and applying slow localized photospheric vortex flows at the ends of a flux tube, the flux tube evolved through a sequence of essentially 2–D equilibria. Considering a numerically generated equilibria they studied its 3–D MHD stability properties, including the stabilizing effect of photospheric line-tying. Their method was applied to a twist profile given by

$$\Phi/L = \begin{cases} \lambda_e (1-A)^2 & , \quad A \leq 1 \\ 0 & , \quad A > 1 \end{cases}$$

where L is the length of the loop, Φ is the winding angle of a field line about the axis as it travels from one end of the loop to the other, A is a magnetic flux function, λ_e is a parameter determining the axial twist of the loop.

In the following analysis, all quantities will be normalized with $\mathbf{B} = B_0\mathbf{B}'$, $p = p_0 p'$, $\rho = \rho_0 \rho'$, $r = ar'$, $\boldsymbol{\xi} = a\boldsymbol{\xi}'$, $t = (a/v_A)\, t'$, where B_0, p_0, ρ_0 and a represent typical values for the coronal magnetic field, plasma pressure, density and loop radius and $v_A = B_0/\sqrt{\mu\rho}$ is the Alfvén velocity in the loop. For convenience, all dashes will be dropped from the equations.

For the untwisted loop, taking the constant normalized axial field

$$B_z = 1$$

gives the flux function, A as

$$A = \frac{1}{2}r^2$$

and the initial boundary for the flux tube surrounded by a uniform plasma with uniform axial magnetic field, given by $A = 1$ is

$$r_0 = \sqrt{2}$$

Mikic, Schnack and Van Hoven (1990) considered an initial uniform plasma beta, $\beta_0 = 0.1$ with a loop length, $L = 4r_0$ and an outer boundary, $R = 4r_0$. They found the equilibrium becomes unstable when the axial twist, $\Phi(0)$ exceeded the critical value, $\Phi_c = 4.8\pi$. They also found that there was a compression of the axial field near to the axis and an expansion of the axial field away from the axis in order to conserve the total longitudinal flux of the flux tube given by $\int_0^1 2\pi r dA = 2\pi \int_0^{r_0} r^2 B_z dr$ for any value of the axial coordinate, z (see Browning and Priest, 1983).

De Bruyne and Hood (1992) investigated how the stability properties of coronal loops to kink modes is transformed into those of localized modes as the poloidal wave number, m, is increased. By developing a set of Fourier truncated equations of motion with rigid-wall line-tied conditions imposed, these equations were then incorporated in a Fortran program with boundary conditions imposed at a small value of the radial component, $r = \epsilon$, due to the singular nature of the linearized

equations of motion at $r = 0$ and a large value of the radial component, $r = R$. Then by using a shooting and matching method, whereby the equations are integrated out from $r = \epsilon$ to a matching point, and integrated inwards from $r = R$ to the matching point, the problem is reduced to one of finding a value of loop length which gives the determinant of a matrix as zero.

They studied two classes of equilibria, the constant-twist Gold-Hoyle field (Gold and Hoyle, 1960) and a variable twist field (Anzer, 1968). For equilibria close to force-free they found that increasing the poloidal wave number stabilizes the equilibria, so that the kink mode is the most unstable mode. As pressure gradients are increased from close to force-free equilibria, the localized mode ($m \to \infty$) becomes the most unstable mode with the kink mode the most stable. However, in the solar context, the close to force-free results are relevant.

3.2 Equilibrium

The magnetostatic equilibrium

$$(\nabla \times \mathbf{B}) \times \mathbf{B} = \mu \nabla p, \tag{3.1a}$$

$$\nabla \cdot \mathbf{B} = 0, \tag{3.1b}$$

written in coordinates for a cylindrically symmetric field

$$B_z \frac{\partial B_r}{\partial z} - B_z \frac{\partial B_z}{\partial r} - \frac{B_\theta}{r} \frac{\partial}{\partial r} (r B_\theta) = \mu \frac{\partial p}{\partial r}, \tag{3.2a}$$

$$\frac{B_r}{r}\frac{\partial}{\partial r}(rB_\theta) + B_z\frac{\partial B_\theta}{\partial z} = 0, \tag{3.2b}$$

$$-B_r\frac{\partial B_r}{\partial z} + B_r\frac{\partial B_z}{\partial r} - B_\theta\frac{\partial B_\theta}{\partial z} = \mu\frac{\partial p}{\partial z}, \tag{3.2c}$$

$$\frac{1}{r}\frac{\partial}{\partial r}(rB_r) + \frac{\partial B_z}{\partial z} = 0, \tag{3.2d}$$

where the equilibrium variables are functions of radial, r, and axial, z, coordinates.

In order to satisfy equation (3.2d), set

$$B_r = -\frac{1}{r}\frac{\partial A}{\partial z}, \tag{3.3a}$$

$$B_z = \frac{1}{r}\frac{\partial A}{\partial r}, \tag{3.3b}$$

where A is a magnetic flux function.

Then using expressions (3.3a) and (3.3b), equation (3.2b) is

$$-\frac{1}{r^2}\frac{\partial A}{\partial z}\frac{\partial}{\partial r}(rB_\theta) + \frac{1}{r}\frac{\partial A}{\partial r}\frac{\partial B_\theta}{\partial z} = 0, \tag{3.4}$$

which is satisfied by

$$B_\theta = \frac{1}{r}K(A), \tag{3.5}$$

where K is an arbitrary function of the flux function, A.

Multiplying equation (3.2a) by B_r and adding equation (3.2c) multiplied by B_z gives the equation

$$-\frac{B_rB_\theta}{r}\frac{\partial}{\partial r}(rB_\theta) - B_\theta B_z\frac{\partial B_\theta}{\partial z} = \mu\left(B_r\frac{\partial p}{\partial r} + B_z\frac{\partial p}{\partial z}\right), \tag{3.6}$$

The left hand side of equation (3.6) is satisfied trivially by substituting expressions (3.3a), (3.3b) and (3.5) for B_r, B_θ and B_z. The right hand side of (3.6) is

$$-\frac{\partial A}{\partial z}\frac{\partial p}{\partial r}+\frac{\partial A}{\partial r}\frac{\partial p}{\partial z}=0, \tag{3.7}$$

which is satisfied by

$$p=p(A), \tag{3.8}$$

Substituting expressions (3.3a), (3.3b) and (3.5) for B_r, B_θ and B_z in equations (3.2a) and (3.2c)

$$-\frac{1}{r^2}\frac{\partial A}{\partial r}\frac{\partial^2 A}{\partial z^2}-\frac{1}{r}\frac{\partial A}{\partial r}\frac{\partial}{\partial r}\left(\frac{1}{r}\frac{\partial A}{\partial r}\right)-\frac{K}{r^2}\frac{dK}{dA}\frac{\partial A}{\partial r}=\mu\frac{dP}{dA}\frac{\partial A}{\partial r}, \tag{3.9}$$

$$-\frac{1}{r^2}\frac{\partial A}{\partial z}\frac{\partial^2 A}{\partial z^2}-\frac{1}{r}\frac{\partial A}{\partial z}\frac{\partial}{\partial r}\left(\frac{1}{r}\frac{\partial A}{\partial r}\right)-\frac{K}{r^2}\frac{dK}{dA}\frac{\partial A}{\partial z}=\mu\frac{dP}{dA}\frac{\partial A}{\partial z}, \tag{3.10}$$

Dividing equation (3.9) by $\partial A/\partial r$, or equation (3.10) by $\partial A/\partial z$ leads to the 2–D Grad-Shafranov equation (after multiplying by r^2)

$$\frac{\partial^2 A}{\partial r^2}-\frac{1}{r}\frac{\partial A}{\partial r}+\frac{\partial^2 A}{\partial z^2}+K\frac{dK}{dA}+r^2\mu\frac{dP}{dA}=0, \tag{3.11}$$

Browning and Hood (1989), and Lothian and Hood (1989) showed that the behaviour of the field for the main part of the loop with a specified twist profile is essentially independent of axial variations. Their analysis is valid for slender flux tubes where the radial length scale is small compared to the flux tube length. This can be observed from equation (3.11) where the ratio of the third to the first terms is of order r^2/L^2, where r is a typical tube radius and L is a typical tube length. The

axial dependence of the Grad-Shafranov equation will be ignored

$$\frac{d^2A}{dr^2} - \frac{1}{r}\frac{dA}{dr} + K\frac{dK}{dA} + r^2\mu\frac{dP}{dA} = 0, \tag{3.12}$$

since this will give good approximations over most of the loop. The main difference is confined to boundary layers at the ends of the loop. Using the 1–D form of the Grad-Shafranov equation (3.12), the central part of the loop is being considered. Cutting off the boundary layers at the ends of the loop by applying boundary conditions at the ends of the 'straight' part of the loop is a stabilizing effect and so any instability found using the 1–D form of the Grad-Shafranov equation (3.12) will be unstable for the 2–D form of the Grad-Shafranov equation (3.11) with the boundary layers added.

The twist on each field line is given by

$$\Phi(A) = \int_{-L/2}^{L/2} \frac{B_\theta}{rB_z} dz, \tag{3.13}$$

where the integral is taken along a field line (i.e. for constant values of the flux function, A).

If the aspect ratio of the loop is large (typically 10 for coronal loops) and excess amounts of twist are not absorbed by the boundary layers, then the twist can be approximated by

$$\Phi = \frac{LB_\theta}{rB_z}, \tag{3.14}$$

so that

$$K(A) = rB_\theta = r^2B_z\frac{\Phi}{L} = r\frac{dA}{dr}\frac{\Phi}{L}, \tag{3.15}$$

and the Grad-Shafranov equation becomes (eliminating K)

$$\left[1+\frac{r^2\Phi^2}{L^2}\right]\frac{d^2A}{dr^2}+\left[-\frac{1}{r}+\frac{d}{dr}\left(\frac{r^2\Phi^2}{2L^2}\right)\right]\frac{dA}{dr}+r^2\mu\frac{dP}{dA}=0, \tag{3.16}$$

The unknown pressure dependence, $P(A)$, can be determined by using either an observed photospheric pressure distribution or conservation of entropy.

For adiabatic processes

$$P/\rho^\gamma = \text{constant}, \tag{3.17}$$

for a volume of plasma contained between two flux surfaces enclosing flux A and $A+\delta A$. The volume of plasma between the flux surfaces A and $A+\delta A$ is

$$\delta V = V(A+\delta A)-V(A)=2\pi\int_{-L/2}^{L/2}\int_{r(A)}^{r(A+\delta A)} r\,dr\,dz$$

$$=2\pi\int_{-L/2}^{L/2}\int_{A}^{A+\delta A}\frac{r}{\partial A/\partial r}dA\,dz=2\pi\int_{A}^{A+\delta A}\int_{-L/2}^{L/2}\frac{dz}{B_z}dA, \tag{3.18}$$

where the z integral is taken at constant A. Lines of constant A give the projection of magnetic fieldlines on the $r-z$ plane. From expression (3.5), rB_θ is constant along fieldlines.

Since plasma cannot cross a flux surface

$$[\rho V]_A^{A+\delta A}=\rho\frac{\delta V}{\delta A}\delta A=\text{constant}, \tag{3.19}$$

and from expression (3.19), using (3.18)

$$2\pi\rho\delta A\int_{-L/2}^{L/2}\frac{dz}{B_z}=\text{constant}, \tag{3.20}$$

We define the pseudo-entropy, S, conserved for adiabatic processes, with $\delta A =$ constant since plasma cannot cross flux surfaces, from (3.17) and (3.20)

$$S(A) = \mu P(A) \left[\int_{-L/2}^{L/2} \frac{dz}{B_z} \right]^{\gamma}, \tag{3.21}$$

In the 1–D case

$$S(A) = \mu P(A) \frac{L^{\gamma}}{B_z^{\gamma}}, \tag{3.22}$$

and the Grad-Shafranov equation (3.16) becomes

$$\left[1 + \frac{r^2\Phi^2}{L^2} + \frac{\gamma S}{L^{\gamma}} \left(\frac{1}{r}\frac{dA}{dr} \right)^{\gamma-2} \right] \frac{d^2A}{dr^2} + \left[-\frac{1}{r} + \frac{r\Phi^2}{L^2} + \frac{r^2\Phi}{L^2}\frac{d\Phi}{dr} \right] \frac{dA}{dr}$$
$$- \frac{\gamma S}{L^{\gamma}} \left(\frac{1}{r}\frac{dA}{dr} \right)^{\gamma-1} + \frac{dS}{dA}\frac{r^2}{L^{\gamma}} \left(\frac{1}{r}\frac{dA}{dr} \right)^{\gamma} = 0, \tag{3.23}$$

By specifying the twist Φ, the pseudo-entropy S as a function of A, the length L, radial coordinate r, and taking γ as $5/3$, the value for an ideal monotonic gas, equation (3.23) was solved numerically to give equilibrium values for B_θ, B_z and p that were then used in the linearized equations of motion.

3.3 Linearized Equations

The ideal linearized equations of motion are decomposed into directions radial, parallel and perpendicular to an equilibrium magnetic field in cylindrical geometry. Then using rigid-wall boundary conditions for loops and Fourier analysing in the poloidal and axial directions, an infinite set of equations of motion connecting the Fourier amplitudes are obtained. The boundary conditions couple the modes in the axial direction.

Starting from an equilibrium magnetic field given by

$$\mathbf{B} = B_\theta(r)\,\mathbf{e}_\theta + B_z(r)\,\mathbf{e}_z, \tag{3.24}$$

and taking unit vectors parallel and perpendicular to the magnetic field as

$$\mathbf{e}_\parallel = \frac{\mathbf{B}}{B}, \tag{3.25a}$$

$$\mathbf{e}_\perp = \frac{B_z\mathbf{e}_\theta - B_\theta\mathbf{e}_z}{B}, \tag{3.25b}$$

as well as the unit vector in the radial direction $\mathbf{e}_r$.

Taking the perturbed Lagrangian displacement vector as

$$\boldsymbol{\xi}(\mathbf{r},t) = \boldsymbol{\xi}(\mathbf{r})\,e^{\sigma t}, \tag{3.26}$$

the linearized equation of motion is

$$\rho\sigma^2\boldsymbol{\xi} = -\nabla p_1 + \frac{1}{\mu}(\nabla\times\mathbf{B})\times\mathbf{B}_1 + \frac{1}{\mu}(\nabla\times\mathbf{B}_1)\times\mathbf{B}, \tag{3.27a}$$

with

$$p_1 = -\boldsymbol{\xi}\cdot\nabla p_0 - \gamma p_0\nabla\cdot\boldsymbol{\xi}, \tag{3.27b}$$

from the linearized adiabatic energy equation, and

$$\mathbf{B}_1 = \nabla\times(\boldsymbol{\xi}\times\mathbf{B}), \tag{3.28}$$

from the linearized induction equation.

After considerable manipulation, the components of the linearized equation of motion can be reduced to

$$\begin{aligned}
\mu\rho\sigma^2\xi_r &= \frac{\partial}{\partial r}\left[\frac{B^2}{r}\frac{\partial\left(r\xi_r\right)}{\partial r}\right] + B^2\left(\mathbf{e}_{\|}\cdot\nabla\right)^2\xi_r - \frac{d}{dr}\left(\frac{{B_\theta}^2}{r^2}\right)r\xi_r \\
&+ \frac{\partial}{\partial r}\left[B^2\mathbf{e}_\perp\cdot\nabla\xi_\perp\right] - \frac{2BB_\theta}{r}\frac{\partial\xi_\perp}{\partial z} + \mu\frac{\partial}{\partial r}\left[\gamma p\nabla\cdot\boldsymbol{\xi}\right], \qquad (3.29a) \\
\mu\rho\sigma^2\xi_\perp &= B^2\left[\left(\mathbf{e}_\perp\cdot\nabla\right)^2 + \left(\mathbf{e}_{\|}\cdot\nabla\right)^2\right]\xi_\perp + \mathbf{e}_\perp\cdot\nabla\frac{B^2}{r}\frac{\partial\left(r\xi_r\right)}{\partial r} \\
&+ 2\frac{BB_\theta}{r}\frac{\partial\xi_r}{\partial z} + \mu\mathbf{e}_\perp\cdot\nabla\left(\gamma p\nabla\cdot\boldsymbol{\xi}\right), \qquad (3.29b) \\
\mu\rho\sigma^2\xi_{\|} &= \mu\mathbf{e}_{\|}\cdot\nabla\left(\gamma p\nabla\cdot\boldsymbol{\xi}\right), \qquad (3.29c) \\
\nabla\cdot\boldsymbol{\xi} &= \frac{1}{r}\frac{\partial}{\partial r}\left(r\xi_r\right) + \mathbf{e}_{\|}\cdot\nabla\xi_{\|} + \mathbf{e}_\perp\cdot\nabla\xi_\perp. \qquad (3.29d)
\end{aligned}$$

Fourier analysing the perturbations in the poloidal and axial directions

$$\begin{aligned}
\xi_r &= Re\sum_{n=-\infty}^{\infty}\sum_{m=-\infty}^{\infty}\xi_{nm}\left(r\right)exp\left\{i\left[m\theta + n\pi\left(2z/L+1\right)\right]\right\}, \qquad (3.30a) \\
\xi_\perp &= Re\sum_{n=-\infty}^{\infty}\sum_{m=-\infty}^{\infty}\zeta_{nm}\left(r\right)exp\left\{i\left[m\theta + n\pi\left(2z/L+1\right)\right] + i\pi/2\right\}, \qquad (3.30b) \\
\xi_{\|} &= Re\sum_{n=-\infty}^{\infty}\sum_{m=-\infty}^{\infty}\eta_{nm}\left(r\right)exp\left\{i\left[m\theta + n\pi\left(2z/L+1\right)\right] + i\pi/2\right\}, \qquad (3.30c)
\end{aligned}$$

where n, m are integers and phase factors have been chosen to make the r-dependent amplitudes real in the linearized equations of motion, since derivatives in the poloidal and axial directions introduce a phase factor of $\pi/2$ into the equations.

Rigid-wall boundary conditions

$$\boldsymbol{\xi} = 0, \text{ at } z = -L/2, L/2, \tag{3.31}$$

imply

$$\forall r, m: \quad \sum_{n=-\infty}^{\infty} \xi_{nm}(r) = 0, \tag{3.32a}$$

$$\forall r, m: \quad \sum_{n=-\infty}^{\infty} \zeta_{nm}(r) = 0, \tag{3.32b}$$

$$\forall r, m: \quad \sum_{n=-\infty}^{\infty} \eta_{nm}(r) = 0, \tag{3.32c}$$

and the modes are coupled in the axial direction but not in the poloidal direction. This means each value of m can be treated separately.

Multiplying equations (3.29) by the appropriate exponential factor and integrating with respect to θ and z

$$\int_0^{2\pi} \int_{-L/2}^{L/2} A \exp\left\{-i\left[m\theta + n\pi\left(2z/L + 1\right)\right]\right\} dz d\theta$$

for (3.29a) and

$$\int_0^{2\pi} \int_{-L/2}^{L/2} A \exp\left\{-i\left[m\theta + n\pi\left(2z/L + 1\right)\right] - i\pi/2\right\} dz d\theta$$

$$\int_0^{2\pi} \int_{-L/2}^{L/2} A \exp\left\{-i\left[m\theta + n\pi\left(2z/L + 1\right)\right] - i\pi/2\right\} dz d\theta$$

for (3.29b) and (3.29c) where A represents any term in the equations (3.29) gives

$$\left[\frac{B^2}{r}(r\xi_n)'\right]' - \left[\mu\rho\sigma^2 + {f_n}^2 + r\left(\frac{{B_\theta}^2}{r^2}\right)'\right]\xi_n + {B_z}^2\lambda_r - [Bg_n\zeta_n]'$$

$$+\frac{2BB_\theta k_n}{r}\zeta_n + \left[\frac{\gamma\mu p}{B}\left\{\frac{B}{r}(r\xi_n)' - f_n\eta_n - g_n\zeta_n\right\}\right]' = 0, \tag{3.33a}$$

$$-\frac{Bg_n}{r}(r\xi_n)' + \left[\mu\rho\sigma^2 + B^2{F_n}^2\right]\zeta_n - B^2\lambda_\perp - \frac{2BB_\theta k_n}{r}\xi_n$$
$$-\frac{\gamma\mu p}{B^2}\left[{B_\theta}^2\lambda_\perp - B_\theta B_z\lambda_\parallel\right] - \frac{\gamma\mu p g_n}{B^2}\left[\frac{B}{r}(r\xi_n)' - f_n\eta_n - g_n\zeta_n\right] = 0, \qquad (3.33b)$$

$$\mu\rho\sigma^2\eta_n + \frac{\gamma\mu p}{B^2}\left[B_\theta B_z\lambda_\perp - {B_z}^2\lambda_\parallel\right]$$
$$-\frac{\gamma\mu p f_n}{B^2}\left[\frac{B}{r}(r\xi_n)' - f_n\eta_n - g_n\zeta_n\right] = 0, \qquad (3.33c)$$

where the suffix m has been dropped, a dash denotes a derivative with respect to r, and

$$f_n = \frac{m}{r}B_\theta + k_n B_z, \qquad (3.34a)$$
$$g_n = \frac{m}{r}B_z - k_n B_\theta, \qquad (3.34b)$$
$$k_n = \frac{2n\pi}{L}, \qquad (3.34c)$$
$$\lambda_r = \frac{1}{L}\left[\int_0^{2\pi}\frac{\partial\xi_r}{\partial z}\exp\{-im\theta\}\,d\theta\right]_{-L/2}^{L/2}, \qquad (3.34d)$$
$$\lambda_\perp = \frac{1}{L}\left[\int_0^{2\pi}\frac{\partial\xi_\perp}{\partial z}\exp\left\{-im\theta - i\frac{\pi}{2}\right\}d\theta\right]_{-L/2}^{L/2}, \qquad (3.34e)$$
$$\lambda_\parallel = \frac{1}{L}\left[\int_0^{2\pi}\frac{\partial\xi_\parallel}{\partial z}\exp\left\{-im\theta - i\frac{\pi}{2}\right\}d\theta\right]_{-L/2}^{L/2}, \qquad (3.34f)$$

The surface terms (3.34d), (3.34e), (3.34f) allow the constraints (3.32) to be applied by rewriting equations (3.33b), (3.33c) in terms of η_n and ζ_n and summing over all

n. Rewriting (3.33b) and (3.33c) as

$$A_n \begin{pmatrix} \eta_n \\ \\ \zeta_n \end{pmatrix} + B_n \left(r\xi_n\right)' + C_n \left(r\xi_n\right) + D_n \begin{pmatrix} \lambda_{\parallel} \\ \\ \lambda_{\perp} \end{pmatrix} = 0, \tag{3.35a}$$

where

$$A_n = \begin{pmatrix} \mu\rho\sigma^2 + \beta f_n^2 & \beta g_n f_n \\ \\ \beta g_n f_n & \mu\rho\sigma^2 + f_n^2 + (1+\beta)\, g_n^2 \end{pmatrix}, \tag{3.35b}$$

$$B_n = \begin{pmatrix} \frac{\beta B f_n}{r} \\ \\ \frac{(1+\beta) B g_n}{r} \end{pmatrix}, \tag{3.35c}$$

$$C_n = \begin{pmatrix} 0 \\ \\ \frac{-2BB_\theta k_n}{r^2} \end{pmatrix}, \tag{3.35d}$$

$$D_n = \begin{pmatrix} -\beta B_z^2 & \beta B_\theta B_z \\ \\ \beta B_\theta B_z & -\left(B^2 + \beta B_\theta^2\right) \end{pmatrix}, \tag{3.35e}$$

and premultiplying (3.35a) by the inverse of A_n gives expressions for η_n and ζ_n in terms of ξ_n, $\lambda_{\parallel}$ and $\lambda_{\perp}$. Summing over all values of n allows the constraints (3.32) to be applied giving expressions for the Lagrange multipliers $\lambda_{\parallel}$ and $\lambda_{\perp}$ in terms of $(r\xi_n)$ and $(r\xi_n)'$. Substituting these expressions back into equation (3.35) gives η_n and ζ_n in terms of $(r\xi_n)$ and $(r\xi_n)'$. The expressions for η_n and ζ_n can be substituted into equation (3.33a) to give an equation involving $(r\xi_n)'$, $(r\xi_n)$ and λ_r

$$\left[\left(\gamma\mu p + B^2\right)\frac{\left(r\xi_n\right)'}{r}\right]' - \left[\frac{\mu\rho\sigma^2 + f_n^2}{r} + \left(\frac{B_\theta^2}{r^2}\right)'\right]\left(r\xi_n\right) - \left(H_n\Phi_n\right)' + K_n\Phi_n + B_z^2\lambda_r = 0, \tag{3.36a}$$

with

$$\Phi_n = \begin{pmatrix} \eta_n \\ \\ \zeta_n \end{pmatrix}, \tag{3.36b}$$

$$H_n = \begin{pmatrix} \beta B f_n & (1+\beta)\, B g_n \end{pmatrix}, \tag{3.36c}$$

$$K_n = \begin{pmatrix} 0 & \frac{2BB_\theta k_n}{r} \end{pmatrix}, \tag{3.36d}$$

and we are left with an infinite set of coupled equations in the Fourier amplitudes ξ_n, $n = 0, \pm 1, \pm 2, \cdots$. By truncating to N equations we can eliminate the Lagrange multiplier, λ_r, by subtracting the N^{th} equation involving λ_r, $(r\xi_N)$ from the remaining $N-1$ equations and $(r\xi_N)$ can be eliminated by using the boundary condition, from (3.32a)

$$\sum_{n=1}^{N} \xi_n = 0, \tag{3.37}$$

to give $N-1$ coupled equations in $N-1$ unknowns $(r\xi_n)$, $n = 1, 2, \cdots, N-1$ which can be written as

$$(U\mathbf{y}')' + V\mathbf{y}' + W\mathbf{y} = \mathbf{0}, \tag{3.38}$$

where $\mathbf{y} = r\boldsymbol{\xi} = r\,(\xi_1,\ \xi_2,\ \cdots,\ \xi_{N-1})^T$.

3.4 Method

A Bulirsch-Stoer variable step integration method was used to find solutions to equation (3.38). The idea is to generate linearly independent solutions to the equations so the required solution can be found as a linear combination of these solutions. Rewrite the $N-1$ second order equations as $2\,(N-1)$ first order equations. A shoot and match method is used to generate solutions. The problem with integrating out from an inner boundary, $r = \epsilon$ is that one of the independent solutions grows while the other decays so that eventually the contribution from the decaying solution is

lost as its value approaches the order of the truncation errors in the numerical integration. The equations are integrated out from the inner boundary, $r = \epsilon$, to a matching point in order to restrict the ratio of the growing solution to that of the decaying solution. By specifying initial values for the eigenfunctions at an outer boundary, $r = R$, the equations are integrated in to the matching point. Generating $N-1$ linearly independent solutions in this way, the eigenfunctions $\boldsymbol{\xi}$ and $d\boldsymbol{\xi}/dr$ are matched as a linear combination of the $N-1$ linearly independent solutions to give the required solution. This reduces to the determinant of a $2(N-1) \times 2(N-1)$ matrix is zero. As it requires several adjustments of the eigenvalue (e.g. loop length) in order to find the zero of the determinant and the equations have to be integrated each time, it is obvious that increasing the number of modes, N, in the Fourier truncated equations will have a large affect on the c.p.u. time required to find a solution. The eigenfunctions, $\boldsymbol{\xi}$, are singular at the origin, $r = 0$, and so a false origin, $r = \epsilon$, is used for the inner boundary. A Frobenius expansion is used to find a relationship between $\boldsymbol{\xi}$ and $d\boldsymbol{\xi}/dr$ to first order. It is found that $\xi \propto r^{m-1}$ for $m \geq 1$ and so $d\boldsymbol{\xi}/dr \approx (m-1)\,\boldsymbol{\xi}/r$ (see Appendix B for derivation).

3.5 Field Profiles

The first field profile investigated allows a check with the results found by Mikic, Schnack and Van Hoven(1990)

$$\Phi/L = \begin{cases} \lambda_e (1-A)^2 & , \quad A \leq 1 \\ 0 & , \quad A > 1 \end{cases}, \tag{3.39a}$$

$$S/L^\gamma = \text{constant}, \tag{3.39b}$$

where Φ is the axial twist of the loop, L is the loop length, λ_e is a parameter measuring the amount of axial twist per unit length of the loop, A is a magnetic flux function and S is the pseudo-entropy defined in section 2.

The second field profile investigated is

$$\Phi/L = \begin{cases} \lambda_e (1-A) & , \quad A \leq 1 \\ 0 & , \quad A > 1 \end{cases}, \tag{3.40a}$$

$$S/L^\gamma = \text{constant}, \tag{3.40b}$$

for which 2–D equilibrium properties have been investigated by Lothian and Hood (1989).

When the number of modes is 2, an analytic solution can be found for the equations in the outer region which can be used directly in place of the integration step in order to check the accuracy of the numerical integration.

The twist, Φ, is zero in the outer region ($A > 1$) and using expression (3.14)

$$B_\theta = 0, \tag{3.41}$$

and from

$$\mathbf{j} = -\frac{1}{\mu}\frac{dB_z}{dr}\mathbf{e}_\theta, \tag{3.42}$$

it is required to take

$$B_z = \text{ constant } = 1, \tag{3.43}$$

in order that the current density is zero.

From expression (3.22) with $S =$ constant

$$pL^\gamma = \text{ constant }, \tag{3.44}$$

The growth rate, σ, is zero as we are interested in the marginal loop length, equations (3.33a), (3.33b) and (3.33c) reduce to

$$\begin{aligned}
&\left[\frac{1}{r}(r\xi_n)'\right]' - f_n^2\xi_n \\
+\lambda_r - (g_n\zeta_n)' + &\left[\gamma p\left(\frac{1}{r}(r\xi_n)' - f_n\eta_n - g_n\zeta_n\right)\right]' = 0, \qquad (3.45a)\\
-\frac{g_n}{r}(r\xi_n)' + F_n^2\zeta_n - \lambda_\perp - \gamma p g_n &\left[\frac{1}{r}(r\xi_n)' - f_n\eta_n - g_n\zeta_n\right] = 0, \qquad (3.45b)\\
-\lambda_{||} - f_n &\left[\frac{1}{r}(r\xi_n)' - f_n\eta_n - g_n\zeta_n\right] = 0, \qquad (3.45c)
\end{aligned}$$

with

$$n = 1, 2 \tag{3.46a}$$

$$f_n = k_n, \tag{3.46b}$$

$$g_n = \frac{m}{r}, \tag{3.46c}$$

$$F_n^2 = \frac{m^2}{r^2} + k_n^2, \tag{3.46d}$$

Equations (3.45) with (3.46a) represent six equations and (3.46a) is used to eliminate the unknowns λ_r, $\lambda_{||}$, $\lambda_\perp$ and reduce the problem to three equations in six unknowns, ξ_1, ξ_2, ζ_1, ζ_2, η_1 and η_2. Then rigid wall boundary conditions

$$\xi_1 + \xi_2 = 0, \tag{3.47a}$$

$$\zeta_1 + \zeta_2 = 0, \tag{3.47b}$$

$$\eta_1 + \eta_2 = 0, \tag{3.47c}$$

are used to reduce the system to three equations in three unknowns, ξ_1, ζ_1, η_1. Choosing $k_1 = k_0 - h$, $k_2 = k_0 + h$, $h = \pi/L$

$$(1+\gamma p)\left[\frac{1}{r}(r\xi_1)'\right]' - \left(k_0^2 + h^2\right)\xi_1 - m(1+\gamma p)\left(\frac{1}{r}\zeta_1\right)' - \gamma p k_0 \eta_1' = 0 \tag{3.48a}$$

$$-\frac{(1+\gamma p)\,m}{r}(r\xi_1)' + \frac{\gamma p m k_0}{r}\eta_1 + \left[\frac{(1+\gamma p)\,m^2}{r^2} + k_0^2 + h^2\right]\zeta_1 = 0 \tag{3.48b}$$

$$\frac{k_0}{r}(r\xi_1)' - \left(k_0^2 + h^2\right)\eta_1 - \frac{m k_0}{r}\zeta_1 = 0 \tag{3.48c}$$

From (3.48b) and (3.48c)

$$\zeta_1 = \frac{m\left(1 + \frac{\gamma p h^2}{k_0^2 + h^2}\right)}{m^2\left(1 + \frac{\gamma p h^2}{k_0^2 + h^2}\right) + \left(k_0^2 + h^2\right) r^2}(r\xi_1)', \tag{3.49a}$$

$$\eta_1 = \frac{k_0 r}{m^2\left(1+\frac{\gamma p h^2}{k_0^2+h^2}\right)+(k_0^2+h^2)\,r^2}\,(r\xi_1)', \tag{3.49b}$$

Substituting (3.49a) and (3.49b) in (3.48a) and simplifying

$$\left[\frac{r}{m^2+K^2r^2}\,(r\xi_1)'\right]' - \xi_1 = 0, \tag{3.50a}$$

with

$$K^2 = \frac{k_0^2+h^2}{\left(1+\frac{\gamma p h^2}{k_0^2+h^2}\right)}, \tag{3.50b}$$

The solution of (3.50) is

$$\xi_1 = a_1 K_m'\left(\frac{[k_0^2+h^2]^{\frac{1}{2}}}{\left[1+\frac{\gamma p h^2}{k_0^2+h^2}\right]^{\frac{1}{2}}}r\right) + a_2 I_m'\left(\frac{[k_0^2+h^2]^{\frac{1}{2}}}{\left[1+\frac{\gamma p h^2}{k_0^2+h^2}\right]^{\frac{1}{2}}}r\right). \tag{3.51}$$

where K_m, I_m are m^{th} order modified Bessel functions. Expression (3.51) represents the analytic solution in the outer region ($A > 1$) with two Fourier modes.

Selecting values for k_0 and L, the equations can be integrated out to the matching point. The values of ξ_1 and $d\xi_1/dr$ are used to calculate a_1 and a_2 in (3.51). Then the value of R, the outer radial boundary, which gives $\xi_1 = 0$ is found. Using a shoot and match method taking this value of R as the outer radial boundary, the marginal loop length is calculated by the numerical program and is equal to L.

In addition to the two numerically generated fields, three analytic field profiles were investigated.

The Gold-Hoyle constant twist field

$$B_\theta = \frac{r}{1+r^2}, \tag{3.52a}$$

$$B_z = \frac{\lambda}{1+r^2}, \tag{3.52b}$$

$$p = p_0 + \frac{1-\lambda^2}{2\left(1+r^2\right)^2}, \tag{3.52c}$$

Anzer field

$$B_\theta = re^{-r/2}, \tag{3.53a}$$

$$B_z = \lambda\left[\sigma + \left(2+2r-r^2\right)e^{-r}\right]^{1/2}, \tag{3.53b}$$

$$p = \frac{1}{2}\left(1-\lambda^2\right)\left[p_0 + \left(2+2r-r^2\right)e^{-r}\right]^{1/2}, \tag{3.53c}$$

and the field

$$B_\theta = r\left(1-r^2\right), \tag{3.54a}$$

$$B_z = \lambda\left[1+\frac{1}{3}\left(1-r^2\right)^2\left(1-4r^2\right)\right]^{1/2}, \qquad r \le 1 \tag{3.54b}$$

$$p = p_0 + \frac{1}{2}\left(1-\lambda^2\right)\left[1+\frac{1}{3}\left(1-r^2\right)^2\left(1-4r^2\right)\right], \tag{3.54c}$$

$$B_\theta = 0, \quad B_z = \lambda, \quad p = \sigma + \frac{1}{2}\left(1-\lambda^2\right), \qquad r > 1 \tag{3.54d}$$

The last field profile is obtained by setting $B_\theta = f(r)$ for some function $f(r)$ with $f(r) = 0$ for $r = 0$ and $r = 1$ and the using the equilibrium equation

$$\frac{d}{dr}\left[p + \frac{1}{2}\left(B_\theta^2 + B_z^2\right)\right] = -\frac{B_\theta^2}{r}, \tag{3.55}$$

to obtain an expression for $p + \frac{1}{2}B_z^2$ in terms of the radial coordinate, r.

4 Stability of line–tied coronal loops

In this chapter, two numerically generated fields and three analytic fields will be considered. By specifying the twist per unit loop length (Φ/L) and the pseudo-entropy per unit length (S/L^{γ}), the field components B_{θ}, B_z and p, and their radial derivatives are calculated.

4.1 Loop Profile 1

The first twist profile to be considered is

$$\Phi/L = \begin{cases} \lambda_e (1-A)^2 & , \quad A \leq 1 \\ 0 & , \quad A > 1 \end{cases} \tag{4.1}$$

with

$$S/L^{\gamma} = \text{constant}, \tag{4.2}$$

where A is a flux function, L is the length of the loop, γ is taken to be $5/3$, Φ is the twist of the loop, and λ_e is a parameter specifying the axial twist per unit length of the loop, and S is the pseudo-entropy. The boundary of the flux tube surrounded by a uniform magnetic field in a uniform plasma is given by $A = 1$. The motivation behind this particular choice of twist profile is to compare with the results obtained by Mikic, Schnack and Van Hoven (1990).

A typical field profile as a function of the radial coordinate is shown in figure 4.1 with $\lambda_e = \pi$ and $S/L^{\gamma} = 0.1$. The axial component of the magnetic field and the

plasma pressure have maxima on the axis, fall to a minimum value within the flux tube and then increase in value out to the edge of the flux tube.

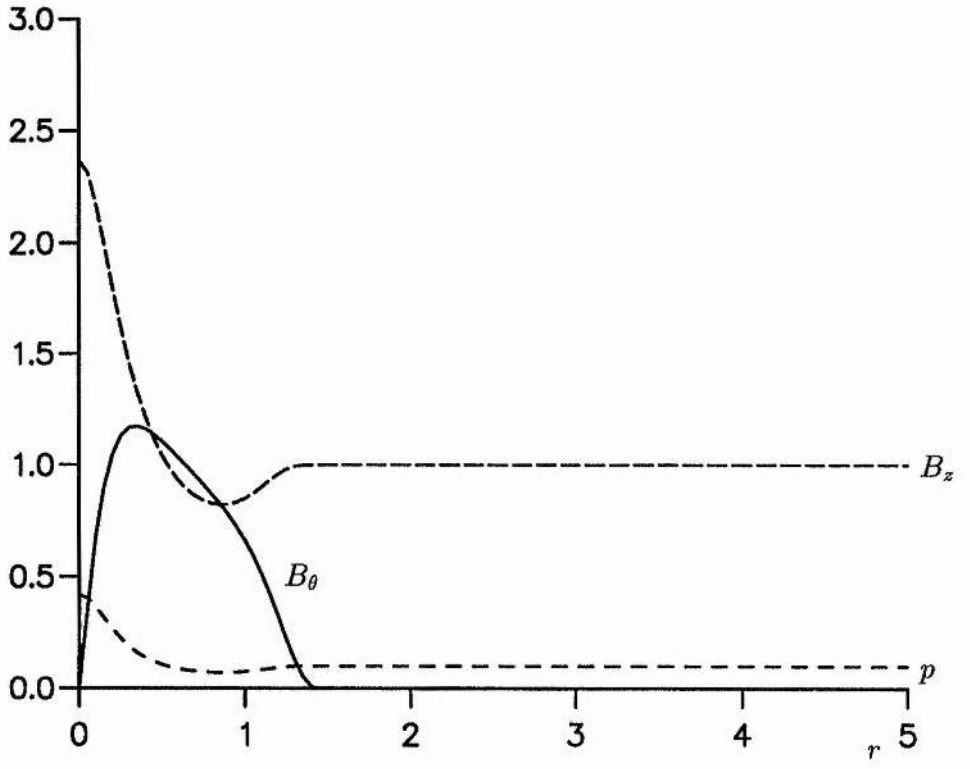

Figure **4.1**: Poloidal magnetic field B_θ (full line), axial magnetic field B_z (upper dashed line) and pressure profiles p (lower dashed line) as a function of the radial coordinate for the first field profile with axial twist per unit length, $\lambda_e = \pi$, and pseudo-entropy per unit length, $S/L^\gamma = 0.1$.

Outside the flux tube the axial magnetic field and plasma pressure are uniform. The poloidal component of the magnetic field increases from zero on the axis to a

maximum value within the flux tube and then decreases to zero at the boundary of the flux tube. There is no component of the poloidal magnetic field outside the flux tube, given by $A > 1$, which is expected from the zero twist in the twist profile (4.1).

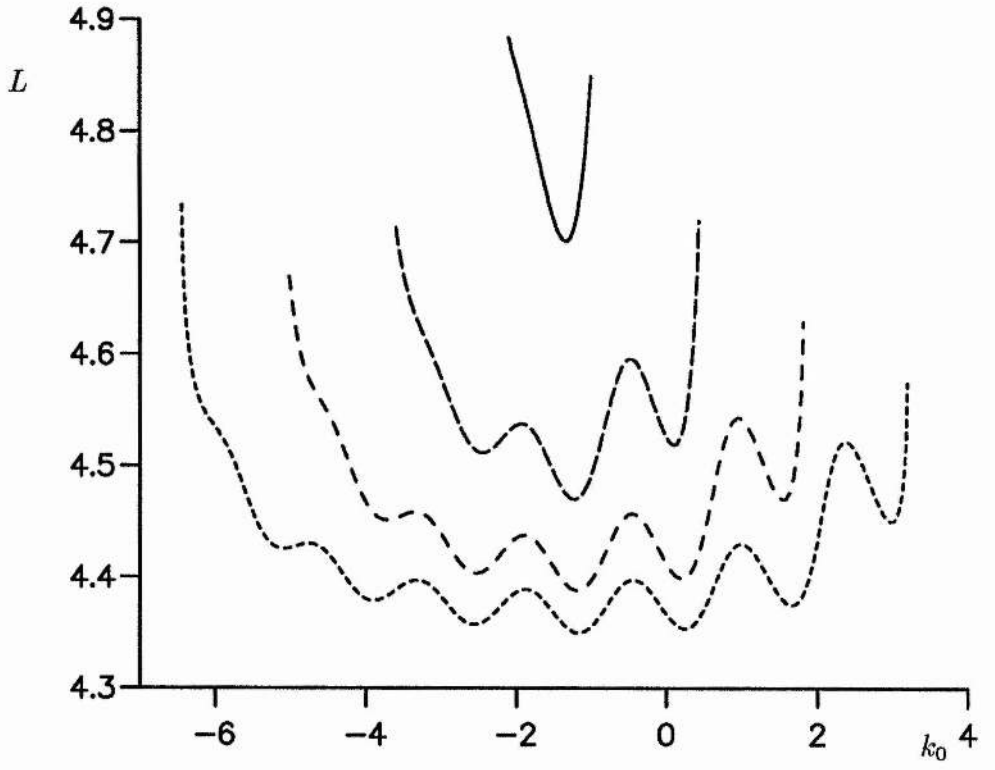

Figure **4.2**: Marginal loop length, L, as a function of the central wavenumber, k_0 with axial twist per unit length, $\lambda_e = \pi$, pseudo-entropy per unit length, $S/L^\gamma = 0.005$ for 3, 5, 7 and 9 Fourier modes (in order of increasing dash length).

A finite number of Fourier modes is being used to approximate an infinite set of Fourier modes. In order to improve the convergence of the Fourier series, a central

wavenumber is introduced. Using $2n + 1$ Fourier modes, one mode is the central wavenumber, k_0, and the other $2n$ are chosen so that n modes lie on one side of the central wavenumber, and n modes on the other side

$$k_i = k_0 + 2\pi i/L, \qquad i = \pm 1, \pm 2, \pm 3, \cdots, \pm n \tag{4.3}$$

By varying the central wavenumber, k_0, the marginal loop length for stability is found. The central wavenumber of interest is given by the smallest value of the marginal loop length as loop lengths greater than this smallest value are unstable. The marginal loop length for the $m = 1$ kink mode as a function of central wavenumber is shown in figure 4.2 for 3, 5, 7 and 9 modes with $\lambda_e = \pi$, $S/L^\gamma = 0.005$. Increasing the number of Fourier modes has the effect of increasing the number of oscillations in the figure as the most unstable modes will be included as sidebands for a greater range of central wavenumber values. Increasing the number of modes decreases the marginal loop length indicating that a finite number of Fourier modes gives an overestimate of the marginal loop length and hence an overestimate of stability. It is noted that the actual choice of central wavenumber becomes less important as n increases. In the limit as $n \to \infty$ there is no need for the central wavenumber k_0.

A problem in the integration of the equations is their singular nature on the axis ($r = 0$). In order to get round this problem a false origin is selected at a small value of r. A Frobenius expansion of the Fourier truncated equations is performed in order to find the relation between the eigenfunction, ξ_r and its radial derivative. A

detailed derivation is performed in Appendix B. Figure 4.3 shows the marginal loop length as a function of the position of the false origin, with $\lambda_e = \pi$, $S/L^\gamma = 0.005$ and 5 Fourier modes. Moving the false origin away from the axis increases the marginal loop length calculated. This is expected since the twist is a maximum on the axis and decreases to zero at the flux tube boundary.

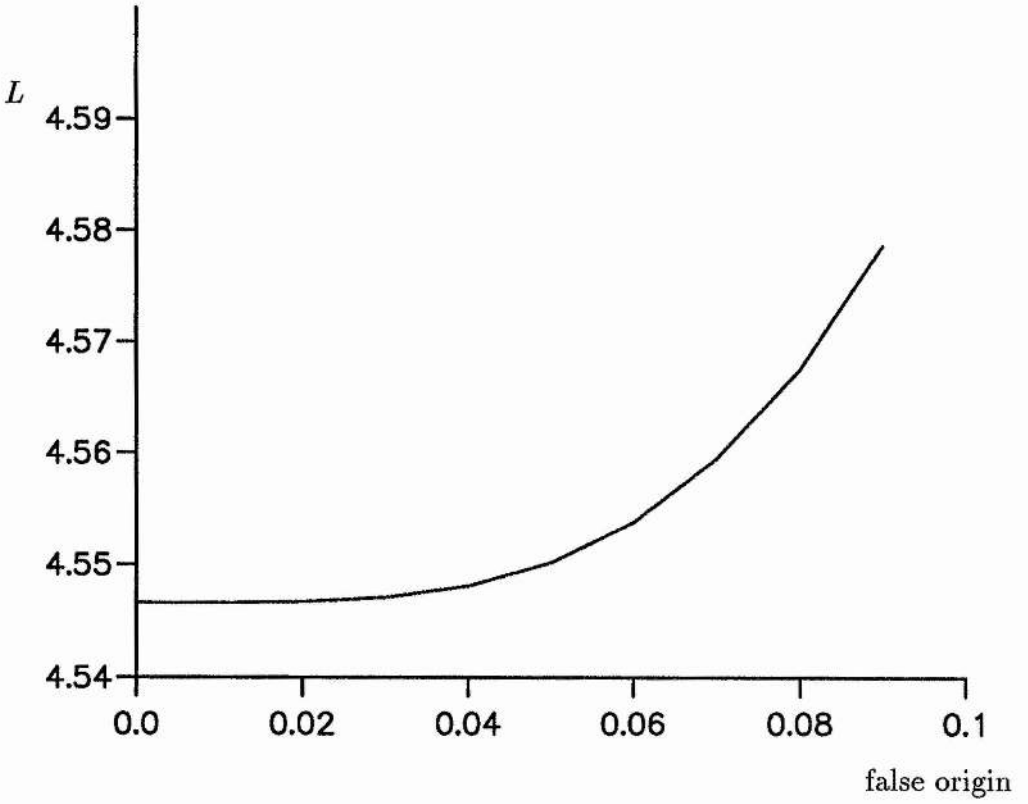

Figure **4.3**: Marginal loop length, L, as a function of the position of the false origin with axial twist per unit length, $\lambda_e = \pi$, pseudo-entropy per unit length, $S/L^\gamma = 0.005$ for 5 Fourier modes.

Moving the false origin away from the axis is equivalent to using a smaller value of

axial twist which is a stabilizing effect. In the calculations a false origin of $\epsilon = 10^{-4}$ was selected as it was found that taking values of $\epsilon = 10^{-5}$, 10^{-4} and 10^{-3} give solutions which agree to the 6 significant figures calculated.

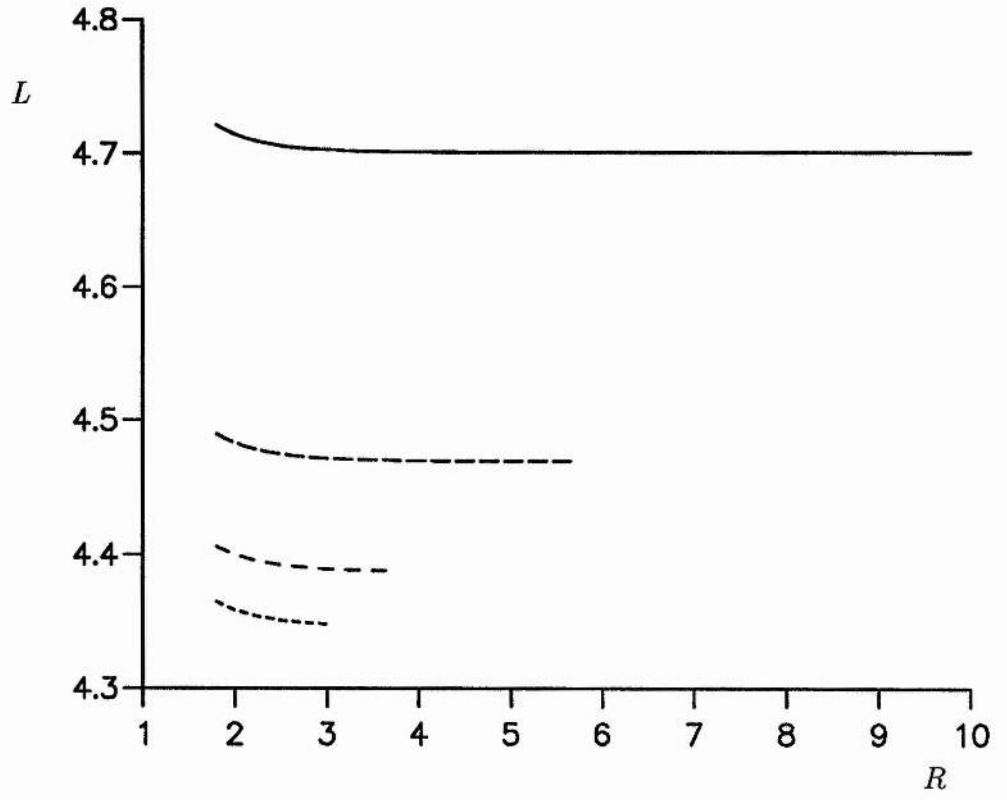

Figure **4.4**: Marginal loop length, L, as a function of the position of the outer radial boundary, R, with axial twist per unit length, $\lambda_e = \pi$, pseudo-entropy per unit length, $S/L^\gamma = 0.005$ for 3, 5, 7 and 9 Fourier modes (in order of decreasing dash length).

An artificial numerical outer boundary where the eigenfunctions are set to zero will have the effect of stabilizing the equilibrium since an extra constraint has been

imposed. The basic idea is to place the outer boundary sufficiently far from the axis in order that the marginal loop lengths calculated are unaffected by the boundary. Taking the outer boundary too far out has two main drawbacks, the first is the extra computational time required to integrate in to the matching point. The second is that the ratio of the growing exponential component of the eigenfunction to the decaying exponential component of the eigenfunction increases and the numerical errors generated ensure that smaller stepsizes have to be taken giving greater computational times or a breakdown of the numerical integration.

Figure 4.4 shows the marginal loop length, L, as a function of the position of the outer radial boundary, R, for $\lambda_e = \pi$, $S/L^\gamma = 0.005$ for 3, 5, 7 and 9 Fourier modes. It was found that taking $R \geq 5.6$ ($\approx 4r_0$) gives no change in the results for the marginal loop length to 6 significant figures. To overcome the numerical integration difficulties, the outer boundary has been selected as shown in Table 4.1.

number of modes	R
3	10.0
5	5.0
7	3.6
9	2.7

Table **4.1**: Values of the outer radial boundary used for different numbers of Fourier modes in this chapter

It was found that increasing the number of Fourier modes leads to an increase in the ratio of the growing exponential component to the decaying exponential component of the eigenfunction. This results in the decaying exponential being 'lost' as it approaches the same order of magnitude as the truncation error of the numerical scheme for a smaller value of the radial component. This makes the numerical scheme an effective random number generator if the outer boundary, R, is chosen too large. It was found that for 9 Fourier modes, solutions could be obtained with an outer boundary of $R = 2.7$ but for $R \geq 2.8$, the numerical scheme was giving random results. The results for 5 Fourier modes are accurate to 5 significant figures using an outer boundary of $R = 5.0$ rather than $R \geq 5.6$. Decreasing the radius of the outer boundary, R, is a stabilizing effect and values of marginal loop length obtained for 7 and 9 Fourier modes will be greater than the values that would be the case for $R \geq 5.6$ required to compare with the results of Mikic, Schnack and Van Hoven (1990).

Figure 4.5 shows the axial twist λ_e/π as a function of the marginal loop length for the kink mode for 5, 7 and 9 Fourier modes in order to compare with the $\Phi = 4.8\pi$, $L = 4r_0$, $R = 4r_0$ result of Mikic, Schnack and Van Hoven (1990). Taking $S/L^\gamma = 0.005$ gives an untwisted value of the plasma beta, $\beta_0 = 0.1$, for a loop length of $L = 4r_0$. The figure shows good agreement with the result obtained by Mikic, Schnack and Van Hoven (1990) shown by a cross in the figure, with the results tending to converge to their value as the number of Fourier modes is increased. The

figure shows that as the loop length, L, is increased the critical twist in the loop, Φ, is increased. As the loop length is increased, the critical twist per unit length, Φ/L, is decreased.

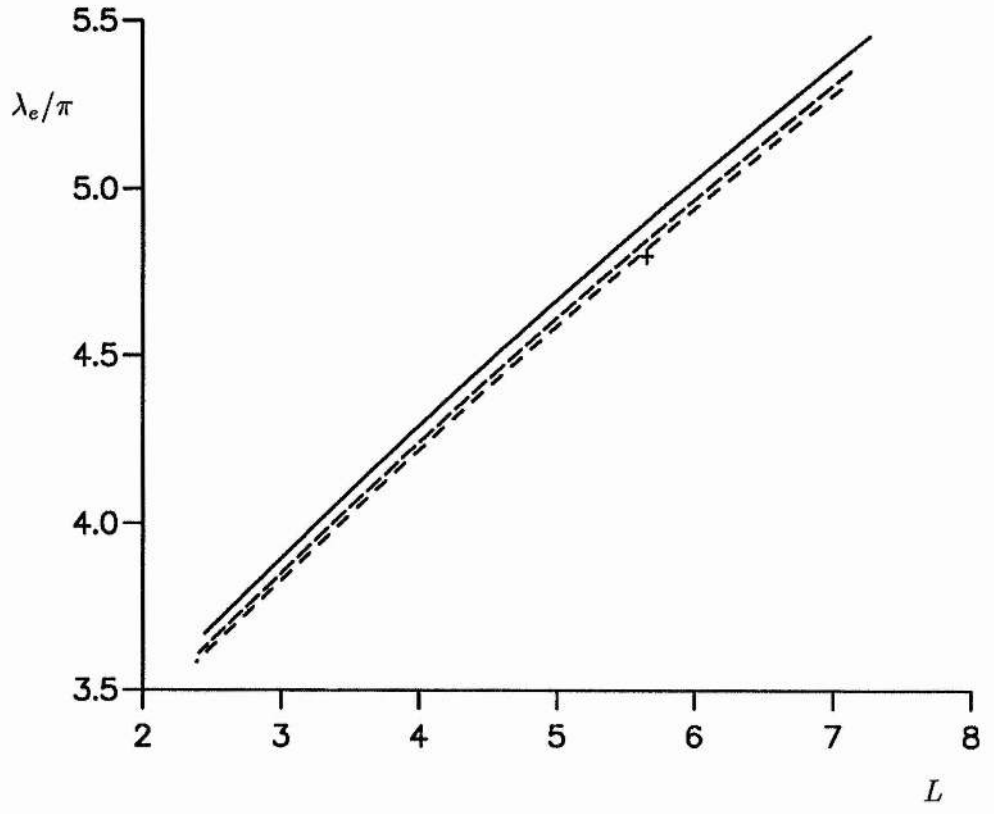

Figure **4.5**: Critical axial twist/π, λ_e/π, as a function of the loop length, L, with pseudo-entropy per unit length, $S/L^\gamma = 0.005$ for 5, 7 and 9 Fourier modes (in order of decreasing dash length). The cross represents the result of Mikic, Schnack and Van Hoven (1990) for comparison.

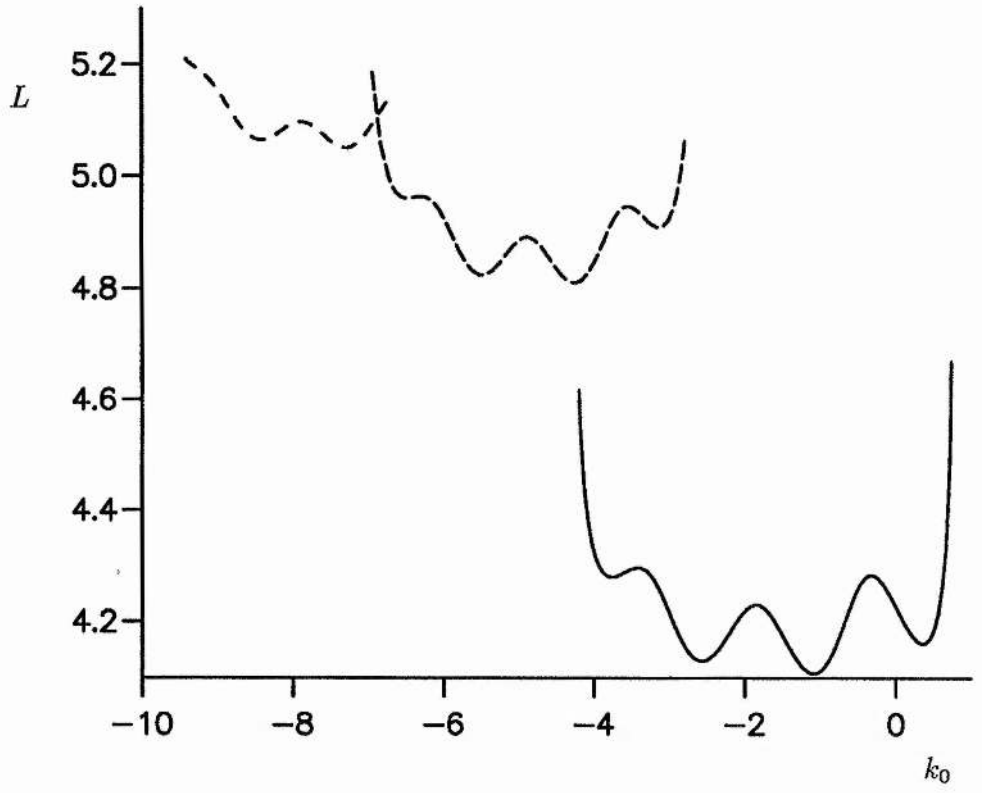

Figure **4.6**: Marginal loop length, L, as a function of central axial wavenumber, k_0 for m=1, 2 and 3 (in order of decreasing dash length) with axial twist per unit length, $\lambda_e = \pi$, and pseudo-entropy per unit length, $S/L^\gamma = 0.3$.

Figure 4.6 shows the marginal loop length as a function of the central wavenumber with 5 Fourier modes, $\lambda_e = \pi$, $S/L^\gamma = 0.3$ for the $m = 1$ kink mode together with the $m = 2$ and $m = 3$ modes. The central wavenumber giving the lowest value of marginal loop length is displaced in the negative direction as the poloidal wavenumber increases. To generate this figure takes a great deal of computing time. An approximate value for the central wavenumber, k_0, has to be known as outside

a small range of values for k_0 the loop length, L, tends to infinity. There is also a problem in making sure that higher harmonic solutions have not been obtained by noting the sign of the matrix determinant for values of L smaller and larger than the marginal loop length solution values. Once a solution for L given k_0 has been found the central wavenumber, k_0, can be adjusted to find a nearby solution. Enough values of k_0 and L have to be calculated in order that all the oscillations of the curve show up and trial values of the marginal loop length are sufficiently close to the marginal loop length to ensure convergence and prevent jumping to other harmonic solutions. The critical value of the loop length is given by the minimum value of L obtained for each curve. Any value of loop length greater than this value will be unstable to modes with central wavenumber corresponding to the critical loop length. The figure was obtained for one value of the axial twist per unit length, λ_e/L, and pseudo-entropy per unit length, S/L^γ. By changing the value of S/L^γ in figure 4.6 and noting the minimum L values, figure 4.7 was obtained. Each point on the curves is taken from the minimum of a set of points similar to that shown by figure 4.6 with $S/L^\gamma = 0.3$.

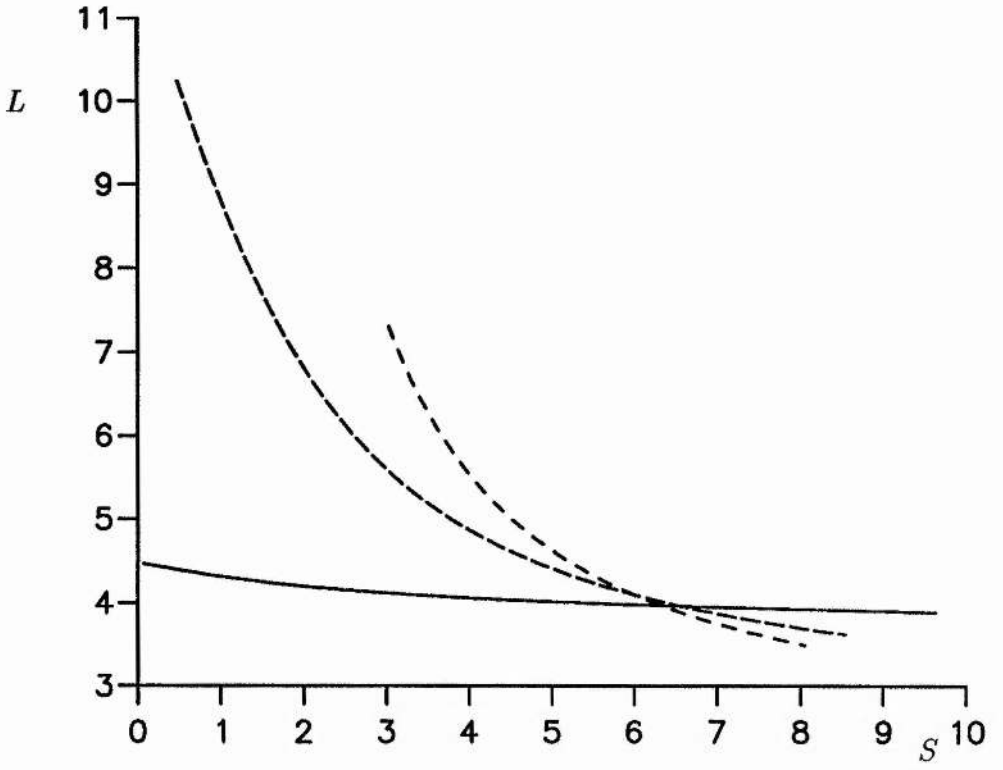

Figure **4.7**: Marginal loop length, L, as a function of the pseudo-entropy, S, with axial twist per unit length, $\lambda_e = \pi$, for 5 Fourier modes with m=1, 2 and 3 (in order of decreasing dash length).

Figure 4.7 shows marginal loop length as a function of the pseudo-entropy, S, with $\lambda_e = \pi$ and 5 Fourier modes for poloidal wavenumbers $m = 1$, $m = 2$ and $m = 3$. For small values of S, near-force-free conditions, the $m = 1$ kink mode is the most unstable. As S increases, plasma pressure and pressure gradients increase. All modes become more unstable and for high values of the pseudo-entropy, the $m = 1$ kink mode is no longer the most unstable mode. This agrees with the results of De

Bruyne and Hood (1992) for the case of the Gold-Hoyle uniform twist field and the Anzer field. However, it needs to be shown that this is still true as the number of Fourier modes is increased. Figure 4.8 shows that the reversal in the stability of the three modes holds also for 7 modes.

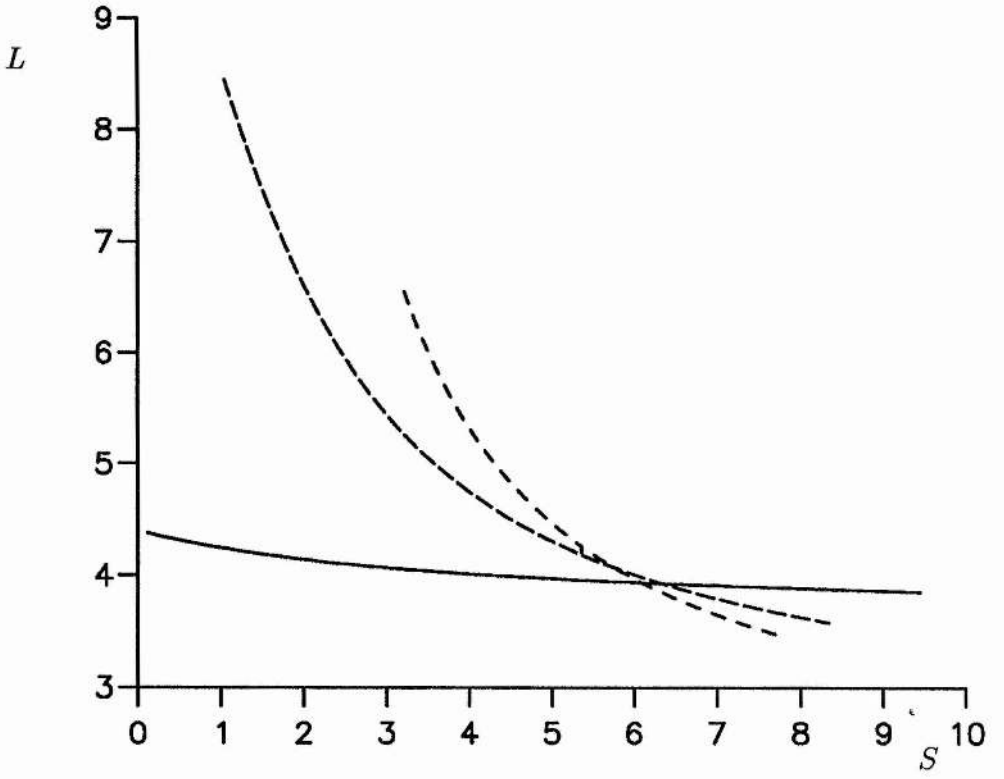

Figure **4.8**: Marginal loop length, L, as a function of the pseudo-entropy, S, with axial twist per unit length, $\lambda_e = \pi$, for 7 Fourier modes with m=1,2 and 3 (in order of decreasing dash length).

4.2 Loop Profile 2

The second twist profile to be considered is

$$\Phi/L = \begin{cases} \lambda_e (1 - A) & , \quad A \leq 1 \\ 0 & , \quad A > 1 \end{cases} \tag{4.4}$$

with

$$S/L^{\gamma} = \text{constant}, \tag{4.5}$$

where A is a flux function, L is the length of the loop, γ is taken to be $5/3$, Φ is the twist of the loop, and λ_e is a parameter specifying the axial twist per unit length of the loop, and S is the pseudo-entropy.

Lothian and Hood (1989) considered this twist profile and looked at the effect of small twist on the equilibrium. They found that twisting the field caused a compression of the magnetic fieldlines within the flux tube and that most of the loop is essentially straight with the axial dependence occurring in a small boundary layer at the ends of the loop extending into the loop a distance of the order of the radius of the flux tube. Thus if the aspect ratio of the loop is taken to be large (typically 10 for coronal loops) most of the loop can be approximated by a one dimensional model which will give good agreement with the results obtained using a two dimensional model.

A typical field profile as a function of the radial coordinate with $\lambda_e = \pi$, $S/L^{\gamma} = 0.1$ is shown in figure 4.9. This is obtained using the 1-D equilibrium equation (3.12). The behaviour of the field is similar in shape to the first profile with the

axial magnetic field and plasma pressure decreasing from maxima to minima within the flux tube and then increasing to the boundary of the flux tube. Outside the flux tube the axial magnetic field and plasma pressure are constant. The poloidal magnetic field increases from zero on the axis to a maximum value within the flux tube and then decreases to zero at the boundary of the flux tube.

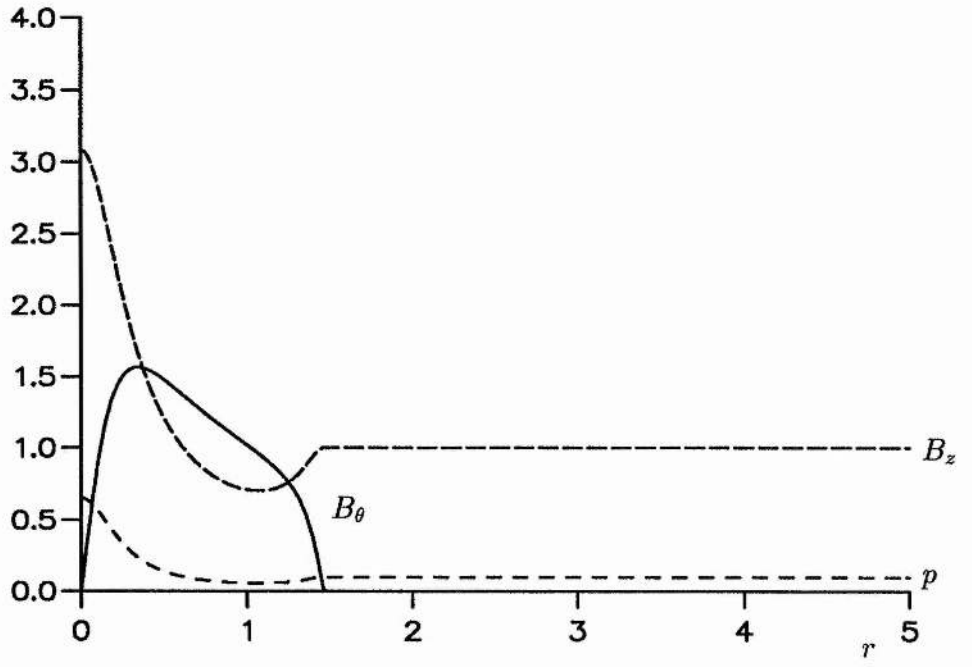

Figure **4.9**: Poloidal magnetic field B_θ (full line), axial magnetic field B_z (upper dashed line) and pressure profiles p (lower dashed line) as a function of the radial coordinate for the second field profile with axial twist per unit length, $\lambda_e = \pi$, and pseudo-entropy per unit length, $S/L^\gamma = 0.1$.

Outside the flux tube the poloidal magnetic field is zero. The field components and their derivatives have greater values than the first profile shown in figure 4.1. As

this happens for profile 1 if the axial twist per unit length, λ_e, is increased which is a destabilizing effect, smaller values of the marginal loop length can be expected for profile 2 compared to profile 1 given the same values of axial twist per unit length, λ_e, and pseudo-entropy per unit length, S/L^γ.

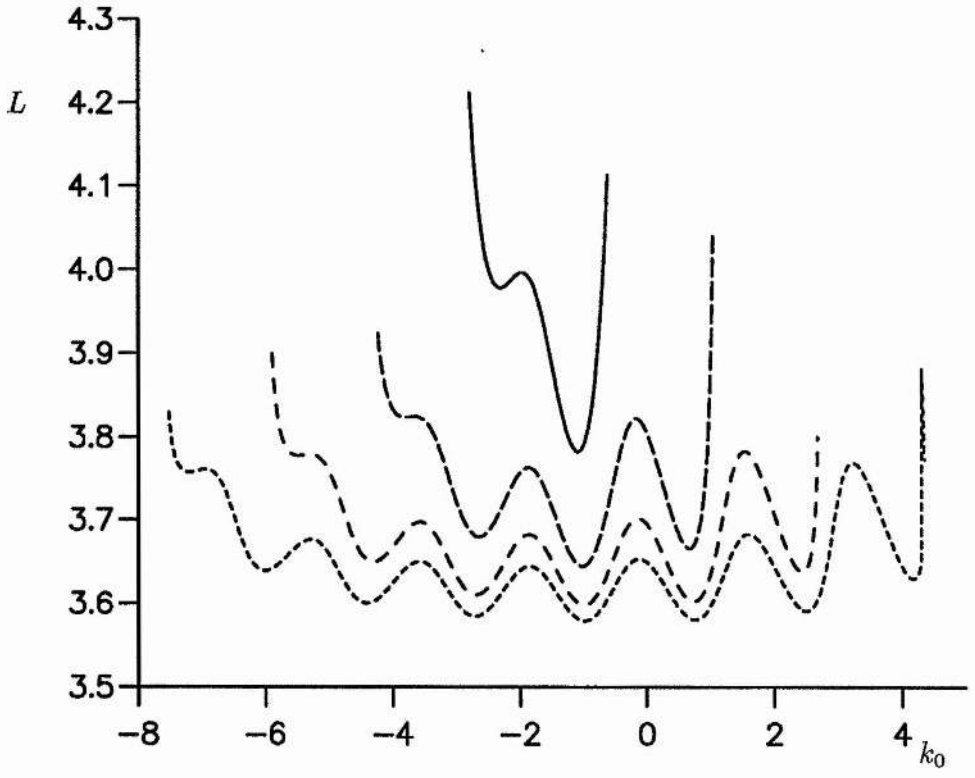

Figure **4.10**: Marginal loop length, L, as a function of the central wavenumber, k_0 with axial twist per unit length, $\lambda_e = \pi$, pseudo-entropy per unit length, $S/L^\gamma = 0.1$ for 3, 5, 7 and 9 Fourier modes (in order of increasing dash length).

The marginal loop length as a function of the central wavenumber, k_0, with $\lambda_e = \pi$ and $S/L^\gamma = 0.1$ is shown by figure 4.10 for 3, 5, 7 and 9 Fourier modes.

As for the first profile, increasing the number of Fourier modes has the effect of increasing the number of oscillations in the figure as the most unstable modes become sidebands for a greater range of central wavenumber values. As the number of Fourier modes is increased, the marginal loop length is decreased. This is expected since the boundary conditions are used to connect the sum of the Fourier modes and the greater the number of Fourier modes the smaller is the restrictive effect of the boundary condition on each of the Fourier modes giving a smaller overestimate of stability. Comparing the curve for 3 Fourier modes for the second profile in figure 4.10 with figure 4.2 for the first profile, there appears to be an extra oscillation. This is not the case as the first profile has a smaller value of S/L^{γ} and so one sideband oscillation is not showing on the scale of figure 4.2.

The marginal loop length as a function of the radial position of the false origin is shown in figure 4.11 with $\lambda_e = \pi$, $S/L^{\gamma} = 0.1$ and 5 Fourier modes. The position of the false origin was chosen to be $\epsilon = 10^{-4}$ as it was found that $\epsilon = 10^{-5}$, $\epsilon = 10^{-4}$ and $\epsilon = 10^{-3}$ give the same value of marginal loop length to the 6 significant figures calculated. The overestimate of the marginal loop length as the false origin is moved away from the axis is expected as the influence of the twisted field within this radius is lost and within this region the twist is greatest as the twist falls from a maximum value on the axis to zero at the flux tube boundary.

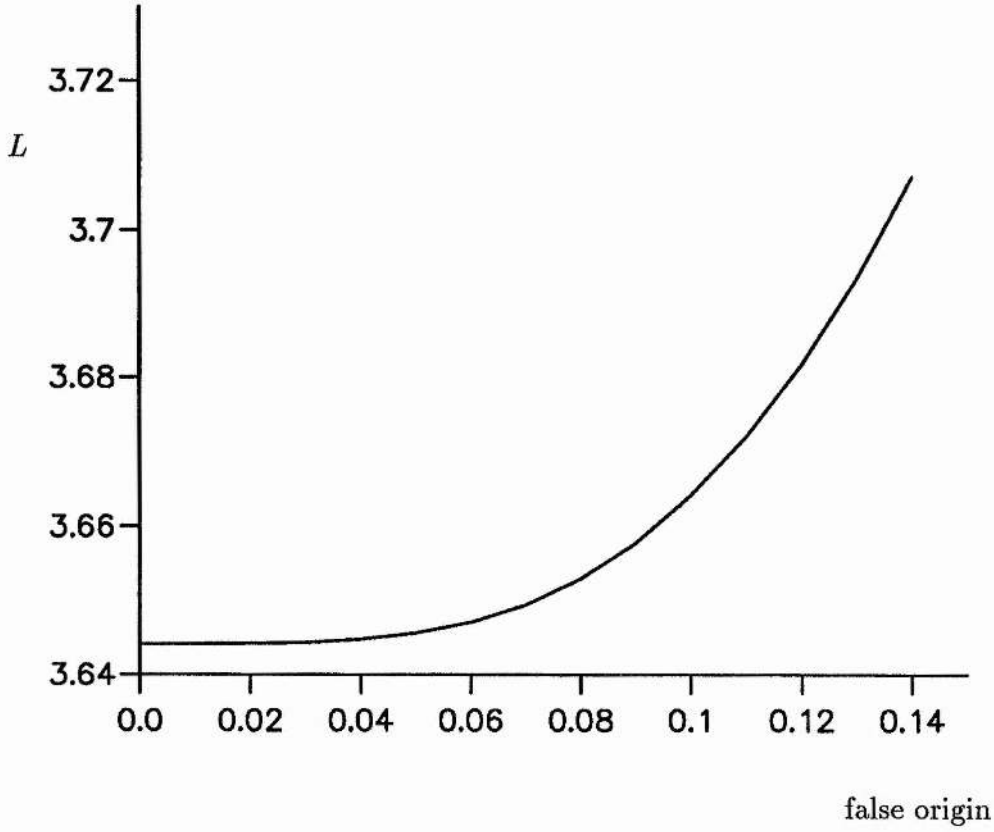

Figure **4.11**: Marginal loop length, L, as a function of the position of the false origin with axial twist per unit length, $\lambda_e = \pi$, pseudo-entropy per unit length, $S/L^\gamma = 0.1$ for 5 Fourier modes.

The marginal loop length as a function of the position of the outer radial boundary is shown in figure 4.12 with $\lambda_e = \pi$, $S/L^\gamma = 0.1$, for 3, 5, 7 and 9 Fourier modes. The stabilizing effect of imposing an extra constraint by this artificial numerical boundary is reduced as the position of the outer boundary moves away from the axis. This is evident in figure 4.12 from the decrease in the marginal loop length as R is increased.

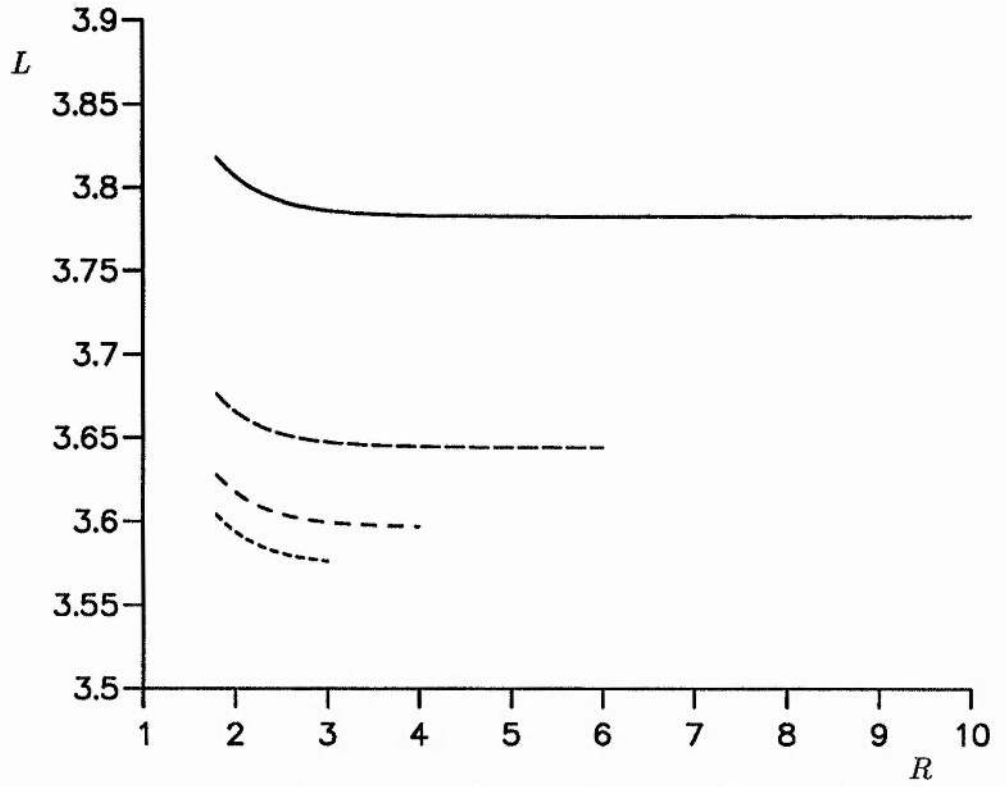

Figure **4.12**: Marginal loop length, L, as a function of the position of the outer radial boundary, R, with axial twist per unit length, $\lambda_e = \pi$, pseudo-entropy per unit length, $S/L^\gamma = 0.1$ for 3, 5, 7 and 9 Fourier modes (in order of decreasing dash length).

The axial twist, λ_e/π, as a function of the marginal loop length, L, with $S/L^\gamma = 0.1$ for the kink mode with 5, 7 and 9 Fourier modes is shown in figure 4.13. For the same twist, increasing the number of Fourier modes increases the marginal loop length and stability of the system. This is not in contradiction with figures 4.7 and 4.10 where marginal loop lengths decrease with an increase in the number of Fourier

modes since the axial twist per unit length is given by $\lambda_e/L = \pi$ and so the axial twist, λ_e, of the different Fourier mode curves in the figures is decreased with an increase in the number of Fourier modes and marginal loop length is increased for greater values of twist as shown by figure 4.13.

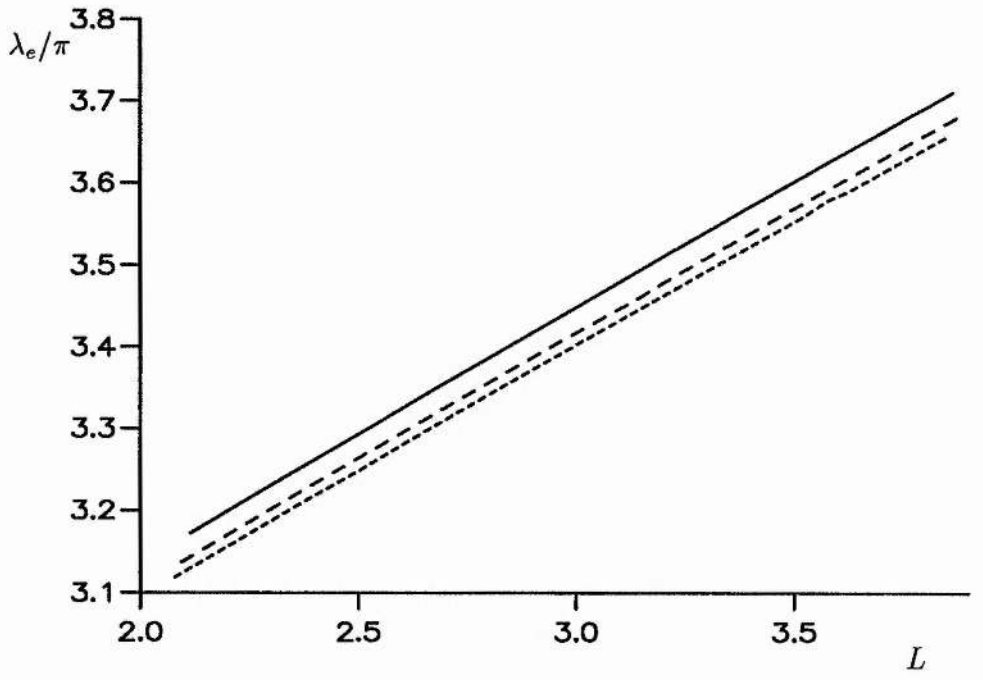

Figure **4.13**: Critical axial twist/π, λ_e/π as a function of the loop length, L, with pseudo-entropy per unit length, $S/L^\gamma = 0.1$ for 5, 7 and 9 Fourier modes (in order of decreasing dash length).

The marginal loop length, L, as a function of the central wavenumber, k_0, for 5 Fourier modes, $\lambda_e = \pi$ and $S/L^\gamma = 0.3$ is shown in figure 4.14 for poloidal wavenumbers m=1, 2 and 3. The same number of oscillations occur for each poloidal

mode as would be expected since this is affected by the number of truncated Fourier modes used. The poloidal modes are displaced towards increasingly negative central axial wavenumbers as the poloidal wavenumber increases.

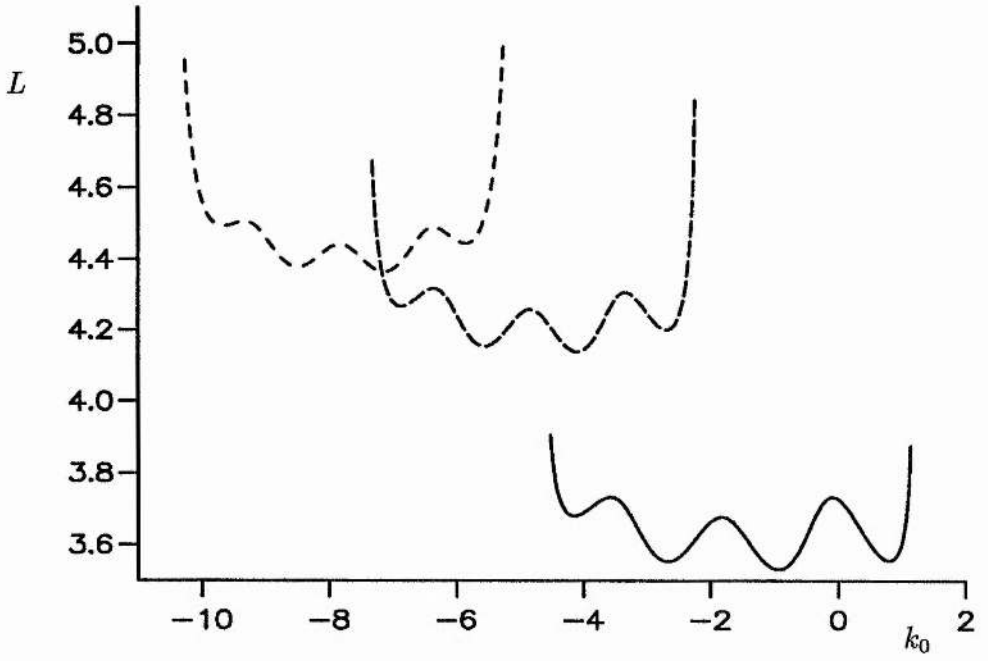

Figure **4.14**: Marginal loop length, L, as a function of central axial wavenumber, k_0 for m=1, 2 and 3 (in order of decreasing dash length) with axial twist per unit length, $\lambda_e = \pi$, and pseudo-entropy per unit length, $S/L^\gamma = 0.3$.

The marginal loop length, L, as a function of the pseudo-entropy, S, with $\lambda_e = \pi$ and 5 Fourier modes is shown in figure 4.15 for the $m = 1$ kink mode and the $m = 2$ and $m = 3$ modes. For small S, near-force-free conditions, the kink mode is the most unstable, and as S is increased all three modes are destabilized by the greater

plasma gradients. For large S, there is a reversal in the relative stability of the three modes in agreement with the earlier result of figure 4.7. As for the first profile, it needs to be shown that this is still true as the number of Fourier modes is increased.

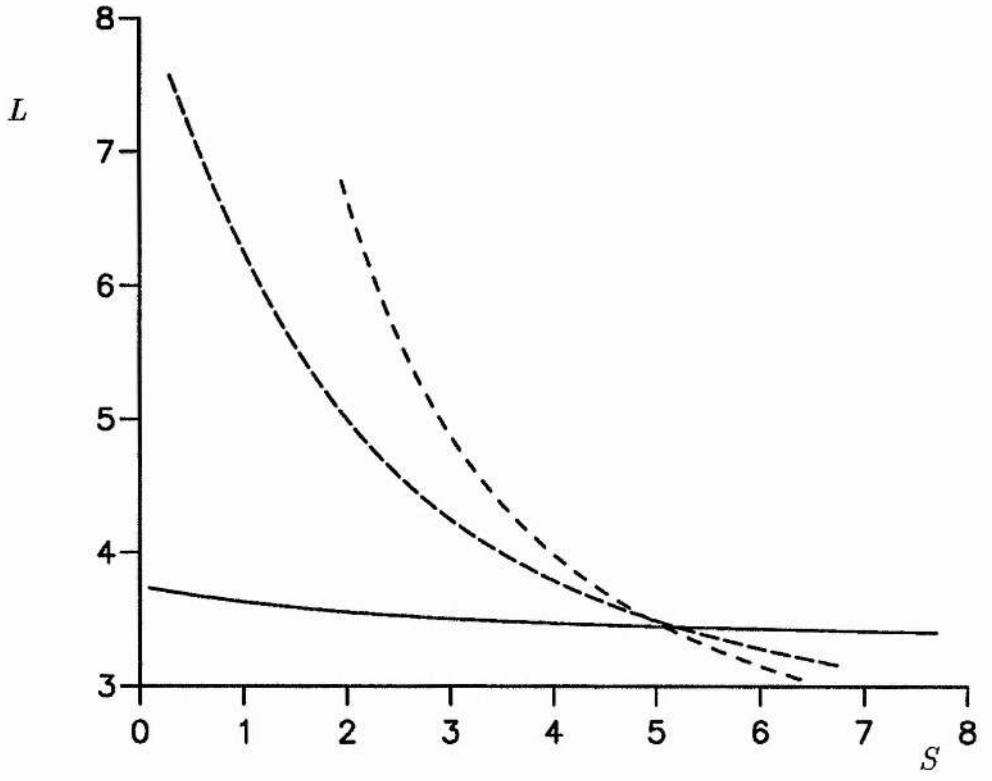

Figure **4.15**: Marginal loop length, L, as a function of the pseudo-entropy, S, with axial twist per unit length, $\lambda_e = \pi$, for 5 Fourier modes with m=1, 2 and 3 (in order of decreasing dash length).

4.3 Analytic profiles

Figures 4.16a, b, c show field profiles for axial and azimuthal magnetic fields and

plasma pressures for the profiles given by,

the Gold-Hoyle constant twist field

$$B_\theta = \frac{r}{1+r^2}, \tag{4.6a}$$

$$B_z = \frac{\lambda}{1+r^2}, \tag{4.6b}$$

$$p = p_0 + \frac{1-\lambda^2}{2\left(1+r^2\right)^2}, \tag{4.6c}$$

Anzer field

$$B_\theta = re^{-r/2}, \tag{4.7a}$$

$$B_z = \lambda\left[p_0 + \left(2+2r-r^2\right)e^{-r}\right]^{1/2}, \tag{4.7b}$$

$$p = \frac{1}{2}\left(1-\lambda^2\right)\left[p_0 + \left(2+2r-r^2\right)e^{-r}\right]^{1/2}, \tag{4.7c}$$

and the field

$$B_\theta = r\left(1-r^2\right), \tag{4.8a}$$

$$B_z = \lambda\left[1+\frac{1}{3}\left(1-r^2\right)^2\left(1-4r^2\right)\right]^{1/2}, \qquad r \le 1 \tag{4.8b}$$

$$p = p_0 + \frac{1}{2}\left(1-\lambda^2\right)\left[1+\frac{1}{3}\left(1-r^2\right)^2\left(1-4r^2\right)\right], \tag{4.8c}$$

$$B_\theta = 0, \quad B_z = \lambda, \quad p = p_0 + \frac{1}{2}\left(1-\lambda^2\right), \qquad r > 1 \tag{4.8d}$$

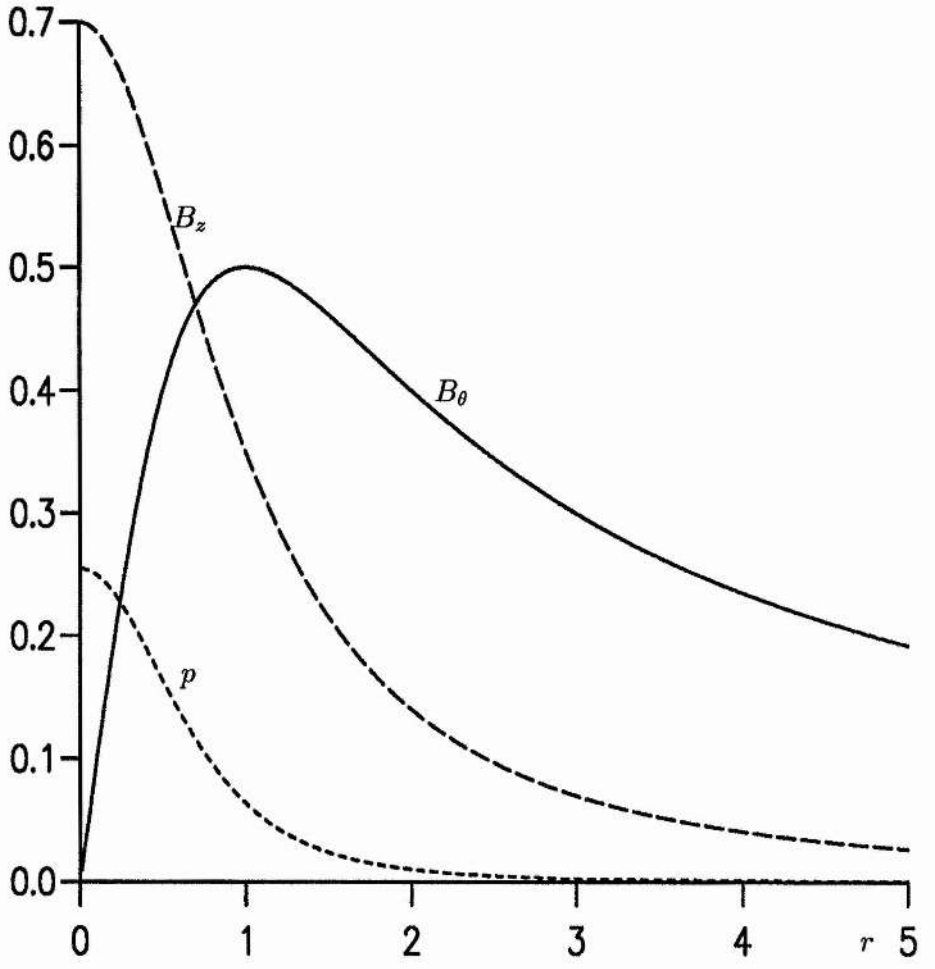

Figure **4.16a**: Poloidal magnetic field B_θ (full line), axial magnetic field B_z (upper dashed line) and plasma pressure profiles p (lower dashed line) as a function of the radial coordinate, r, for the Gold-Hoyle constant twist field with twist parameter, $\lambda = 0.7$, and $p_0 = 0$.

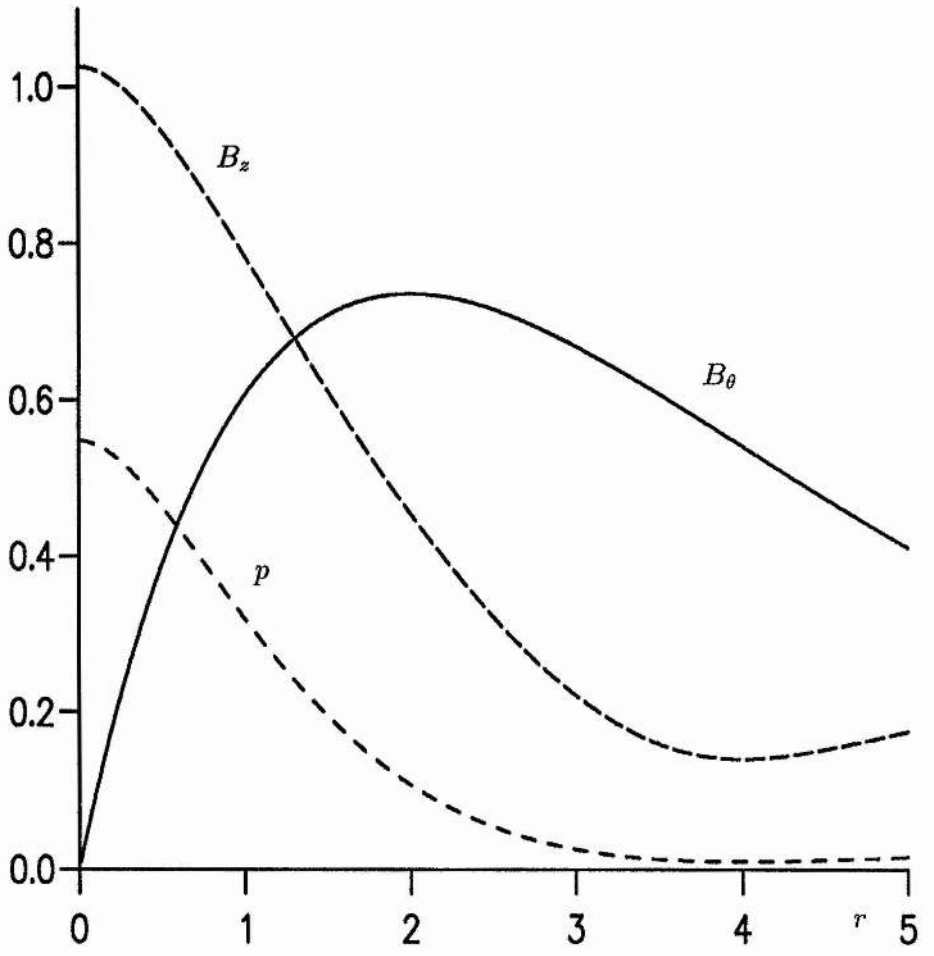

Figure **4.16**b: Poloidal magnetic field B_θ (full line), axial magnetic field B_z (upper dashed line) and plasma pressure profiles p (lower dashed line) as a function of the radial coordinate, r, for the Anzer field with twist parameter, $\lambda = 0.7$, and $p_0 = 0.15$.

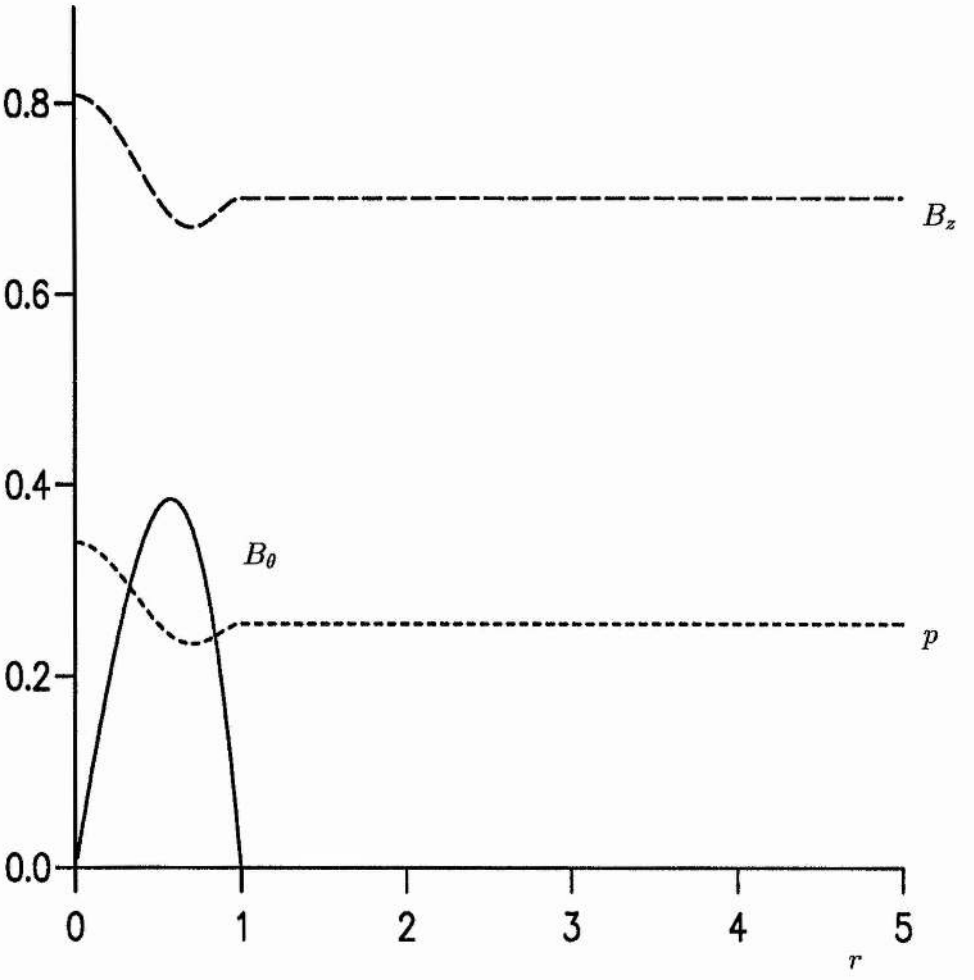

Figure **4.16**c: Poloidal magnetic field B_θ (full line), axial magnetic field B_z (upper dashed line) and plasma pressure profiles p (lower dashed line) as a function of the radial coordinate, r, for the third analytic field with twist parameter, $\lambda = 0.7$, and $p_0 = 0$.

In each case an outer radial boundary of $R = 10$ was taken, $\lambda = 0.7$ and $p_0 = 0.0$ except for the Anzer field with $p_0 = 0.15$ in order to ensure a real plasma pressure.

The Gold-Hoyle constant twist field, figure 4.16a, extends to infinity with the azimuthal magnetic field, B_θ, increasing from zero on the axis to a maximum at $r = 1$ and then monotonically increasing out to infinity. The axial magnetic field and plasma pressure have maxima on the axis and decrease monotonically out to infinity.

The Anzer field, figure 4.16b, has the azimuthal magnetic field, B_θ, increasing from zero on the axis to a maximum at $r = 2$ then monotonically decreasing out to infinity. The axial magnetic field and plasma pressure decrease in value from the axis out to $r = 4$ and the increase out to infinity with axial magnetic field, $B_z \to \lambda\sigma^{1/2}$ as $r \to \infty$. The remaining profile, figure 4.16c, has a similar structure to the numerically generated fields with the azimuthal magnetic field, B_θ, increasing from zero on the axis to a maximum and then decreasing to zero at $r = 1$. The axial magnetic field and plasma pressure decrease from maxima on the axis to minima and then increase to constant values for $r \geq 1$.

Figures 4.17a, b, c show marginal loop length, L, as a function of the twist parameter, λ, for the three analytic profiles (4.6), (4.7) and (4.8). The Gold-Hoyle figure, 4.7a, shows results for $m = 1, 2, 3$, the Anzer figure, 4.7b, for $m = 1, 2, 3, 4, 5$ and the remaining figure, 4.7c, for $m = 1, 2, 3, 4, 5$ and 10. For near-force-free conditions, λ near unity, the smallest marginal loop length is given by the $m = 1$

kink mode showing the kink mode to be the most unstable. Away from near-force-free conditions there is a reversal in the order of the marginal loop lengths of the stability modes indicating that as pressure effects become important, localized modes become the most unstable. All modes are more unstable away from near-force-free conditions. This is in agreement with the results of De Bruyne and Hood (1992) who investigated both the Gold-Hoyle and Anzer fields.

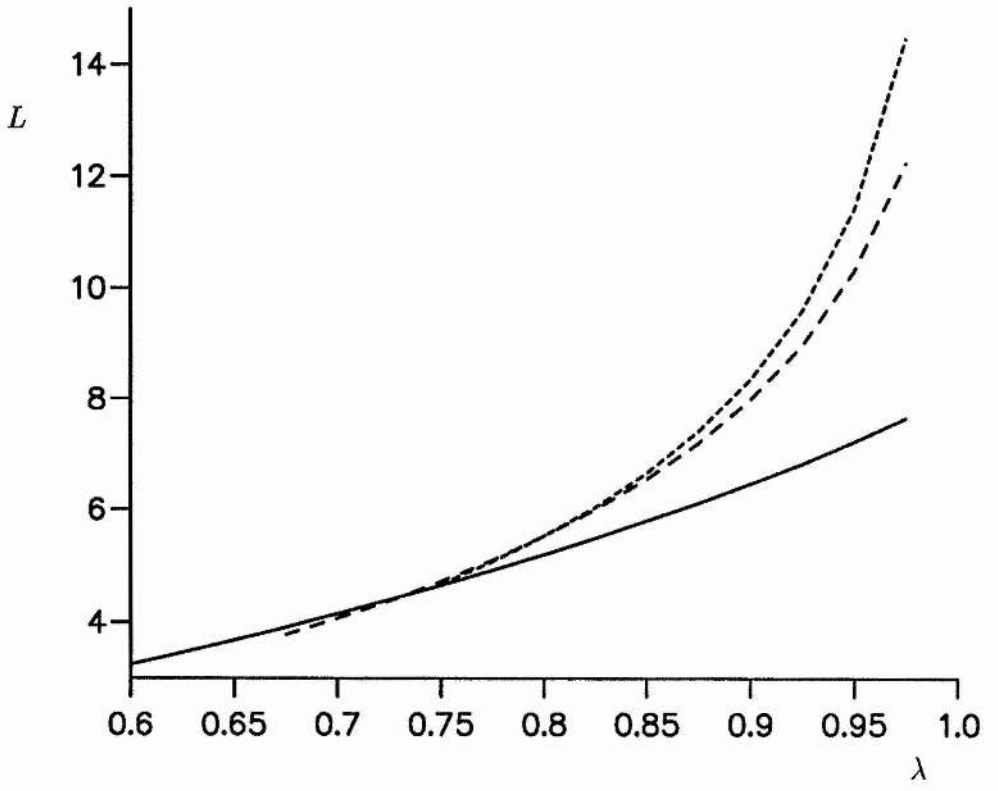

Figure **4.17**a: Marginal loop length, L, as a function of the twist parameter, λ, for 5 Fourier modes with m=1, 2 and 3 (in order of decreasing dash length) for the Gold-Hoyle constant twist field.

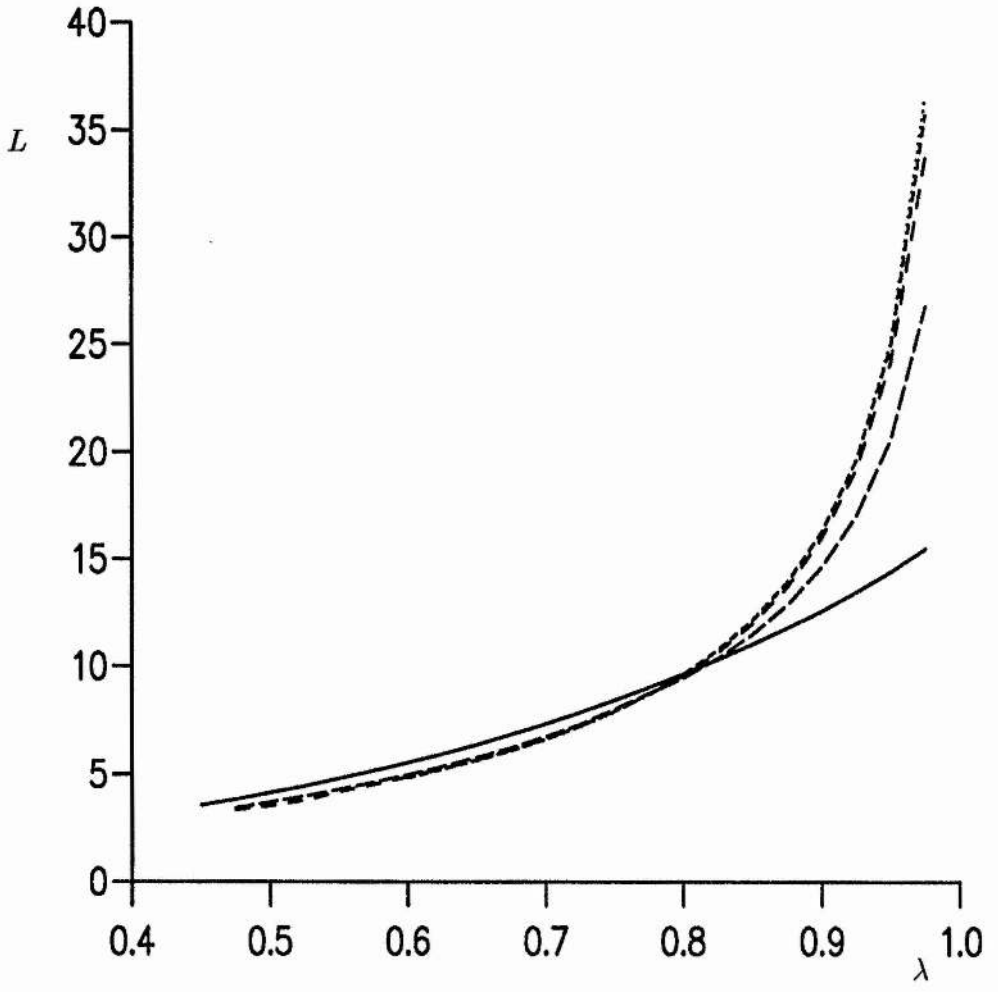

Figure **4.17**b: Marginal loop length, L, as a function of the twist parameter, λ, for 5 Fourier modes with m=1, 2, 3, 4 and 5 (in order of decreasing dash length) for the Anzer field.

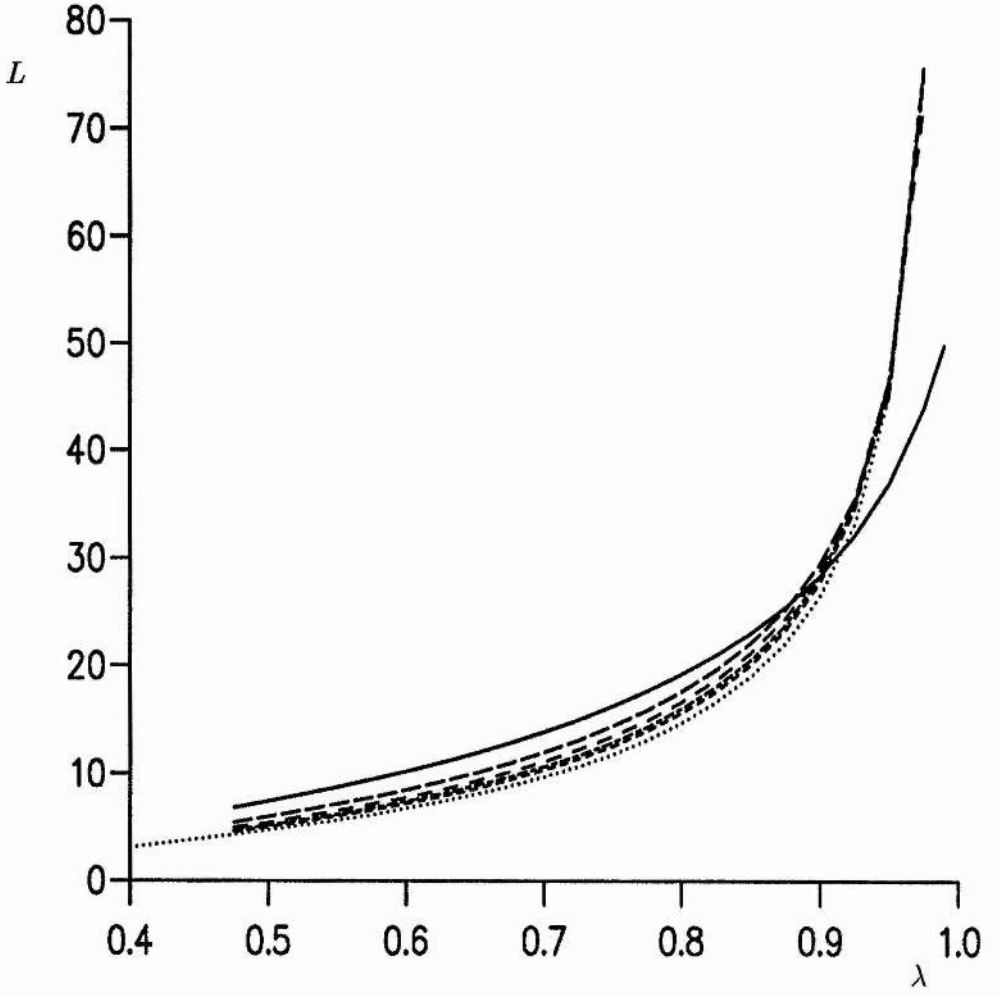

Figure **4.17c**: Marginal loop length, L, as a function of the twist parameter, λ, for 5 Fourier modes with m=1, 2, 3, 4. 5 and 10 (in order of decreasing dash length) for the third analytic field profile.

4.4 Free energy

As the coronal loop is twisted up magnetic energy is stored until the critical twist is reached at which point the loop is marginally stable and no extra energy can be stored without the loop becoming unstable and a flare occurring. The difference in the energy of the critically twisted loop and the untwisted loop is the free energy available to drive a solar flare and is given by

$$\text{free energy} = \int \left(\frac{B^2}{2\mu} + \frac{p}{\gamma - 1}\right) dV - \int \left(\frac{B_{\text{pot}}^2}{2\mu} + \frac{p_{\text{pot}}}{\gamma - 1}\right) dV$$

$$= 2\pi L B_0^2 a^2 \left\{ \int_0^{r'(A=1)} \left(\frac{B'^2}{2\mu} + \frac{p'}{\gamma - 1}\right) r' dr' - \int_0^{r'(A=1)} \left(\frac{B'^2_{\text{pot}}}{2\mu} + \frac{p'_{\text{pot}}}{\gamma - 1}\right) r' dr' \right\}, \tag{4.9}$$

with

$$B'_{\text{pot}} = B'_z = 1, \tag{4.10}$$

giving $\left(r_0 = \sqrt{2}\right)$

$$\int_0^{r'(A=1)} \frac{B'^2_{\text{pot}}}{2\mu} r' dr' = \int_0^{\sqrt{2}} \frac{1}{2} r' dr' = \frac{1}{2\mu}, \tag{4.11}$$

Some values of the terms between the curly brackets in (4.9) are given in table 4.4

Setting

$$B_0 = 500 \ \text{ Gauss}, \tag{4.12a}$$

$$r = 300 \ \text{ km} = 3 \times 10^7 \ \text{ cm}, \tag{4.12b}$$

gives for the first line of data in table 4.4

$$\text{free energy} = 2\pi L B_0^2 a^2 \left(\frac{1}{2\mu} r^2\right) (free)$$

$$= (3.14)\left(\frac{4.47}{\sqrt{2}}\right)\left(3\times 10^{7}\right)^{3}\left(500^{2}\right)(0.250) \quad \text{ergs}$$

$$= 1.7\times 10^{21} \quad \text{Joules}, \tag{4.13}$$

which is at the lower end of the energy required for a compact flare. The results will be modified by aspect ratios more typical of the solar corona (e.g. 10) rather than the value $4.47/\sqrt{2}$ in this example by increasing the free energy available to drive the solar flare.

	λ_e/L	S/L^{γ}	L	free
profile 1	π	0.005	4.47	0.250
	π	0.1	4.30	0.254
profile 2	π	0.01	3.733	0.557
	π	0.1	3.64	0.568

Table **4.2**: Normalized values of free energy available for solar flare.

4.5 Summary

In chapters 3 and 4 the stability of coronal loops to kink modes transformed into localized modes by increasing the poloidal wavenumber, m, has been investigated. Two numerically generated field profiles with twist, Φ, and pseudo-entropy, S, specified as functions of a flux function, A, were investigated as well as three analytic profiles. The first numerical profile provides a comparison with the results of Mikic,

Schnack and Van Hoven (1990). The second numerical profile had its equilibrium properties investigated by Lothian and Hood (1989). Stability of Gold-Hoyle constant twist and Anzer fields have been investigated by De Bruyne and Hood (1992) and provide checks with the results obtained here. Fourier truncated equations of motion with rigid-wall boundary conditions were derived and then incorporated into a Fortran program. Due to the singular nature of the equations on the axis, $r = 0$, it was necessary to take radial boundaries at a small value of radius, $r = \epsilon$, and also at a large radius, $r = R$. The outer radial boundary, R, has to be small enough in order that truncation errors are not significant and computing c.p.u. time is practical, but large enough that the stabilizing effect of imposing an extra constraint does not significantly alter the results. A Bulirsch-Stoer variable step shoot and match method was used to solve the equations. A Bulirsch-Stoer variable step method alters the integration stepsize in order to overcome the difficulties of having large and small gradients in terms of accuracy and time considerations. A shoot and match method integrates out from an inner radial boundary, $r = \epsilon$, and integrates in from an outer radial boundary, $r = R$, to a matching point. Then, by finding a linear combination of the different Fourier mode eigenfunction solutions, the problem is reduced to finding an eigenvalue which gives the determinant of a matrix as zero. Two guesses of the eigenvalue which give opposite signs of the matrix determinant indicate that a solution to the equations is given by an eigenvalue lying between the two guesses. Care has to be taken that the eigenvalue obtained is the one of interest

to the problem under consideration, in this case the smallest positive eigenvalue for marginal loop length and not a higher harmonic. Also two guesses with the same sign of matrix determinant does not necessarily mean that no solution to the equations exists between the two guesses but instead there could be two (or any even number) of solutions between the guesses.

The two numerically generated field profiles were considered in detail. Their respective field profiles, similar in shape, are shown in figures 4.1 and 4.9. By using a finite number of Fourier modes to approximate the infinite set of Fourier modes, it is necessary to introduce a central wavenumber, k_0. By choosing a value of k_0 the equations are solved to find a marginal loop length, L. This is shown by figures 4.2 and 4.10. The oscillations in the figures are caused by the most unstable modes being included as sidebands dependent on the number of Fourier modes selected. The marginal loop length of interest is the smallest value of L obtained since lengths greater than this value are unstable. The effect of the value of the false origin, $r = \epsilon$, is shown by figures 4.3 and 4.11 in order to justify the choice of $\epsilon = 10^{-4}$ by showing that it has a negligible effect on the results. The effect of the position of the outer radial boundary, $r = R$, is shown by figures 4.4 and 4.12. It was found that for 7 and 9 Fourier modes as well as increasing c.p.u. time compared to 5 Fourier modes, the outer radial boundary could not be taken far enough out in order not to significantly alter the eigenvalues obtained by solving the Fourier truncated equations. For this reason most of the analysis in chapter 4 is based on 5 Fourier modes. The critical

axial twist as a function of the loop length is shown by figures 4.5 and 4.13. Figure 4.5 shows a cross representing a result found by Mikic, Schnack and Van Hoven (1990) showing agreement with the Fourier truncated method used here. The marginal loop length, L, as a function of the central axial wavenumber, k_0, for different poloidal wavenumber, m, values is shown by figures 4.6 and 4.14. The figures show that as m increases, the central axial wavenumber, k_0, giving the smallest marginal loop length, L, is displaced in the negative direction. Figures 4.7, 4.8 and 4.15 show marginal loop length, L, as a function of the pseudo-entropy, S, and show that for near-force-free conditions the $m = 1$ kink mode is the most unstable but that away from near-force-free conditions, there is a reversal in the importance of the modes with localized, pressure driven, modes as the most unstable. It has still to be shown that this holds in general and is not an artifact of selecting a small number of Fourier modes. Figures 4.7 and 4.8 show that the result holds for 5 and 7 Fourier modes.

Three analytic field profiles were investigated, the Gold-Hoyle constant twist and Anzer fields extend to infinity and a third profile similar in outline to the two numerically generated field profiles. Again it has been found that kink modes are the most unstable for near-force-free conditions and localized modes are the most unstable when pressure effects are important.

For coronal loops with a small plasma β, it is expected that the near-force-free results are the most relevant with the $m = 1$ kink mode as the most unstable mode. For a prominence inside a flux tube, the magnetic field is larger but plasma pressure

similar to coronal values giving a small plasma β, indicating that kink modes are likely to be the most unstable mode in the flux tube surrounding the prominence.

5 Stability of coronal arcades

5.1 Introduction

In this chapter, the technique for investigating the stability of arcades using Fourier truncated equations of motion with rigid-wall line-tying boundary conditions will be developed. A small r Frobenius expansion will be used to obtain a relation between the eigenfunctions and their derivatives, in order to start the numerical solution of the equations. An alternative finite difference scheme derivation will also be derived. The Bulirsch-Stoer shoot and match method described in Chapters 3 and 4 can then be used to solve the equations.

Barnes and Sturrock (1972) proposed that a potential field structure is distorted by photospheric motions leading to a non-potential field. Energy stored in the magnetic field structure will eventually exceed the energy of an open field structure and so the magnetic field structure must be unstable or metastable. Low (1977) and Birn, Goldstein and Schindler (1978) modelled an arcade in terms of a flux function with the magnetic field along the axis and plasma pressure prescribed. Low found that a catastrophe point exists for a critical value of a parameter, say λ_{crit}, such that no neighbouring equilibria exists for $\lambda > \lambda_{crit}$. For $\lambda < \lambda_{crit}$, there were two solutions. Jockers (1978) proposed that the footpoint displacement should be prescribed rather than the component of the magnetic field along the

axis. Finn and Chen (1990) argued that the entropy should be specified rather than the pressure. Jockers (1978) and Finn and Chen (1990) found no loss of equilibrium or catastrophe point. Melville, Hood and Priest (1983, 1984) extended the results of Low (1977) and Birn, Goldstein and Schindler (1978) to include the effects of gravity. Catastrophe points were found if the pressure exceeds a critical value. Cargill, Hood and Migliuolo (1986) looked at ideal MHD stability of coronal arcades for sheared equilibrium fields. They were unable to find unstable solutions to the three sample force-free equilibrium fields used. For non-force-free fields they found shear to be a stabilizing influence. An, Suess and Wu (1988), Schindler, Birn and Janicke (1983), Galindo-Trejo (1987) and Hu (1988) have all investigated the stability of two-dimensional arcades. Zweibel (1981), Bogdan (1985) and Melville, Hood and Priest (1986, 1987) have investigated the stability of shearless coronal fields.

Rigid-wall line-tying conditions for arcades are given by

$$\boldsymbol{\xi}\left(\theta = \pm\frac{\pi}{2}\right) = 0. \tag{5.1}$$

Taking Fourier series expansions of the form

$$\xi_r = \sum_{m\ even} \xi_m(r)\, exp\left\{i\left[m\left(\theta + \frac{\pi}{2}\right) + kz\right]\right\}, \tag{5.2a}$$

$$\xi_\perp = \sum_{m\ even} \zeta_m(r)\, exp\left\{i\left[m\left(\theta + \frac{\pi}{2}\right) + kz\right] + i\frac{\pi}{2}\right\}, \tag{5.2b}$$

$$\xi_\parallel = \sum_{m\ even} \eta_m(r)\, exp\left\{i\left[m\left(\theta + \frac{\pi}{2}\right) + kz\right] + i\frac{\pi}{2}\right\}, \tag{5.2c}$$

where expansions are taken in the poloidal direction between $\pm\pi/2$ with period π, thus ruling out the odd values of m in the summations in order that the periods of the Fourier terms are 2π. Periodicity in the axial direction of the order of a coronal arcade lengthscale, $k = 2\pi/L$ (typically 6×10^4 km), has been assumed.

The boundary conditions (5.1) imply

$$\sum_{m\ even} \xi_m(r) = 0, \tag{5.3a}$$

$$\sum_{m\ even} \zeta_m(r) = 0, \tag{5.3b}$$

$$\sum_{m\ even} \eta_m(r) = 0, \tag{5.3c}$$

Starting with equations (3.29a), (3.29b) and (3.29c) and integrating all terms by the appropriate exponential factor

$$\int_{\frac{\pi}{2}}^{\frac{\pi}{2}} A \exp\left\{-i\left[m\left(\theta+\frac{\pi}{2}\right)+kz\right]\right\} d\theta, \tag{5.4a}$$

for (3.29a), and

$$\int_{\frac{\pi}{2}}^{\frac{\pi}{2}} A \exp\left\{-i\left[m\left(\theta+\frac{\pi}{2}\right)+kz\right]-i\frac{\pi}{2}\right\} d\theta, \tag{5.4b}$$

for (3.29b) and (3.29c), gives the equations

$$\left[r\left(\frac{B_\theta^2}{r^2}\right)' + f_m^2 + \mu\rho\sigma^2\right]\xi_m - \left[(1+\beta)\frac{B^2}{r}(r\xi_m)'\right]' + [(1+\beta)Bg_m\zeta_m]'$$

$$+ [\beta B f_m \eta_m]' + \frac{2BB_\theta k}{r}\zeta_m + \frac{B_\theta^2}{r^2}\lambda_r = 0, \tag{5.5a}$$

$$\left(f_m^2 + (1+\beta)g_m^2 + \mu\rho\sigma^2\right)\zeta_m - (1+\beta)\frac{Bg_m}{r}(r\xi_m)' - \frac{2BB_\theta k}{r}\xi_m$$

$$+\beta f_m g_m \eta_m - \frac{1}{r^2}\left(B^2 + \beta B_z^2\right)\lambda_\perp - \frac{\beta B_\theta B_z}{r^2}\lambda_\parallel = 0, \tag{5.5b}$$

$$\left(f_m^2 + \frac{\mu\rho\sigma^2}{\beta}\right)\eta_m - \frac{B f_m}{r}(r\xi_m)' + f_m g_m \zeta_m - \frac{B_\theta^2}{r^2}\lambda_\parallel - \frac{B_\theta B_z}{r^2}\lambda_\perp = 0, \tag{5.5c}$$

where a dash denotes a derivative with respect to r, and

$$f_m = \frac{m}{r}B_\theta + kB_z, \tag{5.6a}$$

$$g_m = \frac{m}{r}B_z - kB_\theta, \tag{5.6b}$$

$$k = \frac{2\pi}{L}, \tag{5.6c}$$

$$\lambda_r = \frac{1}{\pi}\left[\frac{\partial \xi_r}{\partial \theta}\exp\left\{-i\left[m\left(\theta + \frac{\pi}{2}\right) + kz\right]\right\}\right]_{-\pi/2}^{\pi/2}, \tag{5.6d}$$

$$\lambda_\perp = \frac{1}{\pi}\left[\frac{\partial \xi_\perp}{\partial \theta}\exp\left\{-i\left[m\left(\theta + \frac{\pi}{2}\right) + kz\right] - i\frac{\pi}{2}\right\}\right]_{-\pi/2}^{\pi/2}, \tag{5.6e}$$

$$\lambda_\parallel = \frac{1}{\pi}\left[\frac{\partial \xi_\parallel}{\partial \theta}\exp\left\{-i\left[m\left(\theta + \frac{\pi}{2}\right) + kz\right] - i\frac{\pi}{2}\right\}\right]_{-\pi/2}^{\pi/2}, \tag{5.6f}$$

Rewrite (5.5b) and (5.5c) as

$$A_m \begin{pmatrix} \eta_m \\ \\ \zeta_m \end{pmatrix} + B_m (r\xi_m)' + C_m (r\xi_m) + D_m \begin{pmatrix} \lambda_\parallel \\ \\ \lambda_\perp \end{pmatrix} = 0, \tag{5.7}$$

where

$$A_m = \begin{pmatrix} \mu\rho\sigma^2 + \beta f_m^2 & \beta g_m f_m \\ \\ \beta g_m f_m & \mu\rho\sigma^2 + f_m^2 + (1+\beta) g_m^2 \end{pmatrix}, \tag{5.8a}$$

$$B_m = \begin{pmatrix} \frac{\beta B f_m}{r} \\ \\ \frac{(1+\beta) B g_m}{r} \end{pmatrix}, \tag{5.8b}$$

$$C_m = \begin{pmatrix} 0 \\ \\ \frac{-2BB_\theta k}{r^2} \end{pmatrix}, \tag{5.8c}$$

$$D_m = \begin{pmatrix} -\beta B_z^2 & \beta B_\theta B_z \\ \\ \beta B_\theta B_z & -(B^2 + \beta B_\theta^2) \end{pmatrix}, \tag{5.8d}$$

$$\beta = \frac{\gamma \mu p}{B^2}. \tag{5.8e}$$

and premultiplying (5.7) by A_m^{-1}, the inverse of A_m, gives expressions for η_m and ζ_m in terms of ξ_m, $\lambda_\parallel$ and $\lambda_\perp$. Summing over all values of m allows the constraints (5.3) to be applied giving expressions for the Lagrange multipliers $\lambda_\parallel$ and $\lambda_\perp$ in terms of $(r\xi_m)$ and $(r\xi_m)'$. Substituting these expressions back into equation (5.7) gives η_m and ζ_m in terms of $(r\xi_m)$ and $(r\xi_m)'$. The expressions for η_m and ζ_m can be substituted into equation (5.5a) to give an equation involving $(r\xi_m)'$, $(r\xi_m)$ and λ_r

$$\left[\left(\gamma\mu p + B^2\right)\frac{(r\xi^m)'}{r}\right]' - \left(\mu\rho\sigma^2 + f_m^2\right)\xi^m - \left(\frac{B_\theta^2}{r^2}\right)' r\xi^m - (H^m\phi^m)' + K^m\phi^m + \frac{B_\theta^2}{r^2}\lambda_r = 0, \tag{5.9}$$

where

$$H^m = (\,\beta B f_m \quad , \quad (1+\beta)\, B g_m\,) \tag{5.10a}$$

$$K^m = (\,0 \quad , \quad \tfrac{2BB_\theta k}{r}\,) \tag{5.10b}$$

$$\phi^m = \begin{pmatrix} \eta_m \\ \\ \zeta_m \end{pmatrix}, \tag{5.10c}$$

giving an infinite set of coupled equations in the Fourier amplitudes ξ_m, $m = \pm 2, \pm 4, \cdots$. By truncating to N equations we can eliminate the Lagrange multiplier, λ_r, by subtracting the N^{th} equation involving λ_r, $(r\xi_{2N})$ from the remaining $N-1$ equations and $(r\xi_{2N})$ can be eliminated by using the boundary condition, from (5.3a)

$$\sum_{m=2}^{m=2N} \xi_n = 0 \qquad \text{m=2n,} \qquad \text{n integer,} \tag{5.11}$$

to give $N-1$ coupled equations in $N-1$ unknowns $(r\xi_m)$, $m = 2, 4, \cdots, 2N-2$ which can be written as

$$(U\mathbf{y}')' + V\mathbf{y}' + W\mathbf{y} = \mathbf{0}, \tag{5.12}$$

where $\mathbf{y} = r\boldsymbol{\xi} = r\,(\xi_2,\ \xi_4,\ \cdots,\ \xi_{2N-2})^T$.

The small r radial boundary conditions are derived in Appendix C from equations (3.5) and (3.6) in Hood (1983). A simpler form for the boundary conditions can be obtained using a finite difference scheme. Rewrite equation (5.12) as

$$U\mathbf{y}'' + (U' + V)\,\mathbf{y}' + W\mathbf{y} = \mathbf{0}, \tag{5.13}$$

In order to start the integration at $r = \epsilon$, a relationship between $\mathbf{y}'(r = \epsilon)$ and $\mathbf{y}(r = \epsilon)$ has to be known. Consider

$$\mathbf{y}_0 \approx \mathbf{y}(r = 0) = 0, \tag{5.14a}$$

$$\mathbf{y}_1 \approx \mathbf{y}(r = \epsilon), \tag{5.14b}$$

$$\mathbf{y}_2 \approx \mathbf{y}(r = 2\epsilon), \tag{5.14c}$$

$$U_1 = U(r = \epsilon), \tag{5.14d}$$

$$V_1 = V(r = \epsilon), \tag{5.14e}$$

$$U_1' = U'(r = \epsilon), \tag{5.14f}$$

$$W_1 = W(r = \epsilon), \tag{5.14g}$$

then equation (5.13) is

$$\frac{U_1(\mathbf{y}_2 - 2\mathbf{y}_1 + \mathbf{y}_0)}{\epsilon^2} + (U_1' + V_1)\frac{\mathbf{y}_2 - \mathbf{y}_0}{2\epsilon} + W_1\mathbf{y}_1 = \mathbf{0}, \tag{5.15}$$

giving

$$\mathbf{y}_2 = A\mathbf{y}_1, \tag{5.16}$$

where

$$A = \left[U_1 + \frac{\epsilon}{2}\left(U_1' + V_1\right)\right]^{-1}\left[2U_1 - \epsilon^2 W_1\right], \tag{5.17}$$

and so the starting conditions at $r = \epsilon$ are

$$\mathbf{y} = \mathbf{y}_1, \tag{5.18a}$$

$$\mathbf{y}' = \frac{\mathbf{y}_2 - \mathbf{y}_0}{2\epsilon} = \frac{1}{2\epsilon} A\mathbf{y}_1. \tag{5.18b}$$

A central azimuthal wavenumber, m_0, is introduced (by analogy to the central axial wavenumber, k_0, for loops). The largest Fourier amplitudes are likely to have the greatest effect on the marginal stability bounds, and by introducing a central azimuthal wavenumber, m_0, with sidebands, $m_0 \pm m$, to represent the other Fourier modes used in the truncation, the most unstable set of Fourier modes can be found to give the approximation for the stability of the system. After carrying out the necessary modifications to the computer program used for the loop equations in order to obtain a program to solve for the arcade equations, I am unable to find marginal stability bounds so far. Arcades are normally more stable than loops and it may be that the wrong parameter region has been investigated. A wider parameter search must be performed but this is left for future work.

6 Discussion

The form of the boundary conditions at the coronal/photospheric interface has been investigated. This has been the subject of controversy (see Hood, 1986) with two main ideas suggested :-

(1) rigid-wall conditions, where all flows are zero at the coronal/photospheric boundary.

(2) flow-through conditions, where flows are allowed across the boundary parallel to the magnetic field provided that energy is conserved.

The large value of the photospheric/coronal density ratio of 10^8 seems to suggest that coronal disturbances propagating to the photospheric boundary would have all components disappearing at the boundary to a high order, in agreement with the rigid-wall conditions. The flow-through conditions require that one end of the loop 'knows' what is happening at the other end simultaneously and it is unlikely that the photosphere can respond so quickly to coronal perturbations.

In order to make the problem tractable, a ballooning approach has been used to give perturbations with short wavelength across the field and long wavelengths along the field in order to reduce the equations to ordinary differential equations along the field. Results obtained are only valid for localized ballooning modes. Ideal and resistive MHD equations are used with a shearless example equilibrium field since results for ideal MHD using this field are already known (Hood, 1986). In the uniform density limit with the poloidal wavenumber, m, taking integer values, two

instabilities exist, the sausage, $m = 0$, mode and kink, $m = 1$, mode. As the density ratio increases, both growth rates decrease with the smaller of the two tending to zero (with $\rho\sigma^2 \approx$ constant for ideal modes) as the density ratio tends to infinity giving at most one unstable solution at the infinite density limit. The infinite density limit ideal unstable mode evolves with $\rho\left(\sigma - \sigma_\infty\right)^3 \approx$ constant for large density ρ. With resistivity included, the unstable mode tending to marginal stability as $\rho \to \infty$ has $\rho\sigma \approx$ constant for large density ρ, whereas the solution which remains unstable at the infinity density limit lies between $\rho\left(\sigma - \sigma_\infty\right)^2 \approx$ constant and $\rho\left(\sigma - \sigma_\infty\right)^3 \approx$ constant depending on the value of radius r and resistivity parameter ηn^2.

The stability of coronal loops to kink modes transformed into localized modes by increasing the poloidal wavenumber, m, was investigated using two numerically generated field profiles and three analytic field profiles. It was found that for near force-free equilibria, kink modes are the most unstable with localized modes the most stable. As pressure gradients become important there is a reversal in the order with localized modes the most unstable and kink modes the most stable. All modes are destabilized by increasing pressure gradients. Future work involves studying the stability of coronal arcades in detail.

REFERENCES

An, C.H., Suess, S., and Wu, S.T.:1989, *Astrophys.J.* **337**, 989.

Anzer, U.:1968, *Solar Phys.* **3**, 298.

Barnes, C., and Sturrock,P.:1972, *Astrophys.J.* **174**, 659.

Bogdan, T.:1985, *Astrophys.J.* **288**, 672.

Bray, R.J., Cram, L.E., Durrant, C.J., and Loughhead,R.E.:1991, *Plasma loops in the solar corona*, C.U.P., England.

Bernstein, I.B., Frieman, E.A., Kruskal, M.D. and Kulsrud, R.M.:1958, *Proc. Roy. Soc. London*, **A244**, 17.

Birn, J., Goldstein, H., and Schindler, K.:1978, *Solar Phys.* **57**, 81.

Browning, P.K., and Hood, A.W.:1989, *Solar Phys.* **124**, 271.

Browning, P.K., and Priest, E.R.:1983, *Astrophys.J.* **266**, 848.

Cargill, P., Hood, A.W., and Migliuolo, S.:1986, *Astrophys.J.* **309**, 402.

Cargill, P., and Hood, A.W.:1989, *Solar Phys.* **124**, 101.

Connor, J.W., Hastie, R.J., and Taylor, J.B.:1979, *Proc. R. Soc. Lon. A.* **365**, 1.

De Bruyne, P., and Hood, A.W.:1992, *Solar Phys.* **142**, 87.

Dewar, R.L., and Glasser, A.H.:1983, *Phys. Fluids* **26**, 3038.

Einaudi, G., and Van Hoven,G.:1981, *Phys.Fluids* **24**, 1092.

Einaudi, G., and Van Hoven,G.:1983, *Solar Phys.* **88**, 163.

Finn, J.M., and Chen, J.:1990, *Astrophys.J.* **349**, 345.

Foote, B., and Craig, I.J.D.:1990, *Astrophys.J.* **350**, 437.

Galindo–Trejo, J.:1987, *Solar Phys.* **108**, 265.

Goedbloed, J.P.:1983, *Lecture Notes on Ideal Magnetohydrodynamics*, Association Euratom-FOM, The Netherlands.

Goedbloed, J.P.:1990,*Computer Phys. Comm* **59**, 39.

Gold, T., and Hoyle, F.:1960, *Mon. Not. Roy. Astron. Soc.***120**, 89.

Hardie, I.S., Hood, A.W., and Allen, H.R.:1991, *Solar Phys.***133**, 313.

Hassam, A.B.:1990, *Astrophys.J.* **348**, 778.

Hood, A.W.:1983, *Solar Phys.* **87**, 279.

Hood, A.W.:1984, *Geophys.,Astrophys.,Fluid dynamics* **28**, 223.

Hood, A.W.:1986, *Solar Phys.* **105**, 307.

Hood, A.W.:1992, *Plasma Phys. and Controlled Fusion* **34**, 411.

Hood, A.W., Van der Linden, R., and Goossens, M.:1989, *Solar Phys.***120**, 261.

Hood, A.W., and Priest, E.R.:1979, *Solar Phys.* **64**, 303.

Hu, Y.Q.:1988, *Astrophys.J.* **331**, 402.

Jockers, K.:1978, *Solar Phys.* **56**, 37.

Lothian, R.M., and Hood, A.W.:1989, *Solar Phys.* **122**, 227.

Lothian, R.M., and Hood, A.W.:1992, *Solar Phys.* **137**, 105.

Low, B.C.:1977, *Astrophys.J.* **217**, 988.

Melville, J.P., Hood, A.W., and Priest, E.R.:1983, *Solar Phys.* **87**, 301.

Melville, J.P., Hood, A.W., and Priest, E.R.:1984, *Solar Phys.* **92**, 15.

Melville, J.P., Hood, A.W., and Priest, E.R.:1986, *Solar Phys.* **105**, 291.

Migliuolo, S., Cargill, P., and Hood, A.W.:1984, *Astrophys.J.* **271**, 820.

Mikic, Z., Schnack, D.D., and Van Hoven, G.V.:1990, *Astrophys.J.*, **361**, 690.

Priest, E.R.:1982, *Solar Magnetohydrodynamics*, D. Reidel Publ. Co. Dordrecht, The Netherlands.

Priest, E.R.:1988, *Dynamics and Structure of Quiescent Solar Prominences.* Kluwer Academic Publ., The Netherlands.

Raadu, M.:1972, *Solar Phys.* **22**, 425.

Robertson, J.A., Hood, A.W., and Lothian, R.M.:1992, *Solar Phys.* **137**, 273.

Rosner, R., Low, B.C., and Holtzer, T.E.:1986, in *Physics of the Sun* , D.Reidel Publ. Co., Dordrecht, The Netherlands.

Schindler, K., Birn, J., and Janicke, L.:1983, *Solar Phys.* **87**, 103.

Steinholfson, R., and Tajima,T.:1987, *Astrophys.J.* **322**, 503.

Svestka, Z.:1976, *Solar Flares*, Dordrecht, The Netherlands.

Van der Linden, R., Goossens, M., and Kerner, W.:1990,*Computer Phys. Comm* **59**, 61.

Velli, M., Einaudi, G.,and Hood, A.W.:1990, *Astrophys.J.*, **350**, 419.

Velli, M., and Hood, A.W.:1986,*Solar Phys.* **106**, 353.

Velli, M., and Hood, A.W.:1987,*Solar Phys.* **109**, 351.

Velli, M., and Hood, A.W.:1989,*Solar Phys.* **119, 107**.

Zweibel, E.:1981, *Astrophys.J.* **249**, 731.

Zweibel, E., and Boozer,A.:1985, *Astrophys.J.* **295**, 642.

Appendix A

Derivation of Resistive Ballooning Equations for Chapter 2

The MHD equations are given by,

Force balance

$$\rho \frac{D\mathbf{v}}{Dt} = -\nabla p + \mathbf{j} \times \mathbf{B}, \tag{A.1}$$

Continuity equation

$$\frac{\partial \rho}{\partial t} + \nabla \cdot (\rho \mathbf{v}) = 0, \tag{A.2}$$

Momentum equation

$$\frac{\partial \mathbf{B}}{\partial t} = \nabla \times (\mathbf{v} \times \mathbf{B}) + \eta \nabla^2 \mathbf{B}, \tag{A.3}$$

Divergence equation

$$\nabla \cdot \mathbf{B} = 0 \tag{A.4}$$

Energy equation

$$\frac{Dp}{Dt} = \frac{\gamma p D\rho}{\rho Dt} + (\gamma - 1)\, \mu \eta j^2, \tag{A.5}$$

make the assumption that all perturbed variables vary as $e^{\sigma t}$,

Take small perturbations about equilibrium in cylindrical geometry

$$p = p_0(r) + p_1(r, \theta, z), \tag{A.6a}$$

$$\mathbf{B} = (0, B_\theta(r), 0) + \mathbf{B}_1(r, \theta, z), \tag{A.6b}$$

$$\mathbf{v} = 0 + \mathbf{v}_1(r, \theta, z), \tag{A.6c}$$

$$\rho = \rho_0(r; \theta) + \rho_1(r, \theta, z), \tag{A.6d}$$

$$\left(\mu p + \frac{{B_\theta}^2}{2}\right)' = -\frac{{B_\theta}^2}{r}, \text{ force balance equation,} \tag{A.6e}$$

the linearized equations, from (A.1) to (A.5) are

$$\rho_0 \sigma \mathbf{v}_1 = -\nabla p_1 + \frac{1}{\mu}(\nabla \times \mathbf{B}_1) \times \mathbf{B}_0 + \frac{1}{\mu}(\nabla \times \mathbf{B}_0) \times \mathbf{B}_1, \tag{A.7}$$

$$\sigma \rho_1 + \nabla.(\rho_0 \mathbf{v}_1) = 0, \tag{A.8}$$

$$\sigma \mathbf{B}_1 = \nabla \times (\mathbf{v}_1 \times \mathbf{B}_0) + \eta \nabla^2 \mathbf{B}_1, \tag{A.9}$$

$$\nabla.\mathbf{B}_1 = 0, \tag{A.10}$$

$$\sigma p_1 + \mathbf{v}_1.\nabla p_0 = \frac{\gamma p_0}{\rho_0}(\sigma \rho_1 + \mathbf{v}_1.\nabla \rho_0) + 2(\gamma - 1)\eta \mathbf{j}_0.(\nabla \times \mathbf{B}_1). \tag{A.11}$$

Substituting equation (A.8) into (A.11) gives

$$\sigma p_1 + \mathbf{v}_1.\nabla p_0 = -\gamma p_0 \nabla.\mathbf{v}_1 + 2(\gamma - 1)\eta \mathbf{j}_0.(\nabla \times \mathbf{B}_1), \tag{A.12}$$

The equations written in cylindrical form are

$$\frac{1}{r}\frac{\partial}{\partial r}(rB_{1r}) + \frac{1}{r}\frac{\partial B_{1\theta}}{\partial \theta} + \frac{\partial B_{1z}}{\partial z} = 0, \tag{A.13}$$

$$\mu \rho \sigma v_{1r} = -\frac{\partial}{\partial r}(\mu p_1 + B_\theta B_{1\theta}) + \frac{B_\theta}{r}\frac{\partial B_{1r}}{\partial \theta} - \frac{2B_\theta B_{1\theta}}{r}, \tag{A.14}$$

$$\mu \rho \sigma v_{1\theta} = -\frac{1}{r}\frac{\partial}{\partial \theta}(\mu p_1) + \frac{B_{1r}}{r}(rB_\theta)', \tag{A.15}$$

$$\mu \rho \sigma v_{1z} = -\frac{\partial}{\partial z}(\mu p_1 + B_\theta B_{1\theta}) + \frac{B_\theta}{r}\frac{\partial B_{1z}}{\partial \theta}, \tag{A.16}$$

$$\sigma B_{1r} = \frac{B_\theta}{r}\frac{\partial v_{1r}}{\partial \theta} + \eta\left[\frac{1}{r}\frac{\partial}{\partial r}\left(r\frac{\partial B_{1r}}{\partial r}\right) + \frac{1}{r^2}\frac{\partial^2 B_{1r}}{\partial \theta^2} + \frac{\partial^2 B_{1r}}{\partial z^2} - \frac{2}{r^2}\frac{\partial B_{1\theta}}{\partial \theta} - \frac{B_{1r}}{r^2}\right], \tag{A.17}$$

$$\sigma B_{1\theta} = -B_\theta\left[\frac{\partial v_{1z}}{\partial z} + \frac{1}{r}\frac{\partial}{\partial r}\left(r v_{1r}\right)\right] + \left(\frac{B_\theta}{r} - B_\theta{}'\right) v_{1r} + \eta\left[\nabla^2 B_{1\theta} + \frac{2}{r^2}\frac{\partial B_{1r}}{\partial \theta} - \frac{B_{1\theta}}{r^2}\right], \tag{A.18}$$

$$\sigma B_{1z} = \frac{B_\theta}{r}\frac{\partial v_{1z}}{\partial \theta} + \eta\nabla^2 B_{1z}, \tag{A.19}$$

$$\sigma p_1 + v_{1r}p' + \gamma p\left[\frac{\partial v_{1z}}{\partial z} + \frac{1}{r}\frac{\partial}{\partial r}\left(r v_{1r}\right)\right]$$
$$+\frac{\gamma p}{r}\frac{\partial v_{1\theta}}{\partial \theta} - 2\left(\gamma - 1\right)\frac{\eta}{\mu r^2}\frac{d}{dr}\left(r B_\theta\right)\left[\frac{\partial}{\partial r}\left(r B_{1\theta}\right) - \frac{\partial}{\partial \theta}\left(B_{1r}\right)\right] = 0, \tag{A.20}$$

$$\sigma\rho_1 + v_{1r}\rho' + \frac{v_{1\theta}}{r}\frac{\partial \rho}{\partial \theta} + \frac{\rho}{r}\frac{\partial}{\partial r}\left(r v_{1r}\right) + \rho\frac{\partial v_{1z}}{\partial z} + \frac{\rho}{r}\frac{\partial v_{1\theta}}{\partial \theta} = 0, \tag{A.21}$$

eliminating $\frac{\partial v_{1z}}{\partial z} + \frac{1}{r}\frac{\partial}{\partial r}\left(r v_{1r}\right)$ between equations (A.18) and (A.20) gives

$$\gamma p\sigma B_{1\theta} = B_\theta\sigma p_1 + \frac{B_\theta\gamma p}{r}\frac{\partial v_{1\theta}}{\partial \theta} + \left(B_\theta p' + \frac{B_\theta}{r} - B_\theta{}'\right) v_{1r} + \eta\left[\nabla^2 B_{1\theta} + \frac{2}{r^2}\frac{\partial B_{1r}}{\partial \theta} - \frac{B_{1\theta}}{r^2}\right]$$
$$-2\left(\gamma - 1\right)\frac{\eta B_\theta}{\mu r^2}\frac{d}{dr}\left(r B_\theta\right)\left[\frac{\partial}{\partial r}\left(r B_{1\theta}\right) - \frac{\partial}{\partial \theta}\left(B_{1r}\right)\right], \tag{A.22}$$

Assume all variables are like $f\left(\theta\right)e^{in(S(r)+z)}$, $n \gg 1$, and take $k^2 = 1 + \left(S'\right)^2$, then,

$O\left(n^2\right)$ terms,

from (A.17), the second and fourth terms of the r.h.s

$$\eta n^2 k^2 B_{1r} = O\left(1\right), \tag{A.23}$$

from (A.18), the fifth term of the r.h.s. to match to the first term

$$\eta n^2 k^2 B_{1\theta} = O\left(n\right), \tag{A.24}$$

from (A.19), the second term of the r.h.s

$$\eta n^2 k^2 B_{1z} = O\left(1\right), \tag{A.25}$$

$O(n)$ terms,

from (A.13), the first and third terms of the r.h.s.

$$n\left[\left(S'\right)B_{1r}+B_{1z}\right]=O\left(1\right), \tag{A.26}$$

from (A.14) or (A.16), the first two terms of the r.h.s

$$n\left[\mu p_1+B_\theta B_{1\theta}\right]=O\left(1\right), \tag{A.27}$$

from (A.21), the fourth and fifth terms

$$n\left[\left(S'\right)v_{1r}+v_{1z}\right]=O\left(1\right), \tag{A.28}$$

from (A.18), the first and fifth terms of the r.h.s.

$$B_\theta in\left[\left(S'\right)v_{1r}+v_{1z}\right]+\eta n^2k^2B_{1\theta}=O\left(1\right), \tag{A.29}$$

or, using (A.28), (A.29) or (A.24) is

$$\eta n^2k^2B_{1\theta}=O\left(1\right), \tag{A.30}$$

So far, there are 3 equations linking the 8 perturbed quantities B_{1r}, $B_{1\theta}$, B_{1z}, v_{1r}, $v_{1\theta}$, v_{1z}, p_1 and ρ_1, namely equations (A.26), (A.27), and (A.28), and so we need to take the equations to the next order.

$O(1)$ equations are,

from (A.13)

$$in\left[\left(S'\right)B_{1r}+B_{1z}\right]+\frac{B_{1r}}{r}+\frac{dB_{1\theta}}{d\theta}=0, \tag{A.31}$$

from (A.14)

$$\mu\rho\sigma v_{1r} = -inS'(\mu p_1 + B_\theta B_{1\theta}) + \frac{B_\theta}{r}\frac{dB_{1r}}{d\theta} - \frac{2B_\theta B_{1\theta}}{r}, \qquad (A.32)$$

from (A.15)

$$\mu\rho\sigma v_{1\theta} = -\frac{\mu}{r}\frac{\partial p_1}{\partial\theta} + \frac{B_\theta B_{1r}}{r} + B_{1r}\frac{dB_\theta}{dr}, \qquad (A.33)$$

from (A.16)

$$\mu\rho\sigma v_{1z} = -in(\mu p_1 + B_\theta B_{1\theta}) + \frac{B_\theta}{r}\frac{dB_{1z}}{d\theta}, \qquad (A.34)$$

from (A.17)

$$\sigma B_{1r} = \frac{B_\theta}{r}\frac{dv_{1r}}{d\theta} - \eta n^2 k^2 B_{1r} + O\left(\frac{1}{n}\right), \qquad (A.35)$$

from (A.19)

$$\sigma B_{1z} = \frac{B_\theta}{r}\frac{dv_{1z}}{d\theta} - \eta n^2 k^2 B_{1z} + O\left(\frac{1}{n}\right), \qquad (A.36)$$

from (A.22)

$$\gamma p\sigma B_{1\theta} = B_\theta\sigma p_1 + \frac{B_\theta\gamma p}{r}\frac{dv_{1\theta}}{d\theta} + \left(B_\theta p' + \frac{\gamma p B_\theta}{r} - \gamma p B_\theta{}'\right)v_{1r}$$
$$-\eta n^2 k^2 \gamma p B_{1\theta} + O\left(\frac{1}{n}\right), \qquad (A.37)$$

Equations (A.31) to (A.37) represent 7 equations in the 7 perturbed quantities B_{1r}, $B_{1\theta}$, B_{1z}, v_{1r}, $v_{1\theta}$, v_{1z} and p_1.

From equation (A.21), a relation for ρ_1 is

$$\sigma\rho_1 + \rho' v_{1r} + \frac{v_{1\theta}}{r}\frac{\partial\rho}{\partial\theta} + \rho in\left[v_{1z} + (S')\,v_{1r}\right] + \frac{\rho}{r}v_{1r} + \frac{\rho}{r}\frac{dv_{1\theta}}{d\theta} = 0, \qquad (A.38)$$

Eliminate $-inS'(\mu p_1 + B_\theta B_{1\theta})$ between equations (A.32) and (A.34)

$$\mu\rho\sigma v_{1r} = \mu\rho\sigma S' v_{1z} - \frac{B_\theta S'}{r}\frac{dB_{1z}}{d\theta} + \frac{B_\theta}{r}\frac{dB_{1r}}{d\theta} - \frac{2B_\theta B_{1\theta}}{r}, \qquad (A.39)$$

using equations (A.26) and (A.28) to eliminate B_{1z}, v_{1z}, equations (A.35) and (A.36) are equivalent, and equation (A.39) becomes

$$\mu\rho\sigma k^2 v_{1r} = \frac{B_\theta k^2}{r}\frac{dB_{1r}}{d\theta} - \frac{2B_\theta B_{1\theta}}{r}, \tag{A.40}$$

The formal equations are (A.27), (A.33), (A.35), (A.37) and (A.40), in the five perturbed variables, v_{1r}, $v_{1\theta}$, B_{1r}, $B_{1\theta}$, p_1 and using (A.27) to eliminate $B_{1\theta}$ and the force balance equation

$$\mu p' + B_\theta \frac{dB_\theta}{dr} + \frac{{B_\theta}^2}{r} = 0$$

to tidy up equations (A.33) and (A.37) by eliminating the $B_\theta{}'$ term, gives

$$\mu\rho\sigma v_{1\theta} = -\frac{\mu}{r}\frac{dp_1}{d\theta} - \frac{\mu p'}{B_\theta}B_{1r}, \tag{A.41}$$

$$\sigma B_{1r} = \frac{B_\theta}{r}\frac{dv_{1r}}{d\theta} - \eta n^2 k^2 B_{1r}, \tag{A.42}$$

$$-\left(\gamma\mu p + {B_\theta}^2\right)\sigma p_1 = \frac{{B_\theta}^2\gamma p}{r}\frac{dv_{1\theta}}{d\theta} + \left({B_\theta}^2 p' + \frac{2\gamma p {B_\theta}^2}{r} + \gamma\mu p p'\right)v_{1r} + \eta n^2 k^2 \gamma\mu p p_1, \tag{A.43}$$

$$\mu\rho\sigma k^2 v_{1r} = \frac{B_\theta k^2}{r}\frac{dB_{1r}}{d\theta} + \frac{2\mu}{r}p_1, \tag{A.44}$$

eliminating p_1 from equation (A.41) using (A.43)

$$\begin{aligned}\left[\left(\gamma\mu p + {B_\theta}^2\right)\sigma + \eta n^2 k^2 \gamma\mu p\right] r\rho\sigma v_{1\theta} \\ = -\frac{rp'}{B_\theta}\left[\left(\gamma\mu p + {B_\theta}^2\right)\sigma + \eta n^2 k^2 \gamma\mu p\right] B_{1r} + \frac{{B_\theta}^2\gamma p}{r}\frac{d^2 v_{1\theta}}{d\theta^2} \\ + \left[\left(\gamma\mu p + {B_\theta}^2\right)p' + \frac{2\gamma p {B_\theta}^2}{r}\right]\frac{dv_{1r}}{d\theta},\end{aligned} \tag{A.45}$$

use equation (A.42) to eliminate B_{1r} from (A.45)

$$\left(\sigma+\eta n^2k^2\right)\frac{{B_\theta}^2\gamma p}{r}\frac{d^2v_{1\theta}}{d\theta^2}-\left(\sigma+\eta n^2k^2\right)\left[\left(\gamma\mu p+{B_\theta}^2\right)\sigma+\eta n^2k^2\gamma\mu p\right]r\rho\sigma v_{1\theta}$$
$$+\left[\frac{2{B_\theta}^2\gamma p\left(\sigma+\eta n^2k^2\right)}{r}+\eta n^2k^2p'{B_\theta}^2\right]\frac{dv_{1r}}{d\theta}=0, \qquad (A.46)$$

eliminating p_1 from equation (A.44) using (A.43)

$$\left[\left(\gamma\mu p+{B_\theta}^2\right)\sigma+\eta n^2k^2\gamma\mu p\right]\frac{\rho\sigma rk^2}{2}v_{1r}$$
$$=\left[\left(\gamma\mu p+{B_\theta}^2\right)\sigma+\eta n^2k^2\gamma\mu p\right]\frac{rB_\theta k^2}{2\mu}\frac{dB_{1r}}{d\theta}-\frac{{B_\theta}^2\gamma p}{r}\frac{dv_{1\theta}}{d\theta}$$
$$-\left[{B_\theta}^2p'+\frac{2{B_\theta}^2\gamma p}{r}+\gamma\mu pp'\right]v_{1r}, \qquad (A.47)$$

eliminate $\frac{dB_{1r}}{d\theta}$ from equation (A.47) using (A.42)

$$\left[\left(\gamma\mu p+{B_\theta}^2\right)\sigma+\eta n^2k^2\gamma\mu p\right]\frac{{B_\theta}^2k^2}{2\mu}\frac{d^2v_{1r}}{d\theta^2}-\left(\sigma+\eta n^2k^2\right){B_\theta}^2\gamma p\frac{dv_{1\theta}}{d\theta}$$
$$-\left(\sigma+\eta n^2k^2\right)\left[\left(\gamma\mu p+{B_\theta}^2\right)\frac{\rho\sigma^2r^2k^2}{2}+r{B_\theta}^2p'\right.$$
$$\left.+2{B_\theta}^2\gamma p+r\gamma\mu pp'+\frac{\eta n^2k^2\gamma\mu p\rho\sigma r^2k^2}{2}\right]v_{1r}=0, \qquad (A.48)$$

The coupled system

$$A\frac{d^2v_\theta}{d\theta^2}+B\frac{dv_r}{d\theta}+Cv_\theta=0, \qquad (A.49a)$$

$$D\frac{d^2v_r}{d\theta^2}+E\frac{dv_\theta}{d\theta}+Fv_r=0, \qquad (A.49b)$$

can be manipulated to give

$$AD\frac{d^4v}{d\theta^4}+\left(AF-BE+CD\right)\frac{d^2v}{d\theta^2}+CFv=0, \qquad (A.50)$$

where v can be replaced by v_r or v_θ.

Comparing with equations (A.46) and (A.48) we have

$$A = \left(\sigma + \eta n^2 k^2\right) \frac{{B_\theta}^2 \gamma p}{r}, \tag{A.51a}$$

$$B = \left[\frac{2{B_\theta}^2 \gamma p \left(\sigma + \eta n^2 k^2\right)}{r} + \eta n^2 k^2 p' {B_\theta}^2\right], \tag{A.51b}$$

$$C = -\left(\sigma + \eta n^2 k^2\right)\left[\left(\gamma \mu p + {B_\theta}^2\right)\sigma + \eta n^2 k^2 \gamma \mu p\right] r\rho\sigma, \tag{A.51c}$$

$$D = \left[\left(\gamma \mu p + {B_\theta}^2\right)\sigma + \eta n^2 k^2 \gamma \mu p\right] \frac{{B_\theta}^2 k^2}{2\mu}, \tag{A.51d}$$

$$E = -\left(\sigma + \eta n^2 k^2\right) {B_\theta}^2 \gamma p, \tag{A.51e}$$

$$F = -\left(\sigma + \eta n^2 k^2\right)\left[\left(\gamma \mu p + {B_\theta}^2\right)\frac{\rho\sigma^2 r^2 k^2}{2} + r{B_\theta}^2 p'\right.$$
$$\left. + 2{B_\theta}^2 \gamma p + r\gamma \mu p p' + \frac{\eta n^2 k^2 \gamma \mu p \rho \sigma r^2 k^2}{2}\right], \tag{A.51f}$$

and equation (A.50) is (dividing through by AD)

$$\frac{d^4 v}{d\theta^4} - \frac{\mu r}{k^2 {B_\theta}^2}\left[\left(\sigma + \eta n^2 k^2\right) 2r\rho\sigma k^2 + \frac{r\rho\sigma^2 k^2 {B_\theta}^2}{\gamma \mu p} + 2p'\right]\frac{d^2 v}{d\theta^2}$$
$$+ \frac{2\mu\rho\sigma r^2}{{B_\theta}^4 \gamma p k^2}\left(\sigma + \eta n^2 k^2\right)\left[\left(\gamma \mu p + {B_\theta}^2\right)\frac{\rho\sigma^2 r^2 k^2}{2} + r{B_\theta}^2 p'\right.$$
$$\left. + 2{B_\theta}^2 \gamma p + r\gamma \mu p p' + \frac{\eta n^2 k^2 \gamma \mu p \rho \sigma r^2 k^2}{2}\right] v = 0, \tag{A.52}$$

writing ${v_A}^2 = {B_\theta}^2/\mu\rho$, ${c_s}^2 = \gamma p/\rho$, then equation (A.52) becomes

$$\frac{d^4 v}{d\theta^4} - \frac{r}{{v_A}^2 k^2}\left[\left(\sigma^2 + \eta n^2 k^2 \sigma\right) 2rk^2 + \frac{rk^2 {v_A}^2 \sigma^2}{{c_s}^2} + \frac{2{c_s}^2}{\gamma}(lnp)'\right]\frac{d^2 v}{d\theta^2}$$
$$+ \frac{r^2}{{c_s}^2 {v_A}^4 k^2}\left(\sigma^2 + \eta n^2 k^2 \sigma\right)\left[\left({c_s}^2 + {v_A}^2\right)\left(r^2 k^2 \sigma^2 + \frac{2r{c_s}^2}{\gamma}(lnp)'\right)\right.$$
$$\left. + 4{v_A}^2 {c_s}^2 + \eta n^2 k^2 r^2 k^2 {c_s}^2 \sigma\right] v = 0, \tag{A.53}$$

Taking v of the form $e^{im\theta}$, $\eta n^2 = 0$ gives

$$m^4 + \frac{r}{{v_A}^2 k^2}\left[2rk^2\sigma^2 + \frac{rk^2{v_A}^2\sigma^2}{{c_s}^2} + \frac{2{c_s}^2}{\gamma}(lnp)'\right]m^2$$

$$+\frac{r^2\sigma^2}{{c_s}^2{v_A}^4k^2}\left[\left({c_s}^2+{v_A}^2\right)\left(r^2k^2\sigma^2 + \frac{2r{c_s}^2}{\gamma}(lnp)'\right) + 4{v_A}^2{c_s}^2\right] = 0, \qquad (A.54a)$$

or, alternatively

$$\frac{r^4}{{c_s}^2{v_A}^4}\left({c_s}^2+{v_A}^2\right)\sigma^4 + \frac{r^2}{{v_A}^2k^2}\left[\left(2k^2 + \frac{{v_A}^2k^2}{{c_s}^2}\right)m^2 + 4 + \frac{2r}{{v_A}^2}\left({c_s}^2+{v_A}^2\right)(lnp)'\right]\sigma^2$$

$$+m^2\left[m^2 + \frac{2r{c_s}^2}{\gamma{v_A}^2k^2}(lnp)'\right] = 0, \qquad (A.54b)$$

in terms of σ^2

$$\sigma^2 = \frac{-E \pm \sqrt{E^2 - F}}{2r^2k^2\left({c_s}^2+{v_A}^2\right)} \qquad (A.55a)$$

where

$$E = {v_A}^2\left(2{c_s}^2+{v_A}^2\right)m^2k^2 + 4{v_A}^2{c_s}^2 + 2r{c_s}^2\left({c_s}^2+{v_A}^2\right)(lnp)', \qquad (A.55b)$$

$$F = 4m^2k^2{c_s}^2{v_A}^2\left({c_s}^2+{v_A}^2\right)\left[m^2k^2{v_A}^2 + \frac{2r{c_s}^2}{\gamma}(lnp)'\right], \qquad (A.55c)$$

This shows that pressure gradient is driving the instability since all other terms in E and F are positive definite.

Using the equilibrium quantities from Hood (1986)

$$B_\theta = \frac{B_0 r}{1+r^2}, \qquad (A.56a)$$

$$\mu p = \frac{{B_0}^2}{2}\frac{1}{(1+r^2)^2}, \qquad (A.56b)$$

$$\mu p' = \frac{{B_0}^2(-2r)}{(1+r^2)^3}, \qquad (A.56c)$$

$$\rho = \frac{{B_0}^2 \rho^*}{\left(1+r^2\right)^2}, \tag{A.56d}$$

$$\gamma = 1, \tag{A.56e}$$

$$k^2 = 1 \tag{A.56f}$$

gives the fourth order equation in v_r or v_θ

$$\frac{d^4 v}{d\theta^4} - \left[\frac{-4}{\left(1+r^2\right)} + 2\left(1+r^2\right)\rho^*\sigma^2 + 2\eta n^2 \rho^* \sigma\right]\frac{d^2 v}{d\theta^2}$$

$$+ \left[\frac{-4r^2}{\left(1+r^2\right)} + \left(1+2r^2\right)\rho^*\sigma^2 + \eta n^2 \rho^* \sigma\right]\left(\sigma + \eta n^2\right)\rho^* \sigma v = 0, \tag{A.57}$$

the coupled ballooning equations are

$$\left(\sigma + \eta n^2\right)\frac{d^2 v_\theta}{d\theta^2} + 2\left[\sigma + \frac{\eta n^2 \left(1-r^2\right)}{1+r^2}\right]\frac{dv_r}{d\theta}$$

$$- \left(\sigma + \eta n^2\right)\left[\left(1+2r^2\right)\sigma + \eta n^2\right]\rho^* \sigma v_\theta = 0, \tag{A.58a}$$

$$\left[\left(1+2r^2\right)\sigma + \eta n^2\right]\frac{d^2 v_r}{d\theta^2} - 2\left(\sigma + \eta n^2\right)\frac{dv_\theta}{d\theta}$$

$$- \left(\sigma + \eta n^2\right)\left[\frac{-4r^2}{1+r^2} + \left(1+2r^2\right)\rho^*\sigma^2 + \eta n^2 \rho^* \sigma\right] v_r = 0, \tag{A.58b}$$

The previous equations have been derived using the assumption that the second order derivative with respect to the poloidal angle, θ, of the perturbed magnetic field is small compared to n^2 in equations (A.17), (A.18) and (A.19). If we drop this assumption, then equations (A.41), (A.42), (A.43) and (A.44) are transformed to

$$\mu \rho \sigma v_{1\theta} = -\frac{\mu}{r}\frac{dp_1}{d\theta} - \frac{\mu p'}{B_\theta} B_{1r}, \tag{A.59}$$

$$\sigma B_{1r} = \frac{B_\theta}{r}\frac{dv_{1r}}{d\theta} - \eta n^2 k^2 B_{1r} - \frac{\eta}{r^2}\frac{d^2 B_{1r}}{d\theta^2}, \tag{A.60}$$

$$-\left(\gamma\mu p + {B_\theta}^2\right)\sigma p_1 = \frac{{B_\theta}^2\gamma p}{r}\frac{dv_{1\theta}}{d\theta} + \left({B_\theta}^2 p' + \frac{2\gamma p {B_\theta}^2}{r} + \gamma\mu p p'\right) v_{1r}$$
$$+\eta n^2 k^2 \gamma\mu p p_1 + \frac{\eta}{r^2}\gamma\mu p\frac{d^2 p_1}{d\theta^2}, \qquad (A.61)$$

$$\mu\rho\sigma k^2 v_{1r} = \frac{B_\theta k^2}{r}\frac{dB_{1r}}{d\theta} + \frac{2\mu}{r}p_1, \qquad (A.62)$$

To reduce equations (A.59), (A.60), (A.61) and (A.62) to two coupled ordinary differential equations in v_{1r} and $v_{1\theta}$, two equations have to be obtained, one involving B_{1r} or one of its derivatives as an expression of v_{1r},$v_{1\theta}$ or some of their derivatives, and the other with p_1 or one of its derivatives as an expression of v_{1r},$v_{1\theta}$ or some of their derivatives. This is in order that p_1 and B_{1r} can be eliminated from (A.59) and (A.62) to give the coupled ordinary differential equations.

Combining (A.60) and the θ-derivative of (A.62)

$$\left(\sigma + \eta n^2 k^2\right) B_{1r} = \left(\frac{B_\theta}{r} - \frac{\eta\mu\rho\sigma}{r B_\theta}\right)\frac{dv_{1r}}{d\theta} + \frac{2\eta\mu}{r^2 B_\theta k^2}\frac{dp_1}{d\theta}, \qquad (A.63)$$

Combining (A.59) and (A.63)

$$\left(\sigma + \eta n^2 k^2 + \frac{2\eta\mu p'}{r{B_\theta}^2 k^2}\right) B_{1r} = \left(\frac{B_\theta}{r} - \frac{\eta\mu\rho\sigma}{r B_\theta}\right)\frac{dv_{1r}}{d\theta} - \frac{2\eta\mu\rho\sigma}{r B_\theta k^2} v_{1\theta}, \qquad (A.64)$$

and B_{1r} is in a suitable form to be eliminated.

Combining (A.61) and the θ-derivative of (A.59)

$$-\left[\left(\gamma\mu p + {B_\theta}^2\right)\sigma + \eta n^2 k^2 \gamma\mu p\right] p_1 = \left(\frac{{B_\theta}^2\gamma p}{r} - \frac{\eta\gamma\mu p\rho\sigma}{r}\right)\frac{dv_{1\theta}}{d\theta}$$
$$+\left({B_\theta}^2 p' + \frac{2\gamma p {B_\theta}^2}{r} + \gamma\mu p p'\right) v_{1r} - \frac{\eta\gamma\mu p p'}{r B_\theta}\frac{dB_{1r}}{d\theta}, \qquad (A.65)$$

Combining (A.62) and (A.65)

$$-\left[\left(\gamma\mu p + {B_\theta}^2\right)\sigma + \eta n^2k^2\gamma\mu p + \frac{2\eta\gamma\mu^2pp'}{r{B_\theta}^2k^2}\right]p_1 = \left(\frac{{B_\theta}^2\gamma p}{r} - \frac{\eta\gamma\mu p\rho\sigma}{r}\right)\frac{dv_{1\theta}}{d\theta}$$

$$+\left({B_\theta}^2p' + \frac{2\gamma p{B_\theta}^2}{r} + \gamma\mu pp' - \frac{\eta\gamma\mu^2pp'\rho\sigma}{{B_\theta}^2}\right)v_{1r}, \qquad (A.66)$$

and p_1 is in a suitable form to be eliminated.

Substituting B_{1r}, p_1 from (A.64) and (A.66) into (A.59) and rearranging

$$\frac{\gamma p}{r}\left(\sigma + \eta n^2k^2 + \frac{2\eta\mu p'}{r{B_\theta}^2k^2}\right)\left({B_\theta}^2 - \eta\mu\rho\sigma\right)\frac{d^2v_{1\theta}}{d\theta^2}$$

$$+\left[\frac{2{B_\theta}^2\gamma p\left(\sigma + \eta n^2k^2\right)}{r} + \eta n^2k^2p'{B_\theta}^2 + \eta\mu p'\left(\frac{2p'}{rk^2} + \frac{4\gamma p}{r^2k^2} + \rho\sigma^2\right)\right]\frac{dv_{1r}}{d\theta}$$

$$-\left(\sigma + \eta n^2k^2\right)\left[\left(\gamma\mu p + {B_\theta}^2\right)\sigma + \eta n^2k^2\gamma\mu p + \frac{2\eta\gamma\mu^2pp'}{r{B_\theta}^2k^2}\right]r\rho\sigma v_{1\theta} = 0, \qquad (A.67)$$

which can be compared with (A.46).

Substituting B_{1r}, p_1 from (A.64) and (A.66) into (A.62) and rearranging,

$$\left[\left(\gamma\mu p + {B_\theta}^2\right)\sigma + \eta n^2k^2\gamma\mu p\right]\left({B_\theta}^2 - \eta\mu\rho\sigma\right)\frac{k^2}{2\mu}\frac{d^2v_{1r}}{d\theta^2}$$

$$-\left[\left(\sigma + \eta n^2k^2\right){B_\theta}^2\gamma p + \eta{B_\theta}^2\rho\sigma^2 + \frac{2\eta\gamma\mu pp'}{rk^2}\right]\frac{dv_{1\theta}}{d\theta}$$

$$-\left(\sigma + \eta n^2k^2\right)\left[\left(\gamma\mu p + {B_\theta}^2\right)\frac{\rho\sigma^2r^2k^2}{2} + r{B_\theta}^2p' + 2{B_\theta}^2\gamma p + r\gamma\mu pp' + \right.$$

$$\left. + \frac{\eta n^2k^2\gamma\mu p\rho\sigma r^2k^2}{2}\right]v_{1r}$$

$$-\frac{\eta\mu p'}{{B_\theta}^2k^2}\left[\left(\sigma + \eta n^2k^2\right)\gamma\mu p\rho\sigma rk^2 + \rho\sigma^2r{B_\theta}^2k^2 + 2{B_\theta}^2p' + \frac{4\gamma p{B_\theta}^2}{r} + 2\gamma pp'\right]v_{1r} = 0, \qquad (A.68)$$

which can be compared with equation (A.48).

For the growth rate, σ, tending to a non-zero positive value as the density ratio, ρ, tends to infinity, $\eta\rho\sigma$ can no longer be neglected by comparison with $\eta n^2 k^2$ as $\rho\sigma$ tends to infinity as ρ tends to infinity. These extra diffusive terms may allow velocities which tended to zero using the previous analysis as ρ tended to infinity, tend to a non-zero value dependent on the extra diffusion terms brought into equation (A.67) and (A.68) as compared with the equations (A.46) and (A.48) giving flows across the boundary.

Appendix B

Derivation of small r radial expansions

With $\sigma = 0$ and $p = 0$, equations (3.29a) and (3.29b) become

$$\frac{\partial}{\partial r}\left[\frac{B^2}{r}\frac{\partial\left(r\xi_r\right)}{\partial r}\right]+B^2\left(\mathbf{e}_{\|}\cdot\nabla\right)^2\xi_r-\frac{d}{dr}\left(\frac{B_\theta^2}{r^2}\right)r\xi_r+\frac{\partial}{\partial r}\left[B^2\mathbf{e}_\perp\cdot\nabla\xi_\perp\right]-\frac{2BB_\theta}{r}\frac{\partial\xi_\perp}{\partial z}=0, \tag{B.1a}$$

$$B^2\left[\left(\mathbf{e}_\perp\cdot\nabla\right)^2+\left(\mathbf{e}_{\|}\cdot\nabla\right)^2\right]\xi_\perp+\mathbf{e}_\perp\cdot\nabla\left[\frac{B^2}{r}\frac{\partial\left(r\xi_r\right)}{\partial r}\right]+\frac{2BB_\theta}{r}\frac{\partial\xi_r}{\partial z}=0, \tag{B.1b}$$

Write

$$\xi_r=\xi_r\left(r,z\right)e^{im\theta}, \tag{B.2a}$$

$$\xi_\perp=\xi_\perp\left(r,z\right)e^{im\theta}, \tag{B.2b}$$

then equations (B.1a) and (B.1b) are

$$\begin{aligned}&\frac{\partial}{\partial r}\left[\frac{B^2}{r}\frac{\partial\left(r\xi_r\right)}{\partial r}\right]+\left(\frac{imB_\theta}{r}+B_z\frac{\partial}{\partial z}\right)^2\xi_r-\frac{d}{dr}\left(\frac{B_\theta^2}{r^2}\right)r\xi_r\\&+\frac{\partial}{\partial r}\left[B\left(\frac{imB_z}{r}-B_\theta\frac{\partial}{\partial z}\right)\xi_\perp\right]-\frac{2BB_\theta}{r}\frac{\partial\xi_\perp}{\partial z}=0,\end{aligned} \tag{B.3a}$$

$$\begin{aligned}&\left[\left(\frac{imB_z}{r}-B_\theta\frac{\partial}{\partial z}\right)^2+\left(\frac{imB_\theta}{r}+B_z\frac{\partial}{\partial z}\right)^2\right]\xi_\perp+\\&+\left(\frac{imB_z}{r}-B_\theta\frac{\partial}{\partial z}\right)\left[\frac{B}{r}\frac{\partial\left(r\xi_r\right)}{\partial r}\right]+\frac{2BB_\theta}{r}\frac{\partial\xi_r}{\partial z}=0.\end{aligned} \tag{B.3b}$$

Equations (B.3a) and (B.3b) simplified, giv

$$\frac{\partial}{\partial r}\left[\frac{B^2}{r}\frac{\partial\left(r\xi_r\right)}{\partial r}\right]-\frac{m^2B_\theta^2}{r^2}\xi_r+\frac{2imB_\theta B_z}{r}\frac{\partial\xi_r}{\partial z}+B_z^2\frac{\partial^2\xi_r}{\partial z^2}-\frac{d}{dr}\left(\frac{B_\theta^2}{r^2}\right)r\xi_r$$

$$+\frac{\partial}{\partial r}\left[\frac{imBB_z}{r}\xi_\perp - BB_\theta\frac{\partial\xi_\perp}{\partial z}\right] - \frac{2BB_\theta}{r}\frac{\partial\xi_\perp}{\partial z} = 0, \qquad (B.4a)$$

$$-\frac{m^2B^2}{r^2}\xi_\perp + B^2\frac{\partial^2\xi_\perp}{\partial z^2} + \frac{imBB_z}{r^2}\frac{\partial(r\xi_r)}{\partial r} - \frac{BB_\theta}{r}\frac{\partial}{\partial r}\left[r\frac{\partial\xi_r}{\partial z}\right] + \frac{2BB_\theta}{r}\frac{\partial\xi_r}{\partial z} = 0. \qquad (B.4b)$$

Expand in a Frobenius expansion about $r = 0$ as

$$\xi_r = r^\nu\left(f_0(z) + f_1(z)\,r^2 + \cdots\right), \qquad (B.5)$$

$$\xi_\perp = r^\nu\left(g_0(z) + g_1(z)\,r^2 + \cdots\right), \qquad (B.6)$$

$$B_\theta = C_0 r + C_1 r^3 + \cdots, \qquad (B.7)$$

$$B_z = b_0 + b_1 r^2 + \cdots. \qquad (B.8)$$

Then using

$$B^2 = B_\theta^2 + B_z^2 = b_0^2 + \left(2b_0b_1 + C_0^2\right)r^2 + \cdots, \qquad (B.9)$$

and the equilibrium equation

$$\frac{B_\theta}{r}(rB_\theta)' + B_zB_z' = 0, \qquad (B.10)$$

equation (B.10) is expanded to give

$$\left[C_0 + C_1r^2 + \cdots\right]\left[2C_0r + 4C_1r^3 + \cdots\right] + \left[b_0 + b_1r^2 + \cdots\right]\left[2b_1r + 4b_2r^3 + \cdots\right] = 0, \qquad (B.11)$$

To O(r)

$$C_0^2 + b_0b_1 = 0, \qquad (B.12)$$

and so from (B.9)

$$B^2 = b_0^2 - C_0^2r^2 + \cdots, \qquad (B.13)$$

$$B = b_0 - \frac{C_0^2}{2b_0} r^2 + \cdots, \tag{B.14}$$

$$B_\theta^2 = C_0^2 r^2 + 2C_0 C_1 r^4 + \cdots, \tag{B.15}$$

$$B_z^2 = b_0^2 - 2C_0^2 r^2 + \cdots, \tag{B.16}$$

$$B_\theta B_z = b_0 C_0 r + \left(b_0 C_1 - \frac{C_0^3}{b_0} \right) r^3 + \cdots, \tag{B.17}$$

$$BB_\theta = b_0 C_0 r + \left(b_0 C_1 - \frac{C_0^3}{2b_0} \right) r^3 + \cdots, \tag{B.18}$$

$$BB_z = b_0^2 - \frac{3}{2} C_0^2 r^2 + \cdots. \tag{B.19}$$

Then equations (B.4a) and (B.4b) are

$$\begin{aligned}
&\frac{\partial}{\partial r}\left[\left\{\frac{b_0^2}{r} - C_0^2 r + \cdots\right\}\left\{(\nu+1) f_0(z) + (\nu+3) f_1(z) r^2 + \cdots\right\} r^\nu\right] \\
&\quad - \left[m^2 C_0^2 + 2m^2 C_0 C_1 r^2 + \cdots\right]\left[f_0(z) + f_1(z) r^2 + \cdots\right] r^\nu \\
&\quad + i\left[2m b_0 C_0 + 2m\left(b_0 C_1 - \frac{C_0^3}{b_0}\right) r^2 + \cdots\right]\left[\frac{df_0}{dz} + \frac{df_1}{dz} r^2 + \cdots\right] r^\nu \\
&\quad + \left[b_0^2 - 2C_0^2 r^2 + \cdots\right]\left[\frac{d^2 f_0}{dz^2} + \frac{d^2 f_1}{dz^2} r^2 + \cdots\right] r^\nu \\
&\quad - \left[4C_0 C_1 r^2 + \cdots\right]\left[f_0(z) + f_1(z) r^2 + \cdots\right] r^\nu \\
&\quad + i\frac{\partial}{\partial r}\left[\left\{\frac{m b_0^2}{r} - \frac{3mC_0^2}{2} r + \cdots\right\}\left\{g_0(z) + g_1(z) r^2 + \cdots\right\} r^\nu\right] \\
&\quad - \frac{\partial}{\partial r}\left[\left\{b_0 C_0 r + \left(b_0 C_1 - \frac{C_0^3}{2b_0}\right) r^3 + \cdots\right\}\left\{\frac{dg_0}{dz} + \frac{dg_1}{dz} r^2 + \cdots\right\} r^\nu\right] \\
&\quad - \left[2b_0 C_0 + \left(2b_0 C_1 - \frac{C_0^3}{b_0}\right) r^2 + \cdots\right]\left[\frac{dg_0}{dz} + \frac{dg_1}{dz} r^2 + \cdots\right] r^\nu = 0, \qquad (B.20a) \\
&\quad - \left[\frac{m^2 b_0^2}{r^2} - m^2 C_0^2 + \cdots\right]\left[g_0(z) + g_1(z) r^2 + \cdots\right] r^\nu \\
&\quad + \left[b_0^2 - C_0^2 r^2 + \cdots\right]\left[\frac{d^2 g_0}{dz^2} + \frac{d^2 g_1}{dz^2} r^2 + \cdots\right] r^\nu
\end{aligned}$$

$$+i\left[\frac{mb_0^2}{r^2}-\frac{3}{2}mC_0^2+\cdots\right]\left[(\nu+1)\,f_0(z)+(\nu+3)\,f_1(z)\,r^2+\cdots\right]r^\nu$$
$$-\left[b_0C_0+\left(b_0C_1-\frac{C_0^3}{2b_0}\right)r^2+\cdots\right]\left[(\nu+1)\,\frac{df_0}{dz}+(\nu+3)\,\frac{df_1}{dz}r^2+\cdots\right]r^\nu$$
$$+\left[2b_0C_0+\left(2b_0C_1-\frac{C_0^3}{b_0}\right)r^2+\cdots\right]\left[\frac{df_0}{dz}+\frac{df_1}{dz}r^2+\cdots\right]r^\nu=0. \qquad (B.20b)$$

Equations (B.20a) and (B.20b) are ($\nu \neq 1$)

$$\left[\frac{(\nu-1)(\nu+1)\,b_0^2}{r^2}f_0(z)+\left\{(\nu+1)(\nu+3)\,b_0^2f_1(z)-(\nu+1)^2\,C_0^2f_0(z)\right\}+\cdots\right]r^\nu\cdot$$
$$-\left[m^2C_0^2f_0(z)+\cdots\right]r^\nu$$
$$+i\left[2mb_0C_0\frac{df_0}{dz}+\cdots\right]r^\nu$$
$$+\left[b_0^2\frac{d^2f_0}{dz^2}+\cdots\right]r^\nu$$
$$-\left[4C_0C_1f_0(z)\,r^2+\cdots\right]r^\nu$$
$$+i\left[\frac{(\nu-1)\,mb_0^2}{r^2}g_0(z)+\left\{(\nu+1)\,mb_0^2g_1(z)-(\nu+1)\,\frac{3mC_0^2}{2}g_0(z)\right\}+\cdots\right]r^\nu$$
$$-\left[(\nu+1)\,b_0C_0\frac{dg_0}{dz}+\cdots\right]r^\nu$$
$$-\left[2b_0C_0\frac{dg_0}{dz}+\cdots\right]r^\nu=0, \qquad (B.21a)$$
$$-\left[\frac{m^2b_0^2}{r^2}g_0(z)+\left\{m^2b_0^2g_1(z)-m^2C_0^2g_0(z)\right\}+\cdots\right]r^\nu$$
$$+\left[b_0^2\frac{d^2g_0}{dz^2}+\cdots\right]r^\nu$$
$$+i\left[\frac{(\nu+1)\,mb_0^2}{r^2}f_0(z)+\left\{(\nu+3)\,mb_0^2f_1(z)-\frac{3}{2}mC_0^2(\nu+1)\,f_0(z)\right\}+\cdots\right]r^\nu$$
$$-\left[(\nu+1)\,b_0C_0\frac{df_0}{dz}+\cdots\right]r^\nu$$
$$+\left[2b_0C_0\frac{df_0}{dz}+\cdots\right]r^\nu=0. \qquad (B.21b)$$

Equation (B.21a) and (B.21b) to O($r^{\nu-2}$)

$$(\nu-1)\, b_0^2 \left[(\nu+1)\, f_0(z) + img_0(z)\right] = 0, \qquad (B.22a)$$

$$imb_0^2 \left[(\nu+1)\, f_0(z) + img_0(z)\right] = 0, \qquad (B.22b)$$

From (B.22a) and (B.22b)

$$i(\nu+1)\, f_0(z) = mg_0(z)\,. \qquad (B.23)$$

Equations (B.21a) and (B.21b) to O(r^{ν})

$$(\nu+1)(\nu+3)\, b_0^2 f_1(z) - (\nu+1)^2 C_0^2 f_0(z) - m^2 C_0^2 f_0(z) +$$

$$+2imb_0 C_0 \frac{df_0}{dz} + b_0^2 \frac{d^2 f_0}{dz^2} + i(\nu+1)\, mb_0^2 g_1(z) +$$

$$+\frac{3}{2}(\nu+1)^2 C_0^2 f_0(z) - i(\nu+1)^2 \frac{b_0 C_0}{m}\frac{df_0}{dz} - \frac{2ib_0 C_0}{m}(\nu+1)\frac{df_0}{dz} = 0, \qquad (B.24a)$$

$$-m^2 b_0^2 g_1(z) + i(\nu+1)\, mC_0^2 f_0(z) + \frac{i(\nu+1)\, b_0^2}{m}\frac{d^2 f_0}{dz^2} + i(\nu+3)\, mb_0^2 f_1(z)$$

$$-\frac{3}{2} imC_0^2(\nu+1)\, f_0(z) - (\nu+1)\, b_0 C_0 \frac{df_0}{dz} + 2b_0 C_0 \frac{df_0}{dz} = 0. \qquad (B.24b)$$

(B.24a) and (B.24b) reduce to

$$\frac{i}{m}\left[m^2 - (\nu+1)^2\right]\left(imC_0 + b_0 \frac{d}{dz}\right)^2 f_0 = 0. \qquad (B.25)$$

The only non-trivial solution is $\mu = \pm m - 1$. Thus, the non-singular solution behaves like $r^{m-1} f_0(z)$ near $r = 0$. $f_0(z)$ is an arbitrary function at this stage and is only known when the correct radial boundary condition at $r = R$ is satisfied.

Derivation of small r radial expansion for equilibrium equations of motion with pressure

With $\sigma = 0$, $p \neq 0$, equations (3.29a), (3.29b) and (3.29c)

$$\frac{\partial}{\partial r}\left[\frac{B^2}{r}\frac{\partial\left(r\xi_r\right)}{\partial r}\right] + B^2\left(\mathbf{e}_{\|}\cdot\nabla\right)^2\xi_r - \frac{d}{dr}\left(\frac{B_\theta^2}{r^2}\right)r\xi_r + \frac{\partial}{\partial r}\left[B^2\mathbf{e}_\perp\cdot\nabla\xi_\perp\right]$$

$$-\frac{2BB_\theta}{r}\frac{\partial\xi_\perp}{\partial z} + \mu\gamma\frac{\partial}{\partial r}\left[p\nabla\cdot\boldsymbol{\xi}\right] = 0, \qquad (B.26a)$$

$$B^2\left[\left(\mathbf{e}_\perp\cdot\nabla\right)^2 + \left(\mathbf{e}_{\|}\cdot\nabla\right)^2\right]\xi_\perp + \mathbf{e}_\perp\cdot\nabla\left[\frac{B^2}{r}\frac{\partial\left(r\xi_r\right)}{\partial r}\right] + \frac{2BB_\theta}{r}\frac{\partial\xi_r}{\partial z} + \mu\gamma\mathbf{e}_\perp\cdot\nabla\left[p\nabla\cdot\boldsymbol{\xi}\right] = 0, \qquad (B.26b)$$

$$\mathbf{e}_{\|}\cdot\nabla\left[p\nabla\cdot\boldsymbol{\xi}\right] = 0, \qquad (B.26c)$$

In addition to (B.2) set

$$\xi_{\|} = \xi_{\|}\left(r,z\right)e^{im\theta}, \qquad (B.27)$$

then equations (B.26a), (B.26b) and (B.26c) are

$$\frac{\partial}{\partial r}\left[\frac{B^2}{r}\frac{\partial\left(r\xi_r\right)}{\partial r}\right] + \left(\frac{imB_\theta}{r} + B_z\frac{\partial}{\partial z}\right)^2\xi_r - \frac{d}{dr}\left(\frac{B_\theta^2}{r^2}\right)r\xi_r$$

$$+\frac{\partial}{\partial r}\left[B\left(\frac{imB_z}{r} - B_\theta\frac{\partial}{\partial z}\right)\xi_\perp\right] - \frac{2BB_\theta}{r}\frac{\partial\xi_\perp}{\partial z}$$

$$+\mu\gamma\frac{\partial}{\partial r}\left[p\left\{\frac{1}{r}\frac{\partial\left(r\xi_r\right)}{\partial r} + \frac{1}{B}\left(\frac{imB_\theta}{r} + B_z\frac{\partial}{\partial z}\right)\xi_{\|} + \frac{1}{B}\left(\frac{imB_z}{r} - B_\theta\frac{\partial}{\partial z}\right)\xi_\perp\right\}\right] = 0, \qquad (B.28a)$$

$$\left[\left(\frac{imB_z}{r} - B_\theta\frac{\partial}{\partial z}\right)^2 + \left(\frac{imB_\theta}{r} + B_z\frac{\partial}{\partial z}\right)^2\right]\xi_\perp + \left(\frac{imB_z}{r} - B_\theta\frac{\partial}{\partial z}\right)\left[\frac{B}{r}\frac{\partial\left(r\xi_r\right)}{\partial r}\right] +$$

$$+\frac{2BB_\theta}{r}\frac{\partial\xi_r}{\partial z} + \mu\gamma\left[\frac{1}{B}\left(\frac{imB_z}{r} - B_\theta\frac{\partial}{\partial z}\right)\left[p\left\{\frac{1}{r}\frac{\partial\left(r\xi_r\right)}{\partial r}\right.\right.\right.$$

$$\left.\left.\left.+\frac{1}{B}\left(\frac{imB_\theta}{r} + B_z\frac{\partial}{\partial z}\right)\xi_{\|} + \frac{1}{B}\left(\frac{imB_z}{r} - B_\theta\frac{\partial}{\partial z}\right)\xi_\perp\right\}\right]\right] = 0, \qquad (B.28b)$$

$$\frac{1}{B}\left(\frac{imB_\theta}{r}+B_z\frac{\partial}{\partial z}\right)\left[p\left\{\frac{1}{r}\frac{\partial\left(r\xi_r\right)}{\partial r}+\frac{1}{B}\left(\frac{imB_\theta}{r}+B_z\frac{\partial}{\partial z}\right)\xi_{\|}+\right.\right.$$
$$\left.\left.+\frac{1}{B}\left(\frac{imB_z}{r}-B_\theta\frac{\partial}{\partial z}\right)\xi_\perp\right\}\right]=0. \qquad (B.28c)$$

Multiplying by B^2, equations (B.28a), (B.28b) and (B.28c) simplify to

$$B^2\frac{\partial}{\partial r}\left[\frac{B^2}{r}\frac{\partial\left(r\xi_r\right)}{\partial r}\right]-\frac{m^2B^2B_\theta^2}{r^2}\xi_r+\frac{2imB^2B_\theta B_z}{r}\frac{\partial\xi_r}{\partial z}+B^2B_z^2\frac{\partial^2\xi_r}{\partial z^2}-B^2\frac{d}{dr}\left(\frac{B_\theta^2}{r^2}\right)r\xi_r$$
$$+B^2\frac{\partial}{\partial r}\left[\frac{imBB_z}{r}\xi_\perp-BB_\theta\frac{\partial\xi_\perp}{\partial z}\right]-\frac{2B^3B_\theta}{r}\frac{\partial\xi_\perp}{\partial z}+\mu\gamma B^2\frac{\partial}{\partial r}\left[\frac{p}{r}\frac{\partial\left(r\xi_r\right)}{\partial r}\right]$$
$$-\mu\gamma p\left(\frac{imB_\theta}{r}\xi_{\|}+\frac{imB_z}{r}\xi_\perp\right)\frac{dB}{dr}+\mu\gamma B\frac{\partial}{\partial r}\left[p\left(\frac{imB_\theta}{r}\xi_{\|}+\frac{imB_z}{r}\xi_\perp\right)\right]$$
$$-\mu\gamma p\left(B_z\frac{\partial\xi_{\|}}{\partial z}-B_\theta\frac{\partial\xi_\perp}{\partial z}\right)\frac{dB}{dr}+\mu\gamma B\frac{\partial}{\partial r}\left[p\left(B_z\frac{\partial\xi_{\|}}{\partial z}-B_\theta\frac{\partial\xi_\perp}{\partial z}\right)\right]=0, \qquad (B.29a)$$

$$-\frac{m^2B^4}{r^2}\xi_\perp+B^4\frac{\partial^2\xi_\perp}{\partial z^2}+\frac{imB^3B_z}{r^2}\frac{\partial\left(r\xi_r\right)}{\partial r}-\frac{B^3B_\theta}{r}\frac{\partial}{\partial r}\left[r\frac{\partial\xi_r}{\partial z}\right]+\frac{2B^3B_\theta}{r}\frac{\partial\xi_r}{\partial z}$$
$$+\mu\gamma\frac{imBB_zp}{r^2}\frac{\partial\left(r\xi_r\right)}{\partial r}-\mu\gamma\frac{BB_\theta p}{r}\frac{\partial}{\partial r}\left(r\frac{\partial\xi_r}{\partial z}\right)$$
$$+\mu\gamma p\left[-\frac{m^2B_\theta B_z}{r^2}+\frac{im}{r}\left(B_z^2-B_\theta^2\right)\frac{\partial}{\partial z}-B_\theta B_z\frac{\partial^2}{\partial z^2}\right]\xi_{\|}$$
$$+\mu\gamma p\left[-\frac{m^2B_z^2}{r^2}-\frac{2imB_\theta B_z}{r}\frac{\partial}{\partial z}-B_\theta^2\frac{\partial^2}{\partial z^2}\right]\xi_\perp=0, \qquad (B.29b)$$

$$\frac{imBB_\theta}{r^2}\frac{\partial\left(r\xi_r\right)}{\partial r}+\frac{BB_z}{r}\frac{\partial}{\partial r}\left(r\frac{\partial\xi_r}{\partial z}\right)+\left(-\frac{m^2B_\theta^2}{r^2}+\frac{2imB_\theta B_z}{r}\frac{\partial}{\partial z}+B_z^2\frac{\partial^2}{\partial z^2}\right)\xi_{\|}$$
$$+\left(-\frac{m^2B_\theta B_z}{r^2}+\frac{im}{r}\left(B_z^2-B_\theta^2\right)\frac{\partial}{\partial z}-B_\theta B_z\frac{\partial^2}{\partial z^2}\right)\xi_\perp=0. \qquad (B.29c)$$

Expand the displacements as (B.5), (B.6) and

$$\xi_{\|}=r^\nu\left(h_0\left(z\right)+h_1\left(z\right)r^2+\cdots\right), \qquad (B.30)$$

$$p=p_0+p_1r^2+\cdots, \qquad (B.31)$$

The equilibrium equation

$$\frac{B_\theta}{r}(rB_\theta)' + B_z B_z' + p' = 0. \tag{B.32}$$

expanded gives

$$\left[C_0 + C_1 r^2 + \cdots\right]\left[2C_0 r + 4C_1 r^3 + \cdots\right] + \left[b_0 + b_1 r^2 + \cdots\right]\left[2b_1 r + 4b_2 r^3 + \cdots\right]$$

$$+ \left[2p_1 r + 4p_2 r^3 + \cdots\right] = 0, \tag{B.33}$$

giving to O(r)

$$C_0^2 + b_0 b_1 + p_1 = 0. \tag{B.34}$$

and from expansion (B.9)

$$B^2 = b_0^2 - \left(C_0^2 + 2p_1\right) r^2 + \cdots, \tag{B.35}$$

$$B = b_0 - \frac{(C_0^2 + 2p_1)}{2b_0} r^2 + \cdots, \tag{B.36}$$

$$\frac{dB}{dr} = -\frac{(C_0^2 + 2p_1)}{b_0} r + \cdots, \tag{B.37}$$

$$B_z = b_0 - \frac{(C_0^2 + p_1)}{b_0} r^2 + \cdots, \tag{B.38}$$

$$B_z^2 = b_0^2 - \left(2C_0^2 + 2p_1\right) r^2 + \cdots, \tag{B.39}$$

$$B_\theta B_z = b_0 C_0 r + \left(b_0 C_1 - \frac{(C_0^3 + C_0 p_1)}{b_0}\right) r^3 + \cdots, \tag{B.40}$$

$$BB_\theta = b_0 C_0 r + \left(b_0 C_1 - \frac{(C_0^3 + C_0 p_1)}{2b_0}\right) r^3 + \cdots, \tag{B.41}$$

$$BB_z = b_0^2 - \left(\frac{3}{2} C_0^2 + 2p_1\right) r^2 + \cdots. \tag{B.42}$$

Then equations (B.29a), (B.29b) and (B.29c) are

$$\left[b_0^2-\left(C_0^2+2p_1\right)r^2+\cdots\right]\frac{\partial}{\partial r}\left[\left\{\frac{b_0^2}{r}-\left(C_0^2+2p_1\right)r+\cdots\right\}\{(\nu+1)\,f_0(z)+\right.$$

$$\left.+\,(\nu+3)\,f_1(z)\,r^2+\cdots\right\}r^\nu\Big]$$

$$-\left[b_0^2-\left(C_0^2+2p_1\right)r^2+\cdots\right]\left[m^2C_0^2+2m^2C_0C_1r^2+\cdots\right]\left[f_0(z)+f_1(z)\,r^2+\cdots\right]r^\nu$$

$$+\left[b_0^2-\left(C_0^2+2p_1\right)r^2+\cdots\right]i\,[2mb_0C_0+2m\,(b_0C_1$$

$$\left.-\frac{(C_0^3+C_0p_1)}{b_0}\right)r^2+\cdots\Big]\left[\frac{df_0}{dz}+\right.$$

$$\left.+\,\frac{df_1}{dz}r^2+\cdots\right]r^\nu$$

$$+\left[b_0^2-\left(C_0^2+2p_1\right)r^2+\cdots\right]\left[b_0^2-2\left(C_0^2+p_1\right)r^2+\cdots\right]\left[\frac{d^2f_0}{dz^2}+\frac{d^2f_1}{dz^2}r^2+\cdots\right]r^\nu$$

$$-\left[b_0^2-\left(C_0^2+2p_1\right)r^2+\cdots\right]\left[4C_0C_1r^2+\cdots\right]\left[f_0(z)+f_1(z)\,r^2+\cdots\right]r^\nu$$

$$+\left[b_0^2-\left(C_0^2+2p_1\right)r^2+\cdots\right]i\frac{\partial}{\partial r}\left[\left\{\frac{mb_0^2}{r}-m\left(\frac{3}{2}C_0^2+2p_1\right)r+\cdots\right\}\{g_0(z)+\right.$$

$$\left.+g_1(z)\,r^2+\cdots\right\}r^\nu\Big]$$

$$-\left[b_0^2-\left(C_0^2+2p_1\right)r^2+\cdots\right]\frac{\partial}{\partial r}\left[\left\{b_0C_0r+\left(b_0C_1-\frac{(C_0^3+C_0p_1)}{2b_0}\right)r^3+\cdots\right\}\left\{\frac{dg_0}{dz}+\right.\right.$$

$$\left.\left.+\,\frac{dg_1}{dz}r^2+\cdots\right\}r^\nu\right]$$

$$-\left[b_0^2-\left(C_0^2+2p_1\right)r^2+\cdots\right]\left[2b_0C_0+\left(2b_0C_1-\frac{(C_0^3+C_0p_1)}{b_0}\right)r^2+\cdots\right]\left[\frac{dg_0}{dz}+\right.$$

$$\left.+\frac{dg_1}{dz}r^2+\cdots\right]r^\nu$$

$$+\mu\gamma\left[b_0^2-\left(C_0^2+2p_1\right)r^2+\cdots\right]\frac{\partial}{\partial r}\left[\left\{\frac{p_0}{r}+p_1r+\cdots\right\}\{(\nu+1)\,f_0(z)+\right.$$

$$\left.+(\nu+3)\,f_1(z)\,r^2+\cdots\right\}r^\nu\Big]$$

$$-\mu\gamma\left[p_0+p_1r^2+\cdots\right]\left[imC_0+imC_1r^2+\cdots\right]\left[h_0(z)+\right.$$

$$\left.+h_1(z)r^2+\cdots\right]\left[-\frac{(C_0^2+2p_1)}{b_0}r+\cdots\right]r^\nu$$

$$-\mu\gamma\left[p_0+p_1r^2+\cdots\right]\left[\frac{imb_0}{r}-\frac{im(C_0^2+p_1)}{b_0}r+\cdots\right]\left[g_0(z)+\right.$$

$$\left.+g_1(z)r^2+\cdots\right]\left[-\frac{(C_0^2+2p_1)}{b_0}r+\cdots\right]r^\nu$$

$$+\mu\gamma\left[b_0-\frac{(C_0^2+2p_1)}{2b_0}r^2+\cdots\right]\frac{\partial}{\partial r}\left[\left\{p_0+p_1r^2+\cdots\right\}\left\{imC_0+\right.\right.$$

$$\left.\left.+imC_1r^2+\cdots\right\}\left\{h_0(z)+h_1(z)r^2+\cdots\right\}r^\nu\right]$$

$$+\mu\gamma\left[b_0-\frac{(C_0^2+2p_1)}{2b_0}r^2+\cdots\right]\frac{\partial}{\partial r}\left[\left\{p_0+p_1r^2+\cdots\right\}\left\{\frac{imb_0}{r}\right.\right.$$

$$\left.\left.-\frac{im(C_0^2+p_1)}{b_0}r+\cdots\right\}\left\{g_0(z)+g_1(z)r^2+\cdots\right\}r^\nu\right]$$

$$-\mu\gamma\left[p_0+p_1r^2+\cdots\right]\left[b_0-\frac{(C_0^2+p_1)}{b_0}r^2+\cdots\right]\left[\frac{dh_0}{dz}+\right.$$

$$\left.+\frac{dh_1}{dz}r^2+\cdots\right]\left[-\frac{(C_0^2+2p_1)}{b_0}r+\cdots\right]r^\nu$$

$$+\mu\gamma\left[p_0+p_1r^2+\cdots\right]\left[C_0r+C_1r^3+\cdots\right]\left[\frac{dg_0}{dz}+\right.$$

$$\left.+\frac{dg_1}{dz}r^2+\cdots\right]\left[-\frac{(C_0^2+2p_1)}{b_0}r+\cdots\right]r^\nu$$

$$+\mu\gamma\left[b_0-\frac{(C_0^2+2p_1)}{2b_0}r^2+\cdots\right]\frac{\partial}{\partial r}\left[\left\{p_0+p_1r^2+\cdots\right\}\left\{b_0\right.\right.$$

$$\left.\left.-\frac{(C_0^2+p_1)}{b_0}r^2+\cdots\right\}\left\{\frac{dh_0}{dz}+\frac{dh_1}{dz}r^2+\cdots\right\}r^\nu\right]$$

$$-\mu\gamma\left[b_0-\frac{(C_0^2+2p_1)}{2b_0}r^2+\cdots\right]\frac{\partial}{\partial r}\left[\left\{p_0+p_1r^2+\cdots\right\}\left\{C_0r+C_1r^3+\cdots\right\}\left\{\frac{dg_0}{dz}+\right.\right.$$

$$\left.\left.+\frac{dg_1}{dz}r^2+\cdots\right\}r^\nu\right]=0, \qquad (B.43a)$$

$$-\left[b_0^2-\left(C_0^2+2p_1\right)r^2+\cdots\right]\left[\frac{m^2b_0^2}{r^2}-m^2\left(C_0^2+2p_1\right)+\cdots\right]\left[g_0(z)+\right.$$

$$+g_1(z)r^2+\cdots\Big]r^\nu$$

$$+\left[b_0^2-\left(C_0^2+2p_1\right)r^2+\cdots\right]\left[b_0^2-\left(C_0^2+2p_1\right)r^2+\cdots\right]\left[\frac{d^2g_0}{dz^2}+\frac{d^2g_1}{dz^2}r^2+\cdots\right]r^\nu$$

$$+\left[b_0^2-\left(C_0^2+2p_1\right)r^2+\cdots\right]i\left[\frac{mb_0^2}{r^2}-m\left(\frac{3}{2}C_0^2+2p_1\right)+\cdots\right]\left[(\nu+1)f_0(z)+\right.$$

$$\left.+(\nu+3)f_1(z)r^2+\cdots\right]r^\nu$$

$$-\left[b_0^2-\left(C_0^2+2p_1\right)r^2+\cdots\right]\left[b_0C_0+\left(b_0C_1-\frac{(C_0^3+C_0p_1)}{2b_0}\right)r^2+\cdots\right]\left[(\nu+1)\frac{df_0}{dz}+\right.$$

$$\left.+(\nu+3)\frac{df_1}{dz}r^2+\cdots\right]r^\nu$$

$$+\left[b_0^2-\left(C_0^2+2p_1\right)r^2+\cdots\right]\left[2b_0C_0+\left(2b_0C_1-\frac{(C_0^3+C_0p_1)}{b_0}\right)r^2+\cdots\right]\left[\frac{df_0}{dz}+\right.$$

$$\left.+\frac{df_1}{dz}r^2+\cdots\right]r^\nu$$

$$+\mu\gamma\left[\frac{imb_0^2}{r^2}-im\left(\frac{3}{2}C_0^2+2p_1\right)+\cdots\right]\left[p_0+p_1r^2+\cdots\right]\left[(\nu+1)f_0(z)+\right.$$

$$\left.+(\nu+3)f_1(z)r^2+\cdots\right]r^\nu$$

$$-\mu\gamma\left[b_0C_0+\left(b_0C_1-\frac{(C_0^3+C_0p_1)}{2b_0}\right)r^2+\cdots\right]\left[p_0+p_1r^2+\cdots\right]\left[(\nu+1)\frac{df_0}{dz}+\right.$$

$$\left.+(\nu+3)\frac{df_1}{dz}r^2+\cdots\right]r^\nu$$

$$-\mu\gamma\left[p_0+p_1r^2+\cdots\right]\left[\frac{m^2b_0C_0}{r}+\left(m^2b_0C_1-\frac{m^2(C_0^3+C_0p_1)}{b_0}\right)r+\cdots\right]\left[h_0(z)+\right.$$

$$\left.+h_1(z)r^2+\cdots\right]r^\nu$$

$$+\mu\gamma\left[p_0+p_1r^2+\cdots\right]\left[\frac{imb_0^2}{r}-2im\left(C_0^2+p_1\right)r+\cdots\right]\left[\frac{dh_0}{dz}+\frac{dh_1}{dz}r^2+\cdots\right]r^\nu$$

$$-\mu\gamma\left[p_0+p_1r^2+\cdots\right]\left[imC_0^2r+2imC_0C_1r^3+\cdots\right]\left[\frac{dh_0}{dz}+\frac{dh_1}{dz}r^2+\cdots\right]r^\nu$$

$$-\mu\gamma\left[p_0+p_1r^2+\cdots\right]\left[b_0C_0r+\left(b_0C_1-\frac{(C_0^3+C_0p_1)}{b_0}\right)r^3+\cdots\right]\left[\frac{d^2h_0}{dz^2}+\right.$$

$$+\frac{d^2h_1}{dz^2}r^2+\cdots\Big]\,r^\nu$$

$$-\mu\gamma\left[p_0+p_1r^2+\cdots\right]\left[\frac{m^2b_0^2}{r^2}-2m^2\left(C_0^2+p_1\right)+\cdots\right]\left[g_0\left(z\right)+g_1\left(z\right)r^2+\cdots\right]r^\nu$$

$$-\mu\gamma\left[p_0+p_1r^2+\cdots\right]\left[2imb_0C_0+\left\{2imb_0C_1-\frac{2im\left(C_0^3+C_0p_1\right)}{b_0}\right\}r^2+\cdots\right]\left[\frac{dg_0}{dz}+\right.$$

$$\left.+\frac{dg_1}{dz}r^2+\cdots\right]r^\nu$$

$$-\mu\gamma\left[p_0+p_1r^2+\cdots\right]\left[C_0^2r^2+2C_0C_1r^4+\cdots\right]\left[\frac{d^2g_0}{dz^2}+\frac{d^2g_1}{dz^2}r^2+\cdots\right]r^\nu=0,$$

(B.43b)

$$\left[\frac{imb_0C_0}{r}+\left\{imb_0C_1-\frac{im\left(C_0^3+C_0p_1\right)}{2b_0}\right\}r+\cdots\right]\left[\left(\nu+1\right)f_0\left(z\right)+\right.$$

$$\left.+\left(\nu+3\right)f_1\left(z\right)r^2+\cdots\right]r^\nu$$

$$+\left[\frac{b_0^2}{r}-\left(\frac{3}{2}C_0^2+2p_1\right)r+\cdots\right]\left[\left(\nu+1\right)\frac{df_0}{dz}+\left(\nu+3\right)\frac{df_1}{dz}r^2+\cdots\right]r^\nu$$

$$-\left[m^2C_0^2+2m^2C_0C_1r^2+\cdots\right]\left[h_0\left(z\right)+h_1\left(z\right)r^2+\cdots\right]r^\nu$$

$$+\left[2imb_0C_0+\left\{2imb_0C_1-\frac{2im\left(C_0^3+C_0p_1\right)}{b_0}\right\}r^2+\cdots\right]\left[\frac{dh_0}{dz}+\frac{dh_1}{dz}r^2+\cdots\right]r^\nu$$

$$+\left[b_0^2-2\left(C_0^2+p_1\right)r^2+\cdots\right]\left[\frac{d^2h_0}{dz^2}+\frac{d^2h_1}{dz^2}r^2+\cdots\right]r^\nu$$

$$-\left[\frac{m^2b_0C_0}{r}+\left(m^2b_0C_1-\frac{m^2\left(C_0^3+C_0p_1\right)}{b_0}\right)r+\cdots\right]\left[g_0\left(z\right)+g_1\left(z\right)r^2+\cdots\right]r^\nu$$

$$+\left[\frac{imb_0^2}{r}-2im\left(C_0^2+p_1\right)r+\cdots\right]\left[\frac{dg_0}{dz}+\frac{dg_1}{dz}r^2+\cdots\right]r^\nu$$

$$-\left[imC_0^2r+2imC_0C_1r^3+\cdots\right]\left[\frac{dg_0}{dz}+\frac{dg_1}{dz}r^2+\cdots\right]r^\nu$$

$$-\left[b_0C_0r+\left\{b_0C_1-\frac{\left(C_0^3+C_0p_1\right)}{b_0}\right\}r^3+\cdots\right]\left[\frac{d^2g_0}{dz^2}+\frac{d^2g_1}{dz^2}r^2+\cdots\right]r^\nu=0.$$

(B.43c)

Equation (B.43a) simplified

$$\left[b_0^2-\left(C_0^2+2p_1\right)r^2+\cdots\right]\frac{\partial}{\partial r}\left[\left\{\frac{b_0^2(\nu+1)f_0(z)}{r}+\right.\right.$$

$$\left.\left.+\left[b_0^2(\nu+3)f_1(z)-\left(C_0^2+2p_1\right)(\nu+1)f_0(z)\right]r+\cdots\right\}r^\nu\right]$$

$$-\left[b_0^2-\left(C_0^2+2p_1\right)r^2+\cdots\right]\left[m^2C_0^2+2m^2C_0C_1r^2+\cdots\right]\left[f_0(z)+f_1(z)r^2+\cdots\right]r^\nu$$

$$+\left[b_0^2-\left(C_0^2+2p_1\right)r^2+\cdots\right]i\left[2mb_0C_0+2m\left(b_0C_1\right.\right.$$

$$\left.\left.-\frac{(C_0^3+C_0p_1)}{b_0}\right)r^2+\cdots\right]\left[\frac{df_0}{dz}+\frac{df_1}{dz}r^2+\cdots\right]r^\nu$$

$$+\left[b_0^2-\left(C_0^2+2p_1\right)r^2+\cdots\right]\left[b_0^2-2\left(C_0^2+p_1\right)r^2+\cdots\right]\left[\frac{d^2f_0}{dz^2}+\frac{d^2f_1}{dz^2}r^2+\cdots\right]r^\nu$$

$$-\left[b_0^2-\left(C_0^2+2p_1\right)r^2+\cdots\right]\left[4C_0C_1r^2+\cdots\right]\left[f_0(z)+f_1(z)r^2+\cdots\right]r^\nu$$

$$+\left[b_0^2-\left(C_0^2+2p_1\right)r^2+\cdots\right]i\frac{\partial}{\partial r}\left[\left\{\frac{mb_0^2g_0(z)}{r}+\right.\right.$$

$$\left.\left.+\left(mb_0^2g_1(z)-m\left(\frac{3}{2}C_0^2+2p_1\right)g_0(z)\right)r+\cdots\right\}r^\nu\right]$$

$$-\left[b_0^2-\left(C_0^2+2p_1\right)r^2+\cdots\right]\frac{\partial}{\partial r}\left[\left\{b_0C_0\frac{dg_0}{dz}r+\right.\right.$$

$$\left.\left.+\left[b_0C_0\frac{dg_1}{dz}+\left(b_0C_1-\frac{(C_0^3+C_0p_1)}{2b_0}\right)\frac{dg_0}{dz}\right]r^3+\cdots\right\}r^\nu\right]$$

$$-\left[b_0^2-\left(C_0^2+2p_1\right)r^2+\cdots\right]\left[2b_0C_0+\left(2b_0C_1-\frac{(C_0^3+C_0p_1)}{b_0}\right)r^2+\cdots\right]\left[\frac{dg_0}{dz}+\right.$$

$$\left.+\frac{dg_1}{dz}r^2+\cdots\right]r^\nu$$

$$+\mu\gamma\left[b_0^2-\left(C_0^2+2p_1\right)r^2+\cdots\right]\frac{\partial}{\partial r}\left[\left\{\frac{p_0}{r}+p_1r+\cdots\right\}\{(\nu+1)f_0(z)+\right.\right.$$

$$\left.\left.+(\nu+3)f_1(z)r^2+\cdots\right\}r^\nu\right]$$

$$-\mu\gamma\left[p_0+p_1r^2+\cdots\right]\left[imC_0+imC_1r^2+\cdots\right]\left[h_0(z)+\right.$$

$$+h_1(z)r^2+\cdots\Big]\left[-\frac{(C_0^2+2p_1)}{b_0}r+\cdots\right]r^\nu$$

$$-\mu\gamma\left[p_0+p_1r^2+\cdots\right]\left[\frac{imb_0}{r}-\frac{im(C_0^2+p_1)}{b_0}r+\cdots\right]\left[g_0(z)+\right.$$

$$\left.+g_1(z)r^2+\cdots\right]\left[-\frac{(C_0^2+2p_1)}{b_0}r+\cdots\right]r^\nu$$

$$+\mu\gamma\left[b_0-\frac{(C_0^2+2p_1)}{2b_0}r^2+\cdots\right]\frac{\partial}{\partial r}\left[\{imC_0p_0h_0(z)+\right.$$

$$\left.+\left[imC_0p_0h_1(z)+imC_1p_0h_0(z)+imC_0p_1h_0(z)\right]r^2+\cdots\right\}r^\nu\Big]$$

$$+\mu\gamma\left[b_0-\frac{(C_0^2+2p_1)}{2b_0}r^2+\cdots\right]\frac{\partial}{\partial r}\left[\left\{\frac{imb_0p_0g_0(z)}{r}+\right.\right.$$

$$\left.\left.+\left[imb_0p_0g_1(z)+imb_0p_1g_0(z)-\frac{imp_0(C_0^2+p_1)}{b_0}g_0(z)\right]r+\cdots\right\}r^\nu\right]$$

$$-\mu\gamma\left[p_0+p_1r^2+\cdots\right]\left[b_0-\frac{(C_0^2+p_1)}{b_0}r^2+\cdots\right]\left[\frac{dh_0}{dz}+\right.$$

$$\left.+\frac{dh_1}{dz}r^2+\cdots\right]\left[-\frac{(C_0^2+2p_1)}{b_0}r+\cdots\right]r^\nu$$

$$+\mu\gamma\left[p_0+p_1r^2+\cdots\right]\left[C_0r+C_1r^3+\cdots\right]\left[\frac{dg_0}{dz}+\right.$$

$$\left.+\frac{dg_1}{dz}r^2+\cdots\right]\left[-\frac{(C_0^2+2p_1)}{b_0}r+\cdots\right]r^\nu$$

$$+\mu\gamma\left[b_0-\frac{(C_0^2+2p_1)}{2b_0}r^2+\cdots\right]\frac{\partial}{\partial r}\left[\left\{b_0p_0\frac{dh_0}{dz}+\right.\right.$$

$$\left.\left.+\left[b_0p_0\frac{dh_1}{dz}+b_0p_1\frac{dh_0}{dz}-\frac{p_0(C_0^2+p_1)}{b_0}\frac{dh_0}{dz}\right]r^2+\cdots\right\}r^\nu\right]$$

$$-\mu\gamma\left[b_0-\frac{(C_0^2+2p_1)}{2b_0}r^2+\cdots\right]\frac{\partial}{\partial r}\left[\left\{C_0p_0\frac{dg_0}{dz}r+\right.\right.$$

$$\left.\left.+\left[C_0p_0\frac{dg_1}{dz}+C_1p_0\frac{dg_0}{dz}+C_0p_1\frac{dg_0}{dz}\right]r^3+\cdots\right\}r^\nu\right]=0. \qquad (B.44)$$

Equation (B.44) and (B.43b) to O($r^{(\nu-2)}$)

$$b_0^4(\nu+1)(\nu-1)f_0(z)+imb_0^4(\nu-1)g_0(z)+\mu\gamma b_0^2p_0(\nu-1)(\nu+1)f_0(z)+$$

$$+i\mu\gamma p_0 m b_0^2 (\nu - 1) g_0 (z) = 0, \tag{B.45a}$$

$$-m^2 b_0^4 g_0 (z) + i m b_0^4 (\nu + 1) f_0 (z) + i\mu\gamma p_0 m b_0^2 (\nu + 1) f_0 (z) - \mu\gamma p_0 m^2 b_0^2 g_0 (z) = 0. \tag{B.45b}$$

Equation (B.45a) and (B.45b) can be rewritten

$$b_0^2 (\nu - 1) \left(b_0^2 + \mu\gamma p_0\right) [(\nu + 1) f_0 (z) + i m g_0 (z)] = 0, \tag{B.46a}$$

$$m b_0^2 \left(b_0^2 + \mu\gamma p_0\right) [i (\nu + 1) f_0 (z) - m g_0 (z)] = 0. \tag{B.46b}$$

Equations (B.46a) and (B.46b) give the relation

$$i (\nu + 1) f_0 (z) = m g_0 (z). \tag{B.47}$$

Equation (B.44), (B.43b) and (B.43c) to O($\nu - 1$)

$$\mu\gamma p_0 \nu b_0 \left[i m C_0 h_0 + b_0 \frac{dh_0}{dz}\right] = 0, \tag{B.48a}$$

$$\mu\gamma p_0 m b_0 \left[-m C_0 h_0 + i b_0 \frac{dh_0}{dz}\right] = 0, \tag{B.48b}$$

$$b_0 \left[m C_0 \{i (\nu + 1) f_0 - m g_0\} + b_0 \frac{d}{dz} \{(\nu + 1) f_0 + i m g_0\}\right] = 0. \tag{B.48c}$$

From equation (B.47), equation (B.48c) is trivial.

Equations (B.48a) and (B.48b) give the relation

$$m C_0 h_0 (z) = i b_0 \frac{dh_0}{dz}. \tag{B.49}$$

which implies $h_0 \equiv 0$ since it cannot satisfy both boundary conditions.

Equations (B.4), (B.43b) and (B.43c) to O(ν)

$$b_0^2 (\nu + 1) \left[b_0^2 (\nu + 3) f_1 - \left(C_0^2 + 2p_1\right) (\nu + 1) f_0\right] - b_0^2 \left(C_0^2 + 2p_1\right) (\nu - 1) (\nu + 1) f_0$$

$$-b_0^2m^2C_0^2f_0+2imb_0^3C_0\frac{df_0}{dz}+b_0^4\frac{d^2f_0}{dz^2}+ib_0^2(\nu+1)\left[mb_0^2g_1-m\left(\frac{3}{2}C_0^2+2p_1\right)g_0\right]$$

$$-imb_0^2\left(C_0^2+2p_1\right)(\nu-1)g_0-b_0^3C_0(\nu+1)\frac{dg_0}{dz}-2b_0^3C_0\frac{dg_0}{dz}+$$

$$+\mu\gamma b_0^2(\nu+1)\left[(\nu+1)p_1f_0+(\nu+3)p_0f_1\right]-\mu\gamma(\nu-1)\left(C_0^2+2p_1\right)p_0(\nu+1)f_0+$$

$$+im\mu\gamma p_0\left(C_0^2+2p_1\right)g_0$$

$$+im\mu\gamma b_0(\nu+1)\left[b_0p_0g_1+b_0p_1g_0-\frac{p_0\left(C_0^2+p_1\right)}{b_0}g_0\right]$$

$$-\frac{1}{2}im\mu\gamma p_0\left(C_0^2+2p_1\right)(\nu-1)g_0-\mu\gamma p_0b_0C_0(\nu+1)\frac{dg_0}{dz}=0, \qquad (B.50a)$$

$$m^2b_0^2\left(C_0^2+2p_1\right)g_0+m^2b_0^2\left(C_0^2+2p_1\right)g_0-m^2b_0^4g_1+$$

$$b_0^4\frac{d^2g_0}{dz^2}-imb_0^2\left(\frac{3}{2}C_0^2+2p_1\right)(\nu+1)f_0$$

$$-imb_0^2\left(C_0^2+2p_1\right)(\nu+1)f_0+imb_0^4(\nu+3)f_1-b_0^3C_0(\nu+1)\frac{df_0}{dz}+2b_0^3C_0\frac{df_0}{dz}$$

$$-im\mu\gamma p_0\left(\frac{3}{2}C_0^2+2p_1\right)(\nu+1)f_0+im\mu\gamma b_0^2p_1(\nu+1)f_0+im\mu\gamma p_0b_0^2(\nu+3)f_1$$

$$-\mu\gamma p_0b_0C_0(\nu+1)\frac{df_0}{dz}+2\mu\gamma p_0m^2\left(C_0^2+p_1\right)g_0-\mu\gamma b_0^2m^2p_1g_0$$

$$-\mu\gamma p_0m^2b_0^2g_1-2im\mu\gamma p_0b_0C_0\frac{dg_0}{dz}=0, \qquad (B.50b)$$

$$-m^2C_0^2h_0+2imb_0C_0\frac{dh_0}{dz}+b_0^2\frac{d^2h_0}{dz^2}=0. \qquad (B.50c)$$

Equations (B.50a), (B.50b) and (B.50c) simplified

$$(\nu+1)(\nu+3)b_0^2\left(b_0^2+\mu\gamma p_0\right)f_1$$

$$+\left[-b_0^2\left(C_0^2+2p_1\right)(\nu+1)^2-\left(b_0^2+\mu\gamma p_0\right)\left(C_0^2+2p_1\right)(\nu-1)(\nu+1)-m^2b_0^2C_0^2+\right.$$

$$\left.+\mu\gamma b_0^2p_1(\nu+1)^2\right]f_0$$

$$+2imb_0^3C_0\frac{df_0}{dz}+b_0^4\frac{d^2f_0}{dz^2}+imb_0^2\left(b_0^2+\mu\gamma p_0\right)(\nu+1)\,g_1$$

$$+\left[-imb_0^2\left(\frac{3}{2}C_0^2+2p_1\right)(\nu+1)-imb_0^2\left(C_0^2+2p_1\right)(\nu-1)+im\mu\gamma b_0^2p_1\,(\nu+1)\right.$$

$$\left.-im\mu\gamma p_0\left(C_0^2+p_1\right)(\nu+1)-\frac{1}{2}im\mu\gamma p_0\left(C_0^2+2p_1\right)(\nu-3)\right]g_0$$

$$-b_0C_0\left[\left(b_0^2+\mu\gamma p_0\right)(\nu+1)+2b_0^2\right]\frac{dg_0}{dz}=0, \qquad (B.51a)$$

$$m^2\left[2b_0^2\left(C_0^2+2p_1\right)+2\mu\gamma p_0\left(C_0^2+p_1\right)-\mu\gamma b_0^2p_1\right]g_0$$

$$-m^2b_0^2\left(b_0^2+\mu\gamma p_0\right)g_1-2im\mu\gamma p_0b_0C_0\frac{dg_0}{dz}+b_0^4\frac{d^2g_0}{dz^2}$$

$$+im\left[-\left(b_0^2+\mu\gamma p_0\right)\left(\frac{3}{2}C_0^2+2p_1\right)(\nu+1)-b_0^2\left(C_0^2+2p_1\right)(\nu+1)+\right.$$

$$\left.+\mu\gamma b_0^2p_1\,(\nu+1)\right]f_0$$

$$+imb_0^2\left(b_0^2+\mu\gamma p_0\right)(\nu+3)\,f_1+b_0C_0\left[-\left(b_0^2+\mu\gamma p_0\right)(\nu+1)+2b_0^2\right]\frac{df_0}{dz}=0, \qquad (B.51b)$$

$$\left(imC_0+b_0\frac{d}{dz}\right)^2h_0\left(z\right)=0. \qquad (B.51c)$$

im(B.51a)$-(\nu+1)$(B.51b)

$$-im\left[\left(b_0^2+\mu\gamma p_0\right)\left(C_0^2+2p_1\right)(\nu-1)\,(\nu+1)+\right.$$

$$\left.m^2b_0^2C_0^2-\left(b_0^2+\mu\gamma p_0\right)\left(\frac{3}{2}C_0^2+2p_1\right)(\nu+1)^2\right]f_0$$

$$+b_0C_0\left[-2m^2b_0^2+\left(b_0^2+\mu\gamma p_0\right)(\nu+1)^2-2b_0^2\,(\nu+1)\right]\frac{df_0}{dz}+imb_0^4\frac{d^2f_0}{dz^2}$$

$$+m^2\left[b_0^2\left(\frac{3}{2}C_0^2+2p_1\right)(\nu+1)-b_0^2\left(C_0^2+2p_1\right)(\nu+3)-\mu\gamma p_0\left(C_0^2+p_1\right)(\nu+1)\right.$$

$$\left.+\frac{1}{2}\mu\gamma p_0\left(C_0^2+2p_1\right)(\nu-3)\right]g_0$$

$$+imb_0C_0\left[-\left(b_0^2+\mu\gamma p_0\right)(\nu+1)-2b_0^2+2\mu\gamma p_0\,(\nu+1)\right]\frac{dg_0}{dz}-b_0^4\,(\nu+1)\,\frac{d^2g_0}{dz^2}=0.$$

$$(B.52)$$

using equation (B.47), equation (B.52) is

$$\frac{ib_0^2}{m}\left[m^2-(\nu+1)^2\right]\left[b_0^2\frac{d^2f_0}{dz^2}+2imb_0C_0\frac{df_0}{dz}+i^2m^2C_0^2f_0\right]=0, \qquad (B.53)$$

which reduces to

$$\frac{ib_0^2}{m}\left[m^2-(\nu+1)^2\right]\left(imC_0+b_0\frac{d}{dz}\right)^2 f_0=0. \qquad (B.54)$$

For the radial dependence of ξ_r near the singularity at $r=0$, without or with pressure, from (B.25) and (B.54)

$$(\nu+1)^2=m^2, \qquad (B.55)$$

or

$$\nu=\pm m-1, \qquad (B.56)$$

Appendix C

Derivation of arcade radial boundary condition near $r = 0$.

Equation (3.5) from Hood (1983) is

$$B^2\frac{\partial^2\xi_r}{\partial r^2}+\frac{B_z^2-B_\theta^2}{r}\frac{\partial\xi_r}{\partial r}+\frac{B_\theta^2}{r^2}\frac{\partial^2\xi_r}{\partial\theta^2}+2ik\frac{B_\theta B_z}{r}\frac{\partial\xi_r}{\partial\theta}$$
$$-\left(k^2B_z^2+\frac{B^2}{r^2}+2\frac{B_\theta B_\theta'}{r}\right)\xi_r$$
$$=-\frac{ik}{r^2}\frac{\partial}{\partial r}\left(r^2B_\theta B\xi_0\right)+\frac{\partial}{\partial r}\left(\frac{B_zB}{r}\frac{\partial\xi_0}{\partial\theta}\right), \qquad (C.1)$$

and equation (3.6) from Hood (1983) is

$$\frac{1}{r^2}\frac{\partial^2}{\partial\theta^2}\left(B\xi_0\right)-k^2B\xi_0=\frac{B_z}{r^2}\frac{\partial}{\partial r}\left(r\frac{\partial\xi_r}{\partial\theta}\right)-ikrB_\theta\frac{\partial}{\partial r}\left(\frac{\xi_r}{r}\right). \qquad (C.2)$$

We expand ξ_r, ξ_0, B_θ and B_z as (see (3.8) from Hood (1983))

$$\xi_r=r^\nu\left(f_0\left(\theta\right)+r^2f_1\left(\theta\right)+\cdots\right), \qquad (C.3a)$$

$$\xi_0=r^\nu\left(g_0\left(\theta\right)+r^2g_1\left(\theta\right)+\cdots\right), \qquad (C.3b)$$

$$B_\theta=C_0r+C_1r^3+\cdots, \qquad (C.3c)$$

$$B_z=b_0+b_1r^2+\cdots, \qquad (C.3d)$$

where $b_0=1$ in Hood (1983). This gives the following expansions

$$B^2=B_\theta^2+B_z^2=b_0^2+\left(2b_0b_1+C_0^2\right)r^2+\left(2b_0b_2+b_1^2+2C_0C_1\right)r^4+\cdots, \qquad (C.4a)$$

$$B_z^2 - B_\theta^2 = b_0^2 + \left(2b_0b_1 - C_0^2\right) r^2 + \left(2b_0b_2 + b_1^2 - 2C_0C_1\right) r^4 + \cdots, \qquad (C.4b)$$

$$B_\theta^2 = C_0^2 r^2 + 2C_0C_1 r^4 + \left(2C_0C_2 + C_1^2\right) r^6 + \cdots, \qquad (C.4c)$$

$$B_\theta B_z = b_0C_0 r + \left(b_0C_1 + b_1C_0\right) r^3 + \left(b_0C_2 + b_1C_1 + b_2C_0\right) r^5 + \cdots, \qquad (C.4d)$$

$$B_z^2 = b_0^2 + 2b_0b_1 r^2 + \left(2b_0b_2 + b_1^2\right) r^4 + \cdots, \qquad (C.4e)$$

$$B_\theta' = C_0 + 3C_1 r^2 + 5C_2 r^4 + \cdots, \qquad (C.4f)$$

$$B_\theta B_\theta' = C_0^2 r + 4C_0C_1 r^3 + \left(6C_0C_2 + 3C_1^2\right) r^5 + \cdots, \qquad (C.4g)$$

$$B = b_0 + \frac{1}{2b_0}\left(2b_0b_1 + C_0^2\right) r^2 +$$

$$+ \left[-\frac{1}{8b_0^3}\left(2b_0b_1 + C_0^2\right)^2 + \frac{1}{2b_0}\left(2b_0b_2 + b_1^2 + 2C_0C_1\right)\right] r^4 + \cdots, \qquad (C.4h)$$

$$r^2 B_\theta B = b_0C_0 r^3 + \left[\frac{C_0}{2b_0}\left(2b_0b_1 + C_0^2\right) + b_0C_1\right] r^5 + \left[-\frac{C_0}{8b_0^3}\left(2b_0b_1 + C_0^2\right)^2 +\right.$$

$$\left. + \frac{C_0}{2b_0}\left(2b_0b_2 + b_1^2 + 2C_0C_1\right) + \frac{C_1}{2b_0}\left(2b_0b_1 + C_0^2\right) + b_0C_2\right] r^7 + \cdots, \qquad (C.4i)$$

$$\frac{B_z B}{r} = \frac{b_0^2}{r} + \left[b_0b_1 + \frac{1}{2}\left(2b_0b_1 + C_0^2\right)\right] r + \left[-\frac{1}{8b_0^2}\left(2b_0b_1 + C_0^2\right)^2 +\right.$$

$$\left. + \frac{1}{2}\left(2b_0b_2 + b_1^2 + 2C_0C_1\right) + \frac{b_1}{2b_0}\left(2b_0b_1 + C_0^2\right) + b_0b_2\right] r^3 + \cdots. \qquad (C.4j)$$

Equation (C.1) expanded is

$$\left[b_0^2 + \left(2b_0b_1 + C_0^2\right) r^2 + \left(2b_0b_2 + b_1^2 + 2C_0C_1\right) r^4 + \cdots\right] \left[\frac{\nu\left(\nu - 1\right) f_0}{r^2} +\right.$$

$$\left. + \left(\nu + 2\right)\left(\nu + 1\right) f_1 + \left(\nu + 4\right)\left(\nu + 3\right) f_2 r^2 + \cdots\right] r^\nu$$

$$+ \left[\frac{b_0^2}{r} + \left(2b_0b_1 - C_0^2\right) r + \left(2b_0b_2 + b_1^2 - 2C_0C_1\right) r^3 + \cdots\right] \left[\frac{\nu f_0}{r} +\right.$$

$$+(\nu+2)\,f_1 r+(\nu+4)\,f_2 r^3+\cdots\Big]\,r^\nu$$

$$+\left[C_0^2+2C_0C_1r^2+\left(2C_0C_2+C_1^2\right)r^4+\cdots\right]\left[\frac{d^2f_0}{d\theta^2}+\frac{d^2f_1}{d\theta^2}r^2+\frac{d^2f_2}{d\theta^2}r^4+\cdots\right]r^\nu$$

$$+2ik\left[b_0C_0+(b_0C_1+b_1C_0)\,r^2+(b_0C_2+b_1C_1+b_2C_0)\,r^4+\cdots\right]\left[\frac{df_0}{d\theta}+\right.$$

$$\left.\frac{df_1}{d\theta}r^2+\frac{df_2}{d\theta}r^4+\cdots\right]r^\nu$$

$$-k^2\left[b_0^2+2b_0b_1r^2+\left(2b_0b_2+b_1^2\right)r^4+\cdots\right]\left[f_0+f_1r^2+f_2r^4+\cdots\right]r^\nu$$

$$-\left[\frac{b_0^2}{r^2}+\left(2b_0b_1+C_0^2\right)+\left(2b_0b_2+b_1^2+2C_0C_1\right)r^2+\cdots\right]\left[f_0+f_1r^2+f_2r^4+\cdots\right]r^\nu$$

$$-2\left[C_0^2+4C_0C_1r^2+\left(6C_0C_2+3C_1^2\right)r^4+\cdots\right]\left[f_0+f_1r^2+f_2r^4+\cdots\right]r^\nu$$

$$=-ik\left[3b_0C_0+5\left(\frac{C_0}{2b_0}\left(2b_0b_1+C_0^2\right)+b_0C_1\right)r^2+7\left(-\frac{C_0}{8b_0^3}\left(2b_0b_1+C_0^2\right)^2+\right.\right.$$

$$\left.\left.+\frac{C_0}{2b_0}\left(2b_0b_2+b_1^2+2C_0C_1\right)+\frac{C_1}{2b_0}\left(2b_0b_1+C_0^2\right)+b_0C_2\right)r^4+\cdots\right][g_0+$$

$$g_1r^2+g_2r^4+\cdots\Big]\,r^\nu$$

$$-ik\left[b_0C_0r+\left(\frac{C_0}{2b_0}\left(2b_0b_1+C_0^2\right)+b_0C_1\right)r^3+\left(-\frac{C_0}{8b_0^3}\left(2b_0b_1+C_0^2\right)^2+\right.\right.$$

$$\left.\left.+\frac{C_0}{2b_0}\left(2b_0b_2+b_1^2+2C_0C_1\right)+\frac{C_1}{2b_0}\left(2b_0b_1+C_0^2\right)+b_0C_2\right)r^5+\cdots\right]\left[\frac{\nu g_0}{r}+\right.$$

$$\left.+(\nu+2)\,g_1r+(\nu+4)\,g_2r^3+\cdots\right]r^\nu$$

$$+\left[\frac{-b_0^2}{r^2}+\left(2b_0b_1+\frac{1}{2}C_0^2\right)+3\left(-\frac{1}{8b_0^2}\left(2b_0b_1+C_0^2\right)^2+\frac{1}{2}\left(2b_0b_2+b_1^2+2C_0C_1\right)+\right.\right.$$

$$\left.\left.+\frac{b_1}{2b_0}\left(2b_0b_1+C_0^2\right)+b_0b_2\right)r^2+\cdots\right]\left[\frac{dg_0}{d\theta}+\frac{dg_1}{d\theta}r^2+\frac{dg_2}{d\theta}r^4+\cdots\right]r^\nu$$

$$+\left[\frac{b_0^2}{r}+\left(2b_0b_1+\frac{1}{2}C_0^2\right)r+\left(-\frac{1}{8b_0^2}\left(2b_0b_1+C_0^2\right)^2+\frac{1}{2}\left(2b_0b_2+b_1^2+2C_0C_1\right)+\right.\right.$$

$$\left.\left.+\frac{b_1}{2b_0}\left(2b_0b_1+C_0^2\right)+b_0b_2\right)r^3+\cdots\right]\left[\frac{\nu}{r}\frac{dg_0}{d\theta}+(\nu+2)\,\frac{dg_1}{d\theta}r+\right.$$

$$+(\nu+4)\frac{dg_2}{d\theta}r^3+\cdots\Big]r^\nu, \tag{C.5}$$

and equation (C.2) expanded is

$$\left[\frac{b_0}{r^2}+\frac{1}{2b_0}\left(2b_0b_1+C_0^2\right)+\left(-\frac{1}{8b_0^3}\left(2b_0b_1+C_0^2\right)^2+\right.\right.$$
$$\left.\left.\frac{1}{2b_0}\left(2b_0b_2+b_1^2+2C_0C_1\right)\right)r^2+\cdots\right]\left[\frac{d^2g_0}{d\theta^2}+\frac{d^2g_1}{d\theta^2}r^2+\frac{d^2g_2}{d\theta^2}r^4+\cdots\right]r^\nu$$
$$-k^2\left[b_0+\frac{1}{2b_0}\left(2b_0b_1+C_0^2\right)r^2+\left(-\frac{1}{8b_0^3}\left(2b_0b_1+C_0^2\right)^2+\right.\right.$$
$$\left.\left.\frac{1}{2b_0}\left(2b_0b_2+b_1^2+2C_0C_1\right)\right)r^4+\cdots\right]\left[g_0+g_1r^2+g_2r^4+\cdots\right]r^\nu$$
$$=\left[\frac{b_0}{r^2}+b_1+b_2r^2+\cdots\right]\left[\frac{df_0}{d\theta}+\frac{df_1}{d\theta}r^2+\frac{df_2}{d\theta}r^4+\cdots\right]r^\nu$$
$$+\left[\frac{b_0}{r}+b_1r+b_2r^3+\cdots\right]\left[\frac{\nu}{r}\frac{df_0}{d\theta}+(\nu+2)\frac{df_1}{d\theta}r+(\nu+4)\frac{df_2}{d\theta}r^3+\cdots\right]r^\nu$$
$$+ik\left[C_0+C_1r^2+C_2r^4+\cdots\right]\left[f_0+f_1r^2+f_2r^4+\cdots\right]r^\nu$$
$$-ik\left[C_0r+C_1r^3+C_2r^5+\cdots\right]\left[\frac{\nu f_0}{r}+(\nu+2)f_1r+(\nu+4)f_2r^3+\cdots\right]r^\nu. \tag{C.6}$$

the $O(\frac{1}{r^2})$ terms from (C.5)

$$b_0^2\nu(\nu-1)f_0+b_0^2\nu f_0-b_0^2f_0=-b_0^2\frac{dg_0}{d\theta}+b_0^2\nu\frac{dg_0}{d\theta}, \tag{C.7}$$

which simplifies to

$$(\nu+1)f_0=\frac{dg_0}{d\theta}. \tag{C.8}$$

the $O(\frac{1}{r^2})$ terms from (C.6)

$$b_0\frac{d^2g_0}{d\theta^2}=b_0\frac{df_0}{d\theta}+b_0\nu\frac{df_0}{d\theta}, \tag{C.9}$$

which simplifies to

$$(\nu+1)\frac{df_0}{d\theta}=\frac{d^2g_0}{d\theta^2}. \tag{C.10}$$

The O(1) terms from (C.5)

$$b_0^2(\nu+2)(\nu+1)f_1+\left(2b_0b_1+C_0^2\right)\nu(\nu-1)f_0+b_0^2(\nu+2)f_1+\left(2b_0b_1-C_0^2\right)\nu f_0+$$

$$+C_0^2\frac{d^2f_0}{d\theta^2}+2ikb_0C_0\frac{df_0}{d\theta}-k^2b_0^2f_0-b_0^2f_1-\left(2b_0b_1+C_0^2\right)f_0-2C_0^2f_0$$

$$=-3ikb_0C_0g_0-ikb_0C_0\nu g_0+(1+\nu)\left(2b_0b_1+\frac{1}{2}C_0^2\right)\frac{dg_0}{d\theta}+b_0^2(\nu+1)\frac{dg_1}{d\theta}, \tag{C.11}$$

which simplifies to

$$\left[2b_0b_1(\nu+1)(\nu-1)+C_0^2(\nu+1)(\nu-3)-k^2b_0^2\right]f_0+b_0^2(\nu+1)(\nu+3)f_1+$$

$$+C_0^2\frac{d^2f_0}{d\theta^2}+2ikb_0C_0\frac{df_0}{d\theta}-(\nu+1)\left(2b_0b_1+\frac{1}{2}C_0^2\right)\frac{dg_0}{d\theta}+$$

$$(\nu+3)ikb_0C_0g_0-b_0^2(\nu+1)\frac{dg_1}{d\theta}=0. \tag{C.12}$$

The O(1) terms from (C.6)

$$b_0\frac{d^2g_1}{d\theta^2}+\frac{1}{2b_0}\left(2b_0b_1+C_0^2\right)\frac{d^2g_0}{d\theta^2}-k^2b_0g_0=b_0\frac{df_1}{d\theta}+$$

$$+b_1\frac{df_0}{d\theta}+b_0(\nu+2)\frac{df_1}{d\theta}+b_1\nu\frac{df_0}{d\theta}+ikC_0f_0-ikC_0\nu f_0, \tag{C.13}$$

rearranging

$$(\nu-1)ikC_0f_0-b_1(\nu+1)\frac{df_0}{d\theta}-b_0(\nu+3)\frac{df_1}{d\theta}+$$

$$+\frac{1}{2b_0}\left(2b_0b_1+C_0^2\right)\frac{d^2g_0}{d\theta^2}-k^2b_0g_0+b_0\frac{d^2g_1}{d\theta^2}=0. \tag{C.14}$$

Take theta-derivative of (C.5)O(1) expansion and $b_0(\nu+1)$ multiplied by (C.6)O(1) expansion to eliminate f_1

$$(\nu-1)(\nu+1)ikb_0C_0f_0 - b_0b_1(\nu+1)^2\frac{df_0}{d\theta} + [2b_0b_1(\nu+1)(\nu-1)+$$
$$+C_0^2(\nu+1)(\nu-3) - k^2b_0^2]\frac{df_0}{d\theta} + C_0^2\frac{d^3f_0}{d\theta^3}+$$
$$2ikb_0C_0\frac{d^2f_0}{d\theta^2} - (\nu+1)\left(2b_0b_1+\frac{1}{2}C_0^2\right)\frac{d^2g_0}{d\theta^2} + (\nu+3)ikb_0C_0\frac{dg_0}{d\theta}$$
$$+\frac{\nu+1}{2}\left(2b_0b_1+C_0^2\right)\frac{d^2g_0}{d\theta^2} - k^2b_0^2(\nu+1)g_0 = 0. \qquad (C.15)$$

Using $O(1/r^2)$ expression from (C.5), and multiplying by $(\nu+1)/b_0^2$

$$\left(\frac{C_0}{b_0}\right)^2\frac{d^4g_0}{d\theta^2} + 2ik\left(\frac{C_0}{b_0}\right)\frac{d^3g_0}{d\theta^3} + \left[-k^2+(\nu+1)(\nu-3)\left(\frac{C_0}{b_0}\right)^2 -\right.$$
$$\left.-4(\nu+1)\left(\frac{b_1}{b_0}\right)\right]\frac{d^2g_0}{d\theta^2} + 2(\nu+1)^2ik\left(\frac{C_0}{b_0}\right)\frac{dg_0}{d\theta} - k^2(\nu+1)^2g_0 = 0. \qquad (C.16)$$

The force-free equilibrium equation in cylindrical geometry

$$\frac{B_\theta}{r}(rB_\theta)' + B_zB_z' = 0. \qquad (C.17)$$

expanded

$$\left[C_0+C_1r^2+\cdots\right]\left[2C_0r+4C_1r^3+\cdots\right] + \left[b_0+b_1r^2+\cdots\right]\left[2b_1r+4b_2r^3+\cdots\right] = 0, \qquad (C.18)$$

giving to $O(r)$ a relation between b_1 and C_0

$$C_0^2 + b_0b_1 = 0. \qquad (C.19)$$

and so

$$\left(\frac{C_0}{b_0}\right)^2\frac{d^4g_0}{d\theta^4} + 2ik\left(\frac{C_0}{b_0}\right)\frac{d^3g_0}{d\theta^3} + \left[-k^2+(\nu+1)^2\left(\frac{C_0}{b_0}\right)^2\right]\frac{d^2g_0}{d\theta^2}$$

$$+2(\nu+1)^2 ik\left(\frac{C_0}{b_0}\right)\frac{dg_0}{d\theta} - k^2(\nu+1)^2 g_0 = 0, \qquad (C.20)$$

which factorizes to

$$\left[\frac{d^2}{d\theta^2} + (\nu+1)^2\right]\left[\left(\frac{C_0}{b_0}\right)^2\frac{d^2}{d\theta^2} + 2ik\left(\frac{C_0}{b_0}\right)\frac{d}{d\theta} - k^2\right] g_0 = 0. \qquad (C.21)$$

as given in Hood (1983) with $b_0 = 1$.

The solution of equation (C.21) is

$$g_0 = (a+b\theta)\, e^{-i\frac{kb_0}{C_0}\theta} + ce^{i(\nu+1)\theta} + de^{-i(\nu+1)\theta}, \qquad (C.22)$$

if $\nu + 1 \neq \pm kb_0/C_0$ or 0. The boundary conditions are

$$g_0 = \frac{dg_0}{d\theta} = 0 \quad \text{at} \quad \theta = \pm\frac{\pi}{2}, \qquad (C.23)$$

Substituting the boundary conditions (C.23) in (C.22) gives the matrix equation

$$\begin{pmatrix} e^{-M\frac{\pi}{2}} & \frac{\pi}{2}e^{-M\frac{\pi}{2}} & e^{N\frac{\pi}{2}} & e^{-N\frac{\pi}{2}} \\ e^{M\frac{\pi}{2}} & -\frac{\pi}{2}e^{M\frac{\pi}{2}} & e^{-N\frac{\pi}{2}} & e^{N\frac{\pi}{2}} \\ -Me^{-M\frac{\pi}{2}} & \left(1-M\frac{\pi}{2}\right)e^{-M\frac{\pi}{2}} & Ne^{N\frac{\pi}{2}} & -Ne^{-N\frac{\pi}{2}} \\ -Me^{M\frac{\pi}{2}} & \left(1+M\frac{\pi}{2}\right)e^{M\frac{\pi}{2}} & Ne^{-N\frac{\pi}{2}} & -Ne^{N\frac{\pi}{2}} \end{pmatrix}\begin{pmatrix} a \\ b \\ c \\ d \end{pmatrix} = 0, \qquad (C.24)$$

where $M = ikb_0/C_0$ and $N = i(\nu+1)$ and the non-trivial solution given by the zero of the matrix determinant is

$$\left[(\nu+1)^2\pi^2 - \left(\frac{kb_0}{C_0}\pi\right)^2\right]\sin(\nu+1)\pi + 2(\nu+1)\pi\left[\cos(\nu+1)\pi - \cos\frac{kb_0}{C_0}\pi\right] = 0. \qquad (C.25)$$